Dissecting the Components of Neuropathic Pain

2018

Dale George
University of Central Florida

DISSECTING THE COMPONENTS OF NEUROPATHIC PAIN

by

DALE SUSAN GEORGE
B.Sc. Garden City College, 2008
M.Sc. Vellore Institute of Technology, 2010

A dissertation submitted in partial fulfillment of the requirements
for the degree of Doctor of Philosophy
in the Burnett School of Biomedical Sciences
in the College of Medicine
at the University of Central Florida
Orlando, Florida

Spring Term
2018

Major Professor: Stephen Lambert

ABSTRACT

Pain is a public health issue affecting the lives of nearly 116 million adults in the US, annually. Understanding the physiological and phenotypic changes that occur in response to painful stimuli is of tremendous clinical interest, but, the complexity of pain and the lack of a representative *in vitro* model hinders the development of new therapeutics. Pain stimuli are first perceived and transmitted by the neurons within the dorsal root ganglia (DRG) which become hyperexcitable under these conditions. It has now been established that satellite glial cells (SGCs) that ensheathe the DRG cell body actively contribute to this neuronal dysregulation. To understand the role of SGCs in this pain circuit, first, we looked at the development of SGCs within the DRG of rats, and we showed that SGCs developed postnatally, and appeared morphologically, transcriptionally and functionally similar to Schwann cells precursors (SCs), supporting the idea that these cells may exhibit multipotent behavior. Secondly, we describe here, a three-dimensional *in vitro* model of the DRG which is functionally characterized on a microelectrode array (MEA). This model can be used to assess the long-term recording of spontaneous activity from bundles of axons while preserving the neuronal-SGC interactions similar to those observed *in vivo*. Furthermore, using capsaicin, an agonist of the TRPV1 nociceptive receptor, we show that this model can be used as an *in vitro* assay to acquire evoked responses from nociceptive neurons. Overall, this study advances our knowledge on the development and differentiation of SGCs and establishes a novel functional three-dimensional model for the study of SGCs. This model can now be used as a tool to study the underlying basis of neuronal dysregulation in pain.

ACKNOWLEDGMENTS

This thesis is a reality because of the collective contribution and efforts of several pivotal individuals. First, my heart filled gratitude to Dr. Stephen Lambert. You are an exemplary scientist and a wonderful human being. Your laid back mentoring style laced with wit and humor is what made graduate training so enjoyable. As I am getting ready to move on to the next phase of training, I realize that I am not the same person who walked into your office six years ago. You have indeed transformed my scientific, and interpersonal skills. Thank you for instilling confidence and for encouraging me throughout this process. I am incredibly grateful to have you as my mentor and friend.

Sincere gratitude to my committee members Dr. Steven Ebert, Dr. Yoon-Seong Kim and Dr. Cristina Fernandez-Valle for their constant guidance, critique, and the much valued scientific input. Dr. Alvaro Estevez, you have been an amazing teacher. Thank you for serving on my committee and for always having your door open for me. Thank you, Dr. Bradley J. Willenberg, for being the second mentor. You were the voice of reason when I needed it the most. I am so grateful for your scientific collaboration and personal guidance. Professor Weigel, it has been a joy being a part of your immunology teaching assistant team.

To my parents who supported me and encouraged me to pursue my dreams. I would not be here if it weren't for the countless sacrifices you both have made. Thank you, mom, for being my hero and for being an embodiment of everything a person needs to be. Dad, you desired to get a Ph.D., but financial pressures kept you away from pursuing it. I hope I have made you proud. A big thank you to my siblings, Bill, Mel, Preetha, and Nita for your unwavering support from the very

beginning of this journey. One of the highlights of my personal life, while in graduate school was getting married to an exceptional person. Reebu, thank you so much for being patient with me and for understanding the pressures of graduate school. To my roommates, Chelsea and Tiffany who have opened not just their homes but their hearts to me. I couldn't have done this without your love and support.

Wesley, thank you for your companionship and positivity. We couldn't be more different from each other and yet, I couldn't have asked for a better lab partner and a friend. These years were so easy and fun because of you. Thank you, Paige, for teaming up with me on those weekends and long hours of work. Alex, your passion for scientific inquiry is contagious and thank you, for those existential luncheons. It was my pleasure to train and to know each of the members of the Lambert lab, especially Anita, Christina, and Peter.

I was fortunate in having great lab neighbors. The Valle lab has played such an essential role in my graduate school life. I would like to thank Nick, who was kind enough to help and guide me when I first started off in the lab. Marga, thank you so much for your expertise and guidance in cell culture and more importantly for your love, care, and concern. I appreciate all the personal and scientific advice Dr. Petrilli offered so generously. Thank you, Marisa, for always helping out with anything I needed.

Thank you to the Burnett family for the scholarship that supported me through five years of graduate school. Thank you to the Burnett School of Biomedical Sciences department for the financial support through graduate teaching opportunities. Thank you to the College of Graduate Studies for the Graduate Dean's Dissertation Completion Fellowship which has enabled me to

ensure timely completion of this thesis. I would like to thank Ryan Dickerson, the medical illustrator for his contributions and creativity with the schematics shown in this thesis. Finally, thank you to the all the staff at the program office, front desk and the vivarium for all your help.

TABLE OF CONTENTS

LIST OF FIGURES

LIST OF TABLES

CHAPTER ONE: GENERAL INTRODUCTION

Scope

Chronic pain is a significant health problem and affects the lives of nearly around 116 million adults in the United States ("Relieving Pain in America: A Blueprint for Transforming Prevention, Care, Education, and Research," 2016). Rather than being curative, the current treatments are aimed at managing the symptoms of pain. Moreover, new drugs in the market are often reformulations of the existing drugs (Backonja & Woolf, 2010; "Relieving Pain in America: A Blueprint for Transforming Prevention, Care, Education, and Research," 2016). This highlights the need to understand the mechanisms underlying neuropathic pain. Neuropathic pain is a highly complex phenomenon that involves not just the neurons, but other important players like the immune and glial cells are integral pieces that contribute to this pathology (Scholz & Woolf, 2007). Often, neurons were the sole focus of these studies, and the contribution of the non-neuronal cells in this dysregulation was overlooked. Satellite glial cells (SGCs) are specialized glial cells in the peripheral nervous system (PNS) that envelops the neuronal cell body of the sensory neurons (E. Pannese, 1981, 2010). Recent studies have demonstrated that SGCs are not just bystanders to injury but, undergo characteristic changes that lead to alterations in the neuronal function that trigger neuropathic pain (P. T. Ohara et al., 2009).

The following dissertation describes the origin of SGCs and investigates the plasticity of this enigmatic cell type. Further, to assess the direct contribution of SGCs to the altered neuronal firing seen in neuropathic conditions, we developed a system where neurophysiological assessments from *in vitro* sensory nerves could be achieved. Understanding the origins and signals involved in

the specification of SGCs, as well as the use of a model which can be used to study the mechanisms by which neuronal activity is regulated is of enormous clinical importance.

Complexity of Pain

Pain is defined as 'an unpleasant sensory and emotional experience associated with actual or potential tissue damage' (Millan, 1999). Pain is a complex and heterogeneous phenomenon, where, manifestations vary depending on the etiology, genes and environmental factors (von Hehn, Baron, & Woolf, 2012). Pain has a protective role wherein; it seeks to act as a warning signal to imminent danger or damage. Symptoms of pain usually disappear when the stimulus is removed (Woolf & Mannion, 1999). In contrast, pain can be pathological and can be thought of as a disease state when the nervous system itself is injured, and changes remain persistent and irreversible (von Hehn et al., 2012). Medical treatment and decreased productivity due to pain in the United States amount to a staggering $600 billion (Holmes, 2016) annually. The widespread prevalence along with the huge economic burden on the society underscores the need to develop new strategies to tackle this debilitating disease.

Acute and Chronic Pain

Pain can be classified as acute when the sensation is momentary or short-term (less than six months) and is reversed with the repair of the damaged tissue. Acute pain is often referred to as physiological pain since it often alarms us of potentially dangerous stimuli and seeks to protect by evoking a flight response (Millan, 1999). Acute pain is easily managed, and several over-the-counter medications help with its management. Whereas, pain is considered chronic when the

sensation of pain persists longer than six months. Chronic pain is deemed to be pathological as there is no biological benefit, and furthermore, it can be more complicated to tackle, as it can often arise in the absence of stimuli (Woolf & Mannion, 1999).

Neuropathic Pain

One of the more common forms of chronic pain is neuropathic pain, which is defined as pain that develops due to injury to the nerves. This sustained injury can lead to sensitization which results in the perception of non-noxious stimuli as painful (allodynia), or this could result in an exaggerated perception of pain in response to a nociceptive stimulus (hyperalgesia). In addition to this hypersensitivity, central and the peripheral nervous system undergo pathological changes that can be detected by employing electrophysiological or imaging techniques (Woolf, 2011). The pain pathway starts at the periphery, and a cascade of events leads to the transmission and perception of pain in the central nervous system (CNS). Afferent neurons within the sensory nervous system generate electrical signals in response to the pain stimuli and transduce it to the secondary neurons in the dorsal horn of the spinal cord. The signal gets modulated at this level before it is transmitted to the thalamus and finally, the tertiary neurons guide the signals to different structures in the cortex (Marchand, 2008) (Figure 1).

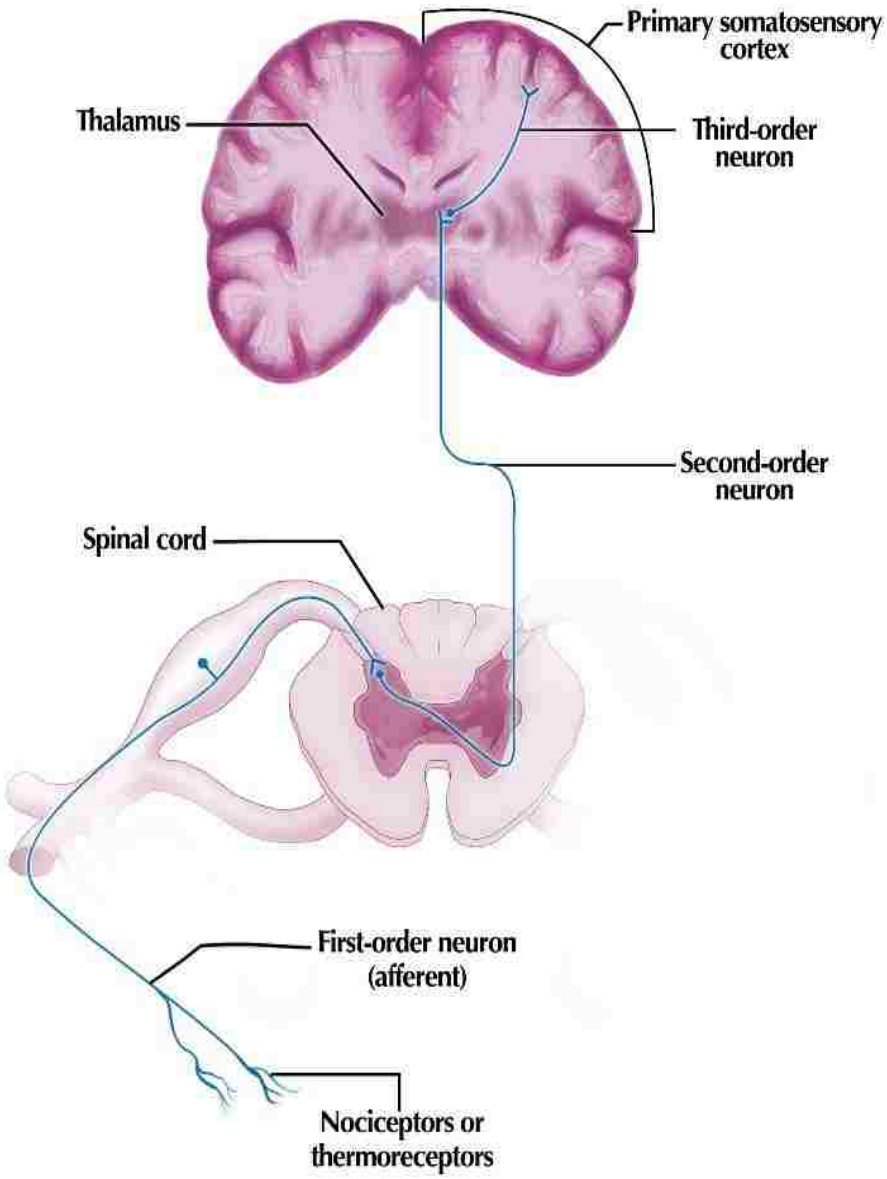

Image by author

Figure 1. Ascending pain pathway

Management of Pain

Several different classes of medication including opioids, anticonvulsants, anti-inflammatory drugs, tricyclic antidepressants or a combination of these is used to manage pain (Egan, 2005). While some treatments appear beneficial for some patients, they provide little to no benefit for others. These treatments often have many adverse side effects given that the molecular targets of these drugs are globally expressed. For example, opioids act by inhibiting the release of neurotransmitters from hyperpolarizing spinal cord neurons but, it can also, in a similar fashion affect other neurons within the CNS (Egan, 2005) causing side effects. The use of opioids can also result in short-term side effects such as dysphoria, nausea, constipation etc., whereas long-term use can lead to addiction and drug abuse. Novel targets and treatments to tackle pain are necessary and significant work needs to be focused in this direction. As pain is initiated in the sensory neurons within the peripheral nervous system, these neurons present themselves as ideal targets for the design of new analgesics. The sensory neurons within the dorsal root ganglia (DRG) are an integral part of this pain pathway, and a detailed understanding of molecular mechanisms underlying changes that occur within the DRG would prove beneficial.

The following section highlights the role of the sensory neurons namely, the neurons within the DRG and their role in the transmission of pain.

Anatomy and Physiology of Dorsal Root Ganglion

Information to the cerebral cortex is conveyed through one of the two somatosensory pathways: posterior column-medial lemniscal pathway (PCML) or the anterolateral system (ALS). ALS pathway transmits modalities of temperature, touch, and pain whereas PCML is involved in the

sensory modality of proprioception and vibration (Haines & Mihailoff, 2018). The sensory stimuli are converted to electrical impulses or action potentials and are transmitted upstream. Parallels exist between the two pathways including the transmission of signals through sensory neurons within the DRG.

The DRG is a structure where sensory neuronal cell bodies are clustered together in the dorsal root of the spinal nerve. DRG neurons are generated from the neural crest cells in three sequential waves during early embryonic development. Spatial and temporal signals from the spinal cord and the adjacent somites generate the different types of neurons seen within the DRG (Marmigere & Ernfors, 2007). These neurons can be classified based on cell size, axonal diameter, conduction velocity, molecular markers they express and by their sensory modality.

Subtypes of Neurons within the DRG

The small neurons typically have small diameter axons which can either be unmyelinated or thinly myelinated, while the larger neurons tend to have a larger diameter, myelinated axons (Lee, Chung, Chung, & Coggeshall, 1986). The larger myelinated Aα/Aβ fibers conduct velocities higher than 2.5m/s while, the smaller thinly myelinated Aδ and unmyelinated C fibers have conduction velocities lower than 2.5m/s (Harper & Lawson, 1985). Large neurons mostly receive non-noxious stimuli and are involved in proprioception (sense limb movement and position) or mechanoreception (receive mechanical stimuli such as touch, pressure, and motion) while the small Aδ and unmyelinated C fibers receive thermal and noxious stimuli and are involved in nociception (Marmigere & Ernfors, 2007). Each of these classes of neurons can also be classified based on the expression a unique set of molecular markers. For instance, capsaicin receptor,

TRPV1 which is known to be important in the transduction of noxious stimuli is uniquely expressed by the nociceptors (Immke & Gavva, 2006). Although this categorization is an over-simplistic generalization, and while there are many exceptions to this classification, interestingly, these neurons establish reproducible patterns of connectivity within the spinal cord (Figure 2) (Marmigere & Ernfors, 2007) For example, C fibers synapse with lamina I and outer lamina II neurons whereas, Aδ neurons synapse with neurons in lamina I and lamina V (Dubin & Patapoutian, 2010).

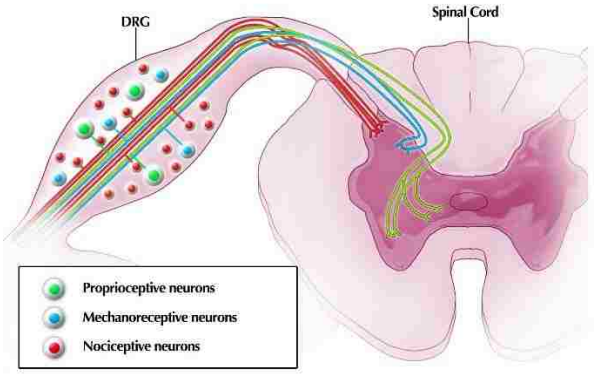

Image by author

Figure 2. Reproducible patterns of connectivity of the DRG neurons to the spinal cord.

Regardless of the subtype of the sensory neuron, these neurons are pseudounipolar in structure. The cell body of the neuron is attached to the bifurcating conducting axonal branches via a short stem axon. These neurons lack dendrites and therefore do not synapse with each other, and no synaptic processing occurs within the DRG. Yet, cross-talk between neurons within DRG commonly occurs in response to nerve injury or neuropathic pain. Recent evidence has alluded to

the fact that this cross-talk could be a result of the coupling of glia within the DRG (Cherkas et al., 2004; Huang, Cherkas, Rosenthal, & Hanani, 2005). The glial organization within the DRG is described in detail below.

Satellite Glial Cells

It is now well established that glial cells are integral to several aspects of neuronal function. Glial cells are involved in the development of the nervous system, formation of synaptic contacts, synaptic transmission and are known to regulate the microenvironment of the brain. (Goldman, 2003; M. Hanani, 2005; HANSSON & RÖNNBÄCK, 2003; Haydon, 2001). Importantly, glial cells are known to play a role in the development and maintenance of certain pathological conditions such as neuropathic pain (Aldskogius & Kozlova, 1998). Considering the importance of glial cells, it is quite surprising that not much is known about the glia within the DRG. Often, Schwann cells (SCs) are the only glial cell type considered when peripheral glia is described.

Structure of SGCs within the DRG

Valentin first described satellite glial cells in 1836, and Pannese in 1981 detailed the structure and organization of these cells in incredible detail. Satellite glial cells (SGCs) surrounds the cell body/soma of sensory neurons and form a tight sheath around them (M. Hanani, 2010; E. Pannese, 1956) (Figure 3) Together, the SGC and the neuron can be considered as a distinct morphological unit where the neurons are separated from each other by this SGC sheath. This unique organization of SGCs distinguishes them from Schwann cells (SCs), the other major peripheral glia which aligns along the axons. SGCs are laminar and do not bear processes. A small extracellular space lies in

between the neuronal soma, and the SGC (about 20nm) and neurons are known to extend microvilli into this space, it is suggested that these processes facilitate chemical exchanges between the SGC and neurons (E. Pannese, 1981; Ennio Pannese, 2002). SGCs offer metabolic support to the neurons they ensheathe, and there is a linear relationship in the number of SGC associated with the neuron to the size of the neuronal soma (Ledda, De Palo, & Pannese, 2004). Interestingly, the number of SGCs associating with the neuron considerably increases after injury (Vera Shinder et al., 1999).

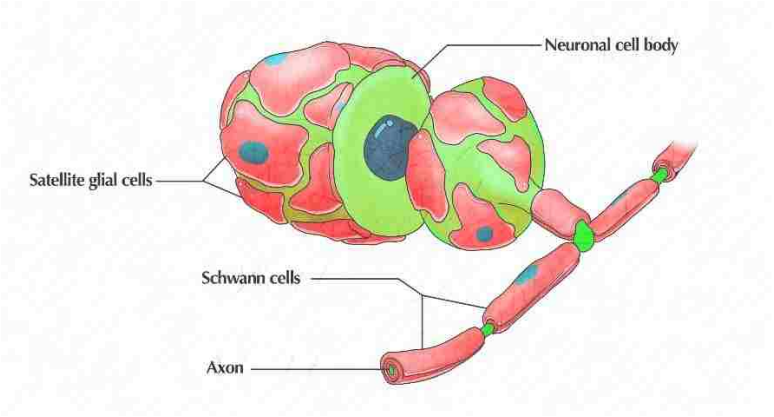

Image by author

Figure 3. Illustration of a single DRG neuron with SGCs enveloping the cell body and with myelinating SCs along the axon

Regulation of Neuronal Microenvironment

Although SGCs envelop the soma of the neurons, it does not form a complete structure like the blood-brain barrier seen in the CNS. Several studies have shown that tracers like La^{3+}, macromolecules, and neurotransmitters can penetrate through the SGC sheath into the neuronal space (Allen & Kiernan, 1994; Arvidson, 1979; M. Hanani, 2005; V. Shinder & Devor, 1994).

Another study examined the effect of heavy metal poisoning in DRGs and it was shown that the neurons were less labeled than the SGCs surrounding them (Kumamoto et al., 1986) suggesting that, even though SGCs do not form a complete barrier, they still exert control over the microenvironment by slowing the diffusion of larger molecules. SGCs exhibit gap junctions composed of mainly Cx43 and studies using tracer molecules have shown that SGCs around a neuron is functionally coupled (M. Hanani, Huang, Cherkas, Ledda, & Pannese, 2002b; E. Pannese, 1981) with bidirectional signaling between the neurons and the glia taking place via calcium waves (Suadicani et al., 2010). It is suggested that this coupling of SGCs may play a role in spatial buffering to control the microenvironment and that the unique arrangement of SGCs around the soma facilitates cross-excitation seen within the DRG neurons (V. Shinder & Devor, 1994).

SGCs express several transporters for neurotransmitters like glutamate and gamma-aminobutyric acid (GABA), and this facilitates the removal of these neurotransmitters from the neuronal extracellular space (Berger & Hediger, 2000). SGCs are also endowed with enzymes that catalyze the conversion and therefore, the removal of the released neurotransmitters. Glutamate released into the neuronal microenvironment is taken up by the glutamate transporters expressed on SGCs and glutamate is converted to glutamine by the activity of enzyme glutamine synthetase (GS). Glutamine is then recycled back to the neuron, and SGCs modulate neuronal activity in this manner. Because of the abundance of GS in SGCs, it has been used as a molecular marker to identify these cells (Miller, Richards, & Kriebel, 2002).

Role of SGCs in Pain

In addition to ensuring the normal function of neurons, SGCs also play an essential role in the dysfunction or disease state of these neurons. SGCs undergo many characteristic changes following injury. Similar to astrocytes in the CNS, SGCs upregulate the expression of the glial fibrillary acidic protein (GFAP) and become activated in response to neuronal injury (Nadeau, Wilson-Gerwing, & Verge, 2014). Although the significance of this upregulation is not apparent, the increase of GFAP is a well-documented phenotype of astrocytes in response to injury (Romao, Sousa Vde, Neto, & Gomes, 2008). SGCs phagocytose the injured and degenerated cells in their vicinity in a manner similar to SCs and microglia (Aldskogius & Arvidsson, 1978).

Under normal conditions, SGCs have a half-life of 600 days and are not highly proliferative cell types (Elson, Ribeiro, Perelson, Simmons, & Speck, 2004). But, in response to injury, SGCs proliferate rapidly and the SGC-neuron ratio changes as early as a day after injury (A. Humbertson, E. Zimmermann, & M. Leedy, 1969). It has been suggested that the SGC-neuron ratio becomes skewed to support the high metabolic needs of the neuron during injury. It is well established that long-term treatment with capsaicin leads to the loss of DRG neurons (Pini, Baranowski, & Lynn, 1990; J. Wood et al., 1988) and interestingly, Gallaher et al., showed that the neuronal numbers are restored 60 days post capsaicin administration. The presence of BrdU/Ki67 positive SGCs along with the expression of nestin (a neuronal progenitor marker) suggested that SGCs were the cell type that replaced the lost neurons (Z. R. Gallaher, Ryu, Larios, Sprunger, & Czaja, 2011). In support of this observation, it has also been shown that after axotomy, SGCs express isolectin IB4, a marker for nociceptive neurons (Li & Zhou, 2001). Together this suggests that SGCs are not

passive players in transmitting pain, but instead are actively involved in contributing to the neuronal changes that underlie neuropathic pain (Peter T. Ohara et al., 2009).

DRG neurons become hyperexcitable in response to injury, and this is identified as a decrease in firing threshold and a measurable increase in the spontaneous activity (M. Hanani, Huang, Cherkas, Ledda, & Pannese, 2002a; Xie, Strong, & Zhang, 2010). The underlying mechanism for this altered neuronal sensitization is still not known. In response to axotomy, increased coupling (around six-fold) between SGCs surrounding an individual neuron and SGCs surrounding different neurons was observed (M. Hanani et al., 2002a). This increase in coupling was due to an increase in the expression of gap junctions between SGC-SGC and between SGC-neuronal units. Although the functional significance of this coupling is not entirely clear, it has been suggested that changes in the number of gap junction lead to alterations in the neuronal microenvironment which could, in turn, reflect changes in the excitability of the neurons. Efforts in this direction could be beneficial in understanding the molecular basis for the sensitization of the DRG neurons.

Physiological Characteristics of SGCs

Patch clamp studies have shown that SGCs are non-excitable, and have a negative resting potential between -33mV to -78mV (Bowery, Brown, & Marsh, 1979). It was shown that SGCs surrounding GABA neurons were depolarized after a small delay period (Hosli, Andres, & Hosli, 1978) and further, it was shown that SGC depolarization occurred only in the presence of neurons. This indicated that SGCs were depolarized indirectly by the neuron suggesting a bidirectional communication that exists between the neuron and SGC.

Although the neuronal soma does not directly participate in the transmission of sensory information to the CNS, invasion of action potentials via the short stem axon can lead to biochemical changes within the soma (Amir & Devor, 2003; Dubin & Patapoutian, 2010) and how the peculiar arrangement of SGCs around the soma contribute to these changes that are observed in the neuronal soma warrants further research. It is also known that DRG soma expresses various receptors and neurotransmitters including capsaicin receptor TRPV1 (Immke & Gavva, 2006). The expression of these receptors on the soma is quite puzzling considering that the sensory information is received at the sensory terminals at the periphery. The expression of these receptors along with the fact that the soma is electrically active promotes the idea that the signals within the DRG may be crucial in uncovering the basis of pathological conditions like neuropathic pain.

Current Models

There are several *in vivo* and *in vitro* models developed to study pain, but most of these models are limited either because of the complexity or the lack thereof, reproducibility, subjective interpretation of behavioral readouts, lack of biological manifestations of pain, etc. The current knowledge in the field is limited partly due to the lack of accurate models.

One of the more commonly used models of peripheral pain is the chronic constriction injury (CCI) model. Here, the sciatic nerve of the mouse is ligated and which causes these mice to display a pain phenotype including allodynia and hyperalgesia (Attal, Jazat, Kayser, & Guilbaud, 1990). Partial sciatic nerve ligation leads to spontaneous pain which is characterized by excessive licking and paw guarding. Other non-surgical *in vivo* models include streptozocin-induced diabetic neuropathic pain model (Courteix, Eschalier, & Lavarenne, 1993) and latent varicella-zoster virus

infected models (Fleetwood-Walker et al., 1999). While the pathophysiological changes of pain are accurately reflected in these models, variability in administering tests, interpretation of the behavioral response, ethical concerns and the cost and time associated with these studies lessen the enthusiasm of their use.

Cell culture models of neuropathic pain have been developed, which include the use of dissociated primary embryonic DRG neurons, reprogrammed fibroblasts and cell lines (Brian J. Wainger et al., 2015; Yin, Baillie, & Vetter, 2016). These models offer a highly reproducible and cost-effective system. The neurons in culture respond to the noxious stimuli and therefore can be used to study pain (Barber & Vasko, 1996). But several of these *in vitro* models lack the complexity that is needed for the precise understanding of the mechanisms of pain. For example, the embryonic DRG neurons are known to differ phenotypically from the adult neurons with respect to their dependence on trophic factors like the nerve growth factor (Zhu & Oxford, 2011). To be able to make meaningful conclusions, these models need to efficiently recapitulate the diversity and physiology of neurons seen within the DRG. Moreover, most of the *in vitro* studies do not include glial cells, as these cultures are often treated with antimitotic agents to remove the contaminating glia to enable acquisition of electrophysiological readings (Newberry et al., 2016).

One of the significant challenges in investigating the direct contribution of SGCs towards neuronal activity lies in the fact that in culture, SGCs migrate away from the soma of the neurons as early as 24 hours (Vitali Belzer, Nathanael Shraer, & Menachem Hanani, 2010). SGCs can be studied in isolation from the neurons, and although electrophysiological readings cannot be acquired, useful information can be extracted from the cells in isolation. But, to date, there has been no description of the isolation of this cell type. Intact explant (organ) culture would be useful, as the

association of SGC and neurons can be preserved. Taking into account the limitations of the field, we have described a novel method of isolation of SGCs and have developed a three-dimensional explant model system where we can acquire electrical readings and, evaluate the contribution of SGCs to the electrical activity of neurons under neuropathic conditions.

CHAPTER TWO: SATELLITE GLIAL CELLS REPRESENT A POPULATION OF DEVELOPMENTALLY ARRESTED SCHWANN CELLS

Preface

This chapter was previously published in Glia, and is reprinted here through Copyright Clearance Center's RightsLink® service.

George D, Ahrens P, Lambert S. Satellite glial cells represent a population of developmentally arrested Schwann cells. Glia. 2018;00:1–11. https://doi.org/10.1002/glia.23320

Introduction

Gap in Knowledge

Although the involvement of SGCs in the generation and maintenance of pain has been widely accepted, much less is known about the mechanisms by which they influence the neuronal activity. Despite their clinical importance, not much is known about the origin and development of these cells. Development of new therapeutics and novel drugs depend on our ability to identify new targets. Hence, understanding their origins and the mechanisms that signal the development of SGCs are important.

The lineage of SGCs remains relatively uncharacterized. The lack of knowledge surrounding the development of SGCs within the trigeminal ganglia and DRG contrasts with what is known about the development of the other PNS glial cell type, Schwann cell (SC), which has been well

characterized in developing nerves such as the sciatic. The origin and development of SCs are briefly discussed below.

Schwann Cell Lineage

SCs are one of the most abundant glia in the peripheral nerves. SCs that associate with the larger diameter axons form myelin around them and increases the conduction velocity of those axons, whereas, SCs that associate with the smaller diameter axons bundles them tightly together to develop structures known as the Remak bundles.

Neural crest cells undergo three different developmental stages to differentiate into a mature myelinating or non-myelinating SC. Neural crest cells are often referred to as the fourth germ layer due to the large variety of cells that they generate. Gliogenesis of the neural crest cell occurs during embryonic development (embryonic day 14 in rats) to give rise to SC precursor cells.

SC precursors are transient and are dependent on axonal contact for survival. Removal of this axonal contact leads to apoptosis but, they can be rescued in culture by the addition of the axonal forms of neuregulin. These cells have extensive processes, have a fibroblast morphology and associate with many axons. In culture, they become flattened and exhibit cell-cell contacts (Jessen et al., 1994). SC precursors have been described as a multipotent cell type capable of becoming endoneurial fibroblasts and even neurons within the parasympathetic ganglia (Espinosa-Medina et al., 2014a; Joseph et al., 2004). Further, it was shown that SC precursors could be specified to generate melanocytes by the addition of basic fibroblast growth factor (Joseph et al., 2004).

Around embryonic day 15-17, SC precursors develop autocrine survival signals and differentiate into immature SCs. This differentiation can be recapitulated *in vitro* as well. Considerable changes

to the nerve also accompany these transition points such as the deposition of extracellular matrix, formation of connective tissue, etc. To match the axon and SC numbers, a delicate balance of proliferation and apoptosis of the immature SCs is seen during this stage. Axons are grouped into bundles with the immature SCs surrounding them.

The immature SCs then differentiate to either a mature myelinating or a mature non-myelinating SC during perinatal stages (reviewed in (Jessen & Mirsky, 1997; Mirsky et al., 2008)). SCs defasciculate the axons to establish a 1:1 ratio and myelination is initiated in the large diameter axons. The small diameter axons remain unmyelinated and are surrounded by non-myelinating SCs. Different signals specify the differentiation of the immature SC to the two different mature phenotypes.

The ensheathment of axons destined to be myelinated is initiated around birth, and the process of myelination continues after birth. SCs aligned along the length of the axon form a myelin sheath around them. The node of Ranvier that exists between each of these myelinating SCs is packed with voltage-gated sodium channels. The arrangement of myelin interspaced with the nodes of Ranvier facilitates the salutatory conduction of impulses. Myelin is composed mainly of lipids and about 20% of proteins. Proteins in myelin are important for the structure, compaction, and stability of the myelin sheath. Myelin basic protein (MBP) is one such protein involved in the compaction of myelin and is often used as a marker to identify myelin segments in culture (Martini, Mohajeri, Kasper, Giese, & Schachner, 1995).

Each of the stages in the development of the SC is well defined by the set of markers they express (Jessen & Mirsky, 1998). Markers like Sox 10, $P75^{NTR}$ are expressed through all stages of

development while certain antigens are expressed only during specific developmental stages and this allows us to distinguish the cells at each stage of development (Figure 4). For example, cadherin-19 (CDH19), is a unique marker that is expressed solely during the SC precursor stage (Takahashi & Osumi, 2005) and the expression of this antigen is downregulated as SC precursors transition into immature SCs.

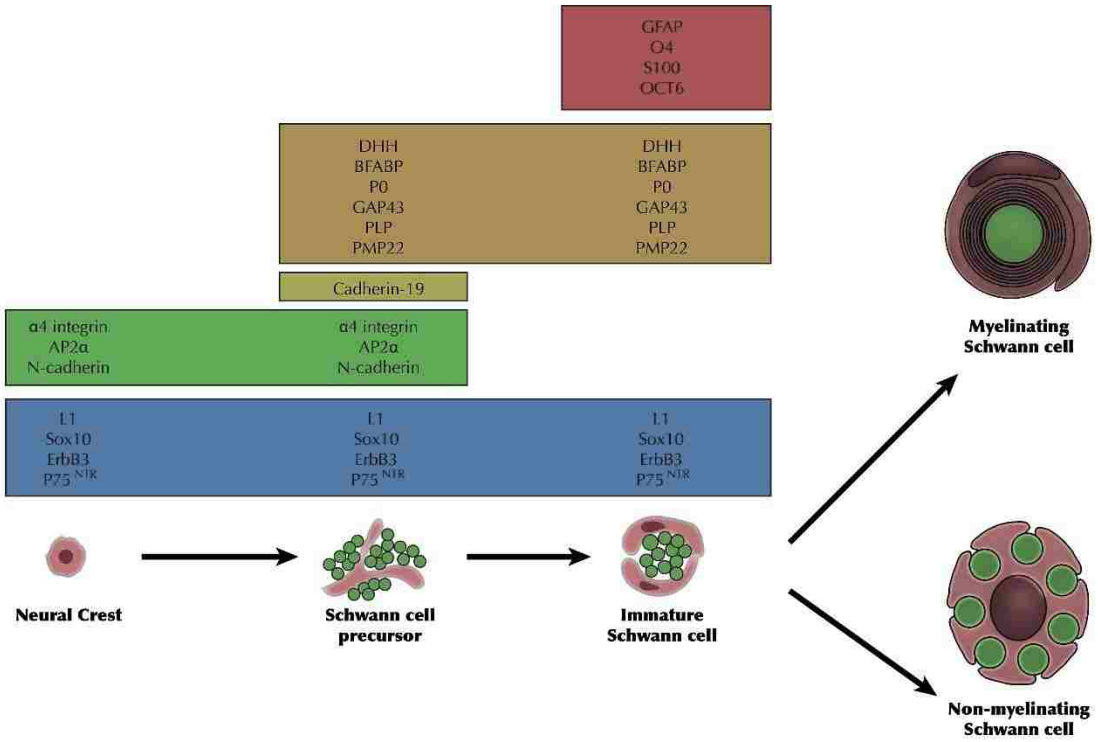

Image by author

Figure 4. Progression of the Schwann cell lineage

Origin and Development of SGCs

Neural crest cell gives rise to boundary cap cells around embryonic day 11 in rats. Studies have shown that the boundary cap cells migrate along the axons and populate the DRG. It has been thought that SGCs arise from boundary cap cells during the development of the small diameter nociceptive neurons (Maro et al., 2004) but, this topic has not been explored. Certain clues suggest that SGCs may be closely related to SCs. In Sox 10 mutants, both SGCs and SC precursors fail to develop, indicating the potential for a common lineage (Britsch et al., 2001). Moreover, when cultured independently of neurons, SGCs start to adopt the characteristic bipolar morphology associated with SCs (V. Belzer, N. Shraer, & M. Hanani, 2010; Poulsen, Larsen, Duroux, & Gazerani, 2014) and express several biomarkers (e.g., GFAP, S100 and L1) also observed in SCs. Whether SGCs and SCs have similar developmental stages and the signals that lead to their specification has not been investigated.

Plasticity of SGCs

SGCs have been proposed to be highly plastic, giving rise to a range of cells that includes oligodendrocytes (Fex Svenningsen, Colman, & Pedraza, 2004; M. Hanani et al., 2002b; Weider et al., 2015). SGCs have also been shown to undergo enhanced proliferation in response to nerve injury (A. Humbertson, Jr., E. Zimmermann, & M. Leedy, 1969). Their plastic nature and the fact that elevated levels of the Sox 10 transcription factor promote the conversion of SGCs into an oligodendrocyte type cell, suggest that SGCs may not represent a fully differentiated cell type (Weider et al., 2015), an idea supported by the expression of the transcription factor Sox 2, which

has been described as a stem cell marker, in the nuclei of SGCs (Koike, Wakabayashi, Mori, Hirahara, & Yamada, 2015).

In this study, we provide data to support the hypothesis that SGCs in the DRG represent a population of cells arrested in the SC lineage progression. We observed that SGCs did not associate with neuronal soma, until after birth, and SGCs expressed the SC precursor marker CDH19 along with other markers of the early SC lineage are then expressed by these cells through adulthood. Using a novel purification technique, we observed that purified cultures of SGCs are almost transcriptionally identical to adult SC cultures. Finally, we showed that coculturing SGCs with pure populations of embryonic DRG neurons allowed them to myelinate DRG axons in the same manner similar to the adult SCs. These observations raise new questions about the DRG microenvironment as a stem cell niche and the hierarchy of glial cell development in the PNS.

Materials and Methods

Reagents and Antibodies

All cell culture media and the supplements were purchased from Gibco and Invitrogen respectively. The culture media formulation for neurons and cocultures were previously described (Callizot, Combes, Steinschneider, & Poindron, 2011).

Culture media

NB media: Neurobasal with 2% B27, 1X GlutaMax, 1X penicillin-streptomycin (P/S) and 50ng/ml NGF (Harlan).

D10M media: DMEM with 10% heat-inactivated FBS (Hyclone), 2µM forskolin (Sigma), 20 µg/ml bovine pituitary extract (Biomedical technologies) and 1X P/S. D10M culture media was used for SCs and SGCs when cultured in the absence of neurons (Sparrow et al., 2012).

Antibodies

Primary antibodies against mouse TUBB3 (1:300), rabbit MBP (1:200), collagen (1: 200), and Ki67 (1:50) were purchased from Abcam. Rabbit GS (1:10,000) was purchased from Sigma. Rabbit, S100 (1:200) from purchased from Dako. Rabbit CDH19 (1:100) and mouse TRPV1 (1:50) were from Santa Cruz. The secondary antibodies goat, donkey-Alexa Fluor, and DAPI were purchased from Invitrogen. HRP-conjugated goat secondary antibodies were purchased from Jackson ImmunoResearch.

Animal Use

All animal protocols were approved by the University of Central Florida Institutional Animal Care and Use Committee (IACUC). Cervical DRGs were harvested from embryos at 15 days of gestation (E15), two days after birth (P2) or from 90 day old (P90) Sprague-Dawley rats (Charles River Laboratories).

Isolation of DRGs

Embryonic DRG

For embryonic dissection, a standard procedure was followed (Fex Svenningsen, Shan, Colman, & Pedraza, 2003; Pacifici & Peruzzi, 2012). Briefly, the pregnant rats were euthanized by CO_2 asphyxiation after which a secondary physical means was used ensure euthanization. The abdomen was sterilized with 70% isopropanol. The lower abdominal skin was cut to expose the muscles, and a transverse incision was made using a pair of sterile scissors to expose the uterus. The fetuses were removed using sterile curved forceps and placed into sterile Hibernate E media. The embryos were released aseptically from the amniotic sac and transferred to a 100mm dish with fresh Hibernate E media. Under a dissection microscope, the embryos were laid on the side, and the head was removed using microdissection scissors. The embryos were positioned dorsal side up, and nicks were made on either side of the spinal cord from the rostral to the caudal end. The vertebral column was then gently and carefully teased apart to release the spinal cord with the attached DRGs. The DRGs were isolated using fine dissecting forceps and placed directly on to a coated coverslip for organotypic cultures or into a 15mL conical tube for further processing.

P2 and P90 DRG

Previously published procedures were followed for the isolation of P90 DRG (Malin, Davis, & Molliver, 2007; Sleigh, Weir, & Schiavo, 2016) with minor modifications. 90-day old rats were euthanized as mentioned earlier and the skin was doused with 70% isopropanol and the head removed. The animal was then placed dorsal side up, and the skin was gently lifted using a curved

forceps and was cut to expose the muscles of the vertebral column. Using sterile forceps to lift the spinal column, cuts were made along either side of the column all the way to the sacral region ensuring the viscera and the internal organs were not punctured. The ribs were detached close to the spinal column on both sides, and a deep medial cut at the sacral region was made to release the spinal column. The spinal column was transferred to 70% isopropanol for a few seconds to wash off any contaminating hair and was quickly moved to a dish containing L15 media. Under aseptic conditions, the spinal column was transferred to a dissecting board with the ventral side up. The spinal column is secured using pins on the board, and a cut was made in the middle of the spinal column at the rostral end. The spinal cord was then removed using forceps to expose the cervical DRGs. The meninges were removed using fine dissecting forceps to reduce cellular contamination. DRGs can be seen with long white axon bundles projecting into the spinal column, and each DRG was carefully removed by tugging and lifting up the axon bundle close to the DRG in the column. The isolated DRGs were transferred to cold L15 media in a 60mm dish. Under a dissecting scope, the axon bundles were then carefully trimmed to minimize SC contamination and myelin debris. The same procedure was adapted for DRG isolation from P2 rat pups.

Preparation of Dissociated Embryonic DRG Neurons

DRGs were isolated from E15 embryos as stated above and were collected in a centrifuge tube containing L15 media. The tube was centrifuged at 1500rpm for 5 minutes at 4°C to remove the L15 media. The cells were incubated with 0.25% trypsin (Life Technologies) for 20-30 minutes. At the end of the incubation, the suspension was homogenized by pipetting. The activity of trypsin was inhibited by the addition of 10% FBS. Trypsin solution was removed by discarding the

supernatant after centrifuging (Fex Svenningsen et al., 2003; Hall, 2006). The pellet was resuspended in NB media and was plated on acid-washed coverslips coated with 0.01% poly-L-ornithine and 50µg/ml laminin. 50% media was exchanged every 2-3 days.

Isolation of SGCs and Preparation of Dissociated Adult DRG Neurons

P90 DRGs were isolated as described and special care was taken to ensure that the axon bundles attached to the DRGs were trimmed and the epineurium covering the DRG was removed. DRGs were transferred to a 15mL tube containing L15 media and centrifuged at 1500 rpm for 5 minutes at 4°C. The supernatant was discarded and the pelleted DRGs was incubated at 37°C for about an hour with 5mg/mL type 2 collagenase (Worthington). The suspension was agitated by vortexing every 15 minutes. At the end of the incubation, the DRGs were further homogenized by tituration using a fire-polished glass pipette rinsed with FBS. The cell suspension was spun at 1500 rpm at 4°C to remove the enzyme. The pellet was resuspended in NB media and extensively titurated to ensure complete dissociation. 10% and 5% BSA (Amresco) solutions were freshly prepared in neurobasal media and the dense 10% BSA solution was first transferred to a 15mL tube and equal volume of 5% BSA solution was layered on top. The homogenized cell suspension was then carefully layered on top of the BSA cushion and was centrifuged at 115g for 4 minutes at a low brake. The myelin debris and the lighter non-neuronal cells settled at the interface between the 10 and 5% BSA whereas, the heavier neurons enveloped with SGCs were pelleted down. The supernatant was discarded and the BSA cushion separation was repeated to remove any remaining contaminating cells and debris. The pellet which contains neurons with tightly adhered SGCs were referred to as fraction 1. To separate SGCs from the neurons, fraction 1 was treated with 0.25%

trypsin at 37°C for 45 minutes. After incubation, the activity of trypsin was inhibited by the addition of 10% FBS and the cell suspension was centrifuged and the supernatant was discarded. The pellet was resuspended to obtain a homogenous solution and was layered on top of the BSA cushion, and the separation was performed as mentioned previously. The heavy neurons settle at the bottom (fraction 2), and this time, SGCs that were released from the neurons were captured at the interface of the cushion. This enriched population of SGCs is referred to as fraction 3. SGCs were carefully aspirated from the BSA cushion interface to a fresh tube containing NB media. BSA was then removed by centrifugation at 1500rpm. The cells from each fraction were plated on 0.01% poly-L-ornithine (Sigma) and 50µg/ml laminin (Invitrogen). 50% media exchanges were made 2-3 days. Pictorial representation of the isolation process is shown in Figure 5.

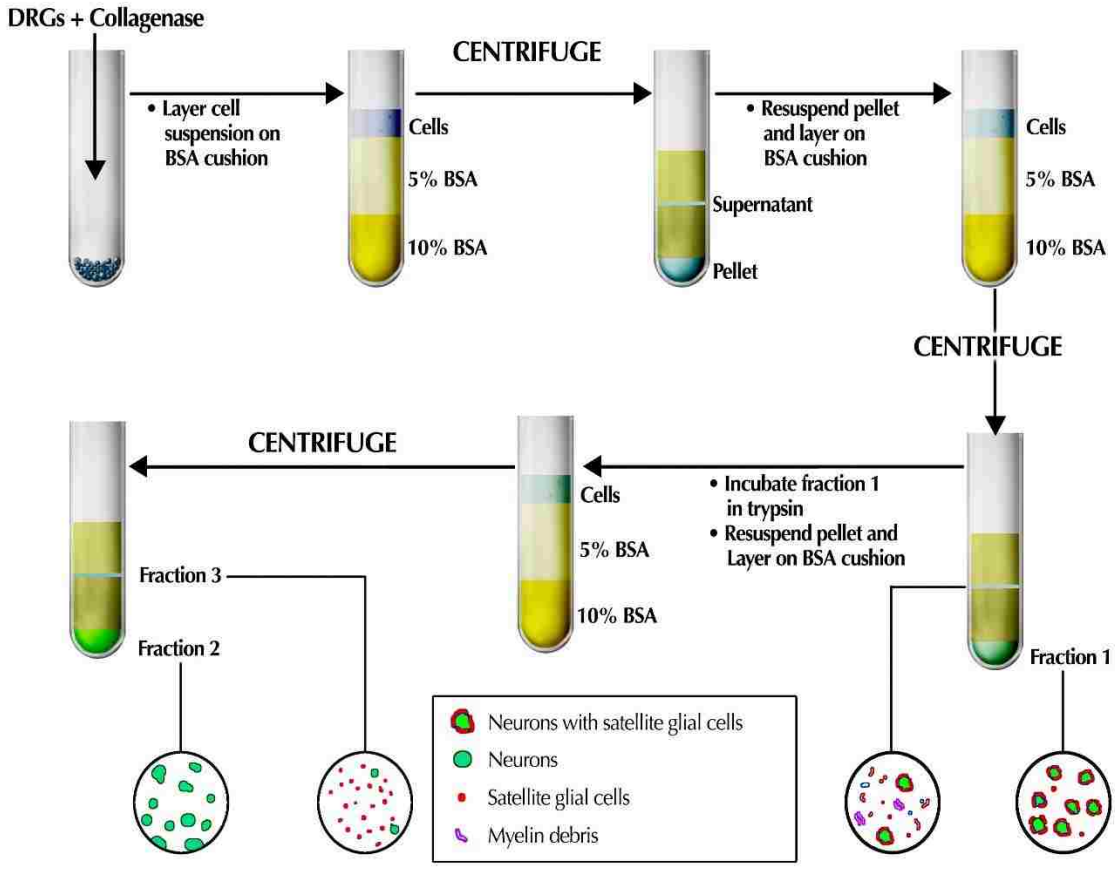

Image by author

Figure 5: BSA cushion separation for the isolation of SGCs

Generation of Adult SCs

SCs were isolated from P90 rat sciatic nerve. The animal was placed dorsal side up, and the legs were splayed and pinned down. The skin was disinfected with 70% isopropanol. The skin along the posterior face of the thigh was retracted and using sterile forceps and scissors, a superficial incision was made, and the muscles of the posterior thigh were split to expose the sciatic nerve.

Using curved forceps, the sciatic nerve was gently lifted to release it from the muscles. The sciatic nerve was released by making two cuts, one at the proximal and the other at the distal end (Bala, Tan, Ling, & Cheah, 2014; Savastano et al., 2014). The harvested sciatic nerve was transferred to a dish containing L15 media, and the outer epineurium was removed using sterile forceps. SCs were generated as described previously by Morrissey *et al*. (Morrissey, Kleitman, & Bunge, 1991) with modifications. Briefly, the sciatic nerve was trimmed into 1mm long segments and was transferred to uncoated 24 well culture plates. A successive series of plating was done to facilitate migration of fibroblasts from the segments and their attachment to the culture plate, as these cells are the major contaminants in the preparation of SCs. Fibroblast can be easily distinguished from SCs based on their morphology as they appear as large flat irregular cells whereas SCs appear as phase bright, bipolar spindle-shaped cells. Once a confluent layer of fibroblast was observed, the segments were transferred to new uncoated wells. This process of cell migration and re-plating was repeated about 3-7 times until the migrating cells appeared to resemble an SC morphology. The segments were then incubated in a solution of 0.05% stemzyme (Worthington Biochemical Corp, 25mM HEPES (Sigma) supplemented with 15% FBS in DMEM at 37°C for about 16-18 hours. After the incubation period, the segments were homogenized by tituration with a fire-polished pipette. The cell suspension was centrifuged at 235g for 5 minutes. The pellet which contains SCs is also abundant in myelin debris. To remove the myelin debris, laminin selection was performed (Pannunzio et al., 2005). Briefly, the cell pellet is resuspended in D10M media and the cells were plated on coverslips coated with 50µg/ml Poly-L-Lysine (Sigma) and 10µg/ml laminin for about 10 minutes. After the initial seeding, media from the coverslip containing cells (well 1) was aspirated and re-plated on a newly coated coverslip (well 2) and fresh media was

added to well 1. Myelin debris settles on to the coated coverslips and so, at each successive re-plating, less debris were observed. Laminin selection was repeated three to four times to effectively remove the myelin debris.

Coculture of Neuron/SC and Neuron/SGCs

Dissociated E15 DRG neurons were used for coculture experiments. To remove the endogenous cells from the dissociated neurons, the culture was treated with one three-day pulse of 10µM FUdR (Wood, 1976) one day after seeding. A full media change was made after the treatment, to remove any residual FUdR and half changes of media were made every two days. Seven days after the removal of FUdR (12DIV), pure neurons were seeded with either SGCs or SCs at a density of 100,000 cells/coverslip. SCs were grown in media containing FBS and a complete withdrawal of FBS from the growth media leads to apoptosis. Therefore, to prevent apoptosis, SCs were weaned off FBS containing media by decreasing the concentration of FBS over a week's time. At 19DIV, the cocultures were switched to myelin permissive media. To induce myelination, 50µg/ml ascorbic acid is added fresh to the media. Cultures were maintained for another 21 days in myelin permissive media after which the cultures were fixed for analysis (40DIV). Myelin segments were quantified using Volocity® 6.3 software.

Endogenous Myelination of Embryonic DRGs and Adult DRGs

To induce endogenous myelination of E15 DRG, the dissociated DRGs were prepared as described in the previous section and at 7DIV, 50µg/ml of ascorbic acid was added. Cells were maintained in myelin permissive media for 14 days (21DIV) (Callizot et al., 2011).

Adult DRGs were maintained either as an organotypic explant culture or a dissociated culture. For explant cultures, to facilitate attachment, the media was kept low. Fraction 1 from the BSA cushion separation was used for endogenous myelination of adult neurons. Both explant and dissociated cultures were allowed to grow for 14 days in NB media before being switched to myelin permissive media for another 21 days (35DIV).

Immunohistochemistry and Immunocytochemistry

DRGs were fixed in 4% paraformaldehyde (PFA, Electron Microscopy Sciences) for 30 minutes on ice, rinsed and transferred to 30% sucrose (Sigma) with 0.02% sodium azide (Fisher Scientific) solution overnight at 4°C. Tissues were embedded in OCT (Sakura) compound in plastic molds, frozen on dry ice and stored at -80°C. Using a cryostat, 10µm sections were made and collected on positively charged microscopic slides (Medline Industries).

For cells, the media was removed and the cells were fixed in 4% PFA for 10 minutes on ice. After this step, the procedure was the same for both immunohistochemistry and immunocytochemistry. The samples were permeabilized with 0.3% Triton X-100 in 4% PFA for 10 minutes. The samples were then washed with PBS and 10% normal goat serum was used as an agent to block non-specific epitopes. Samples, where myelin was induced or expected, were incubated in 10% goat serum with 0.1% Triton X-100 to facilitate penetration of the antibody. After 30 minutes of incubation with the block solution, primary antibodies prepared in block solution were added to the samples for overnight incubation at 4°C. After removing the primary antibodies, the samples were rinsed with PBS and secondary antibodies were added and incubated for 45 minutes at room temperature.

After washing out the secondary antibodies, the samples were mounted using fluoro-gel (Electron Microscopy Sciences).

Image Acquisition and Analysis

All fluorescent images were acquired with Zeiss LSM710 confocal microscope and ZEN 2.1 software. Antibody concentrations were optimized and a no primary control and negative controls were used to confirm the specificity of the antibodies. Image acquisition was also optimized and fluorescence was recorded using 488nm and 568nm excitation lasers on separate channels. Each image shown for comparison is acquired using the same optimized settings.

Western Blot Analysis

E15, P2 and P90 DRGs were homogenized in cold RIPA buffer (25mM Tris-HCl (pH 7.4), 1% NP-40, 150mM NaCl, 1% sodium deoxycholate, 0.2% SDS and 1X protease inhibitor cocktail) using a tissue grinder. The homogenate was collected into a microfuge tube and was centrifuged at 14,000g for 15 minutes at 4°C. The supernatant was carefully transferred to a chilled microfuge tube. The proteins were prepared for quantification using DC protein assay (Biorad Laboratories) and were read using a microplate reader at an absorbance of 750nm. The protein samples were prepared for SDS-PAGE by dissolving the proteins in laemmli buffer (300mM Tris-HCl (pH 6.8), 10% SDS, 50% glycerol and 0.05% bromophenol blue) and DTT at 95°C for 5 minutes. Equal amounts of proteins (20µg) were loaded onto the 10% mini-protean TGX pre-cast gel (Biorad Laboratories) and were samples run at 40V for 30 minutes and which was then increased to 100V until the samples reached the bottom of the gel. The samples were transferred to PVDF Immobilon

membranes overnight at 10V. Non-specific protein binding sites on the membrane were blocked using 5% milk for 1 hour at room temperature before the membrane is incubated overnight with primary antibodies. HRP-conjugated secondary antibodies and SuperSignal West Pico (Pierce Biotechnology) chemiluminescent substrate were used for the detection of signals. ImageJ was used to measure the signal intensity and the signals obtained were normalized to an internal GAPDH control. Statistical analysis was performed using one-way ANOVA followed by Bonferroni's post hoc test (n = 2 for all experiments).

Transcriptome Analysis

SGC passage 1 cells obtained by performing the BSA cushion separation, along with early passages of adult SCs were plated on 60mm dishes coated with poly-L-Lysine. Both cell types were maintained in D10M media for 7 days till they were about 90% confluent. RNAeasy mini kit (Qiagen) was used to isolate RNA from both cell types. Manufacturer's instructions were followed. The concentration and purity of RNA were measured using 2100 Bioanalyzer (Agilent Technologies). Affymetrix Rat Gene ST 2.0 was used for the transcriptome analysis and only main category probe-sets were used (29,489) (Affymetrix, Santa Clara, CA). Transcripts that are $\log_2$ fold change ≥ 2, $p \leq 0.05$ and FDR ≥ 0.05 were identified as differentially expressed transcripts.

Results

SGCs Develop Postnatally

Previous studies have utilized both embryonic and adult DRGs as potential sources of SGCs. Figure 6 shows dissociated embryonic (E15) and adult (P90) DRGs at 1DIV. The DRGs are stained with antibodies to β-3 tubulin (TUBB3) to recognize neurons and glutamine synthase (GS) for SGCs. There were several non-neuronal cells in the E15 culture (indicated by arrows) but they neither enveloped the neuronal soma nor expressed GS, the unique marker for SGCs (Figure 6A). In addition to clear increases in neuronal volume (Lawson, Caddy, & Biscoe, 1974), SGCs ensheathing the cell bodies of DRG neurons (indicated by asterisks) were observed only in the adult cultures (Figure 6B), suggesting that SGCs might arise later in the development of the PNS. To investigate this idea more closely we examined cervical DRGs from a series of developmental time points for the presence of GS-positive cells ensheathing neuronal cell bodies. As can be seen (Figure 6C-E), GS expressing cells appear predominantly in the postnatal period and can be seen surrounding neurons. Analysis by western blot showed a significant increase in the expression of GS in the postnatal DRGs (Figures. 6F-G). This window follows the disappearance of proliferating cells from the developing ganglia as determined by Ki67 staining of the nucleus. Most of the non-neuronal cells of E15 DRG were Ki67 positive (Figure 6H) as shown previously by Lawson et al., (Lawson et al., 1974) and these proliferative cells are absent in P2 and P90 DRGs (Figure 6I-J).

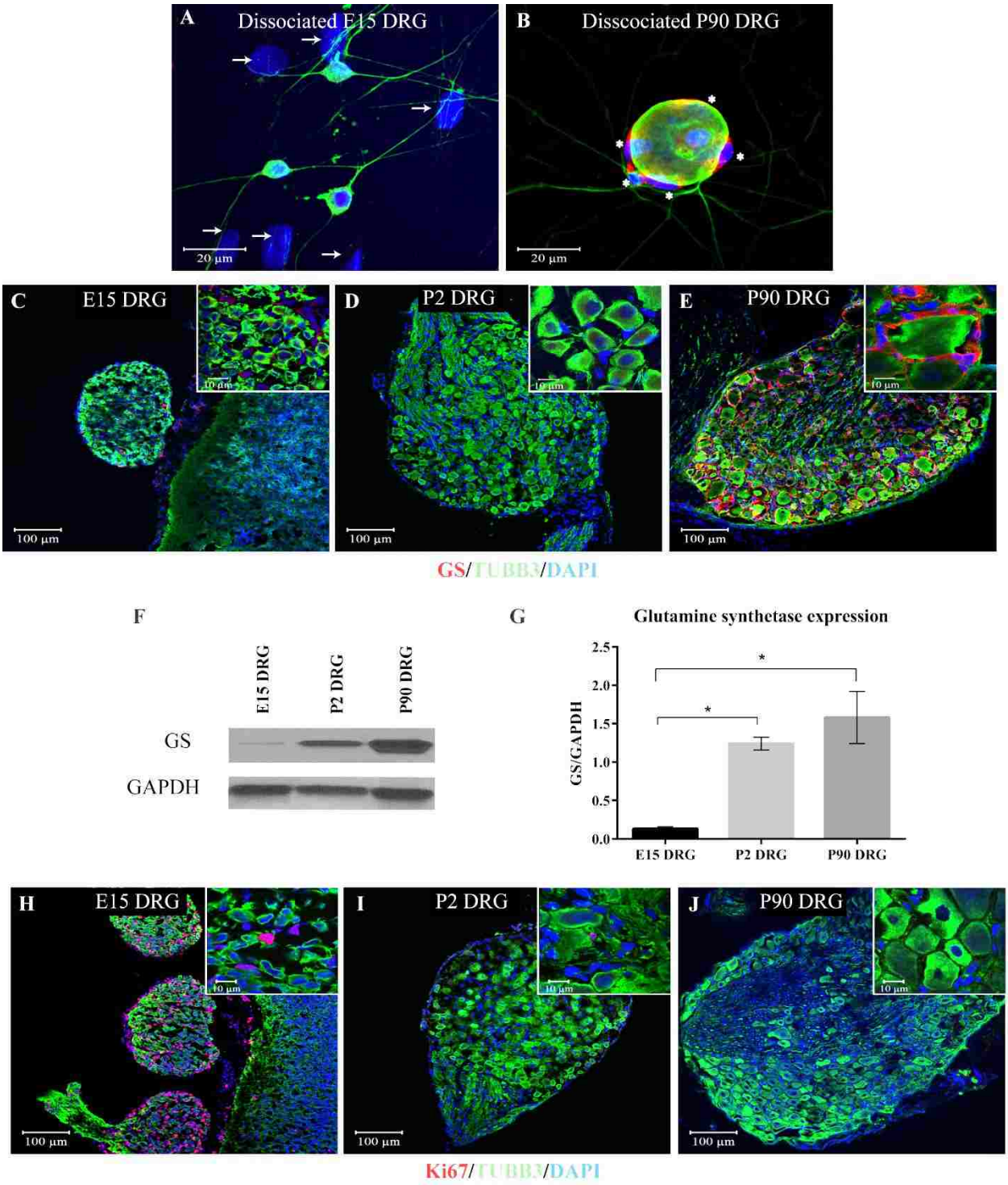

Figure 6. Postnatal development of SGCs

(**A**) Dissociated embryonic (E15) and (**B**) dissociated adult (P90) DRGs at one day in culture showed the presence of several SGCs around the adult neuron (indicated by asterisks) while no SGCs are seen enveloping the embryonic neuron. Arrows point to non-neuronal cells. (**C-E**) 10µm sections of E15, P2 and P90 cervical DRGs. (**A-E**) Cultures were immunostained for GS, TUBB3 and DAPI to identify SGCs, neurons and nuclei respectively. (**F**) Western blot showing GS expression at the different developmental stages and (**G**) the quantification of GS expression normalized with GAPDH expression (n = 2) showed a significant increase in GS expression in the postnatal developmental stages. Data are presented as mean ($\bar{x}$) ± SEM. *$p < 0.05$. (**H-J**) 10µm sections of cervical DRGs identifying proliferative cells by Ki67 staining in E15, P2 and P90 female rats.

We also observed that we could recapitulate the time course of SGC development *in vitro*. Dissociated E15 DRG cultures were monitored over time for the appearance of GS-positive SGCs, ensheathing the neuronal cell bodies (Figure 7A-C). When we maintained dissociated E15 DRGs for about 5 days, non-neuronal cells started to associate with the neuronal soma (Figure 7A). By 12DIV, the number of cells enveloping the neurons increased (Figure 7B) and GS positive cells were clearly visible by 18DIV (Figure 7C), correlating with our observations *in vivo*. Interestingly, dissociated E15 DRG cultures have been commonly utilized as a model for PNS myelination (Callizot et al., 2011) where SCs were observed throughout the culture that could be stimulated to form myelin sheaths (identified by myelin basic protein (MBP) upon the addition of ascorbate (Figure 7D-E). Here, we also see SGCs around the neuronal soma (indicated by asterisks). The

generation of both SGCs and SCs from E15 DRG support the idea of a common lineage for SC and SGCs in the developing ganglia.

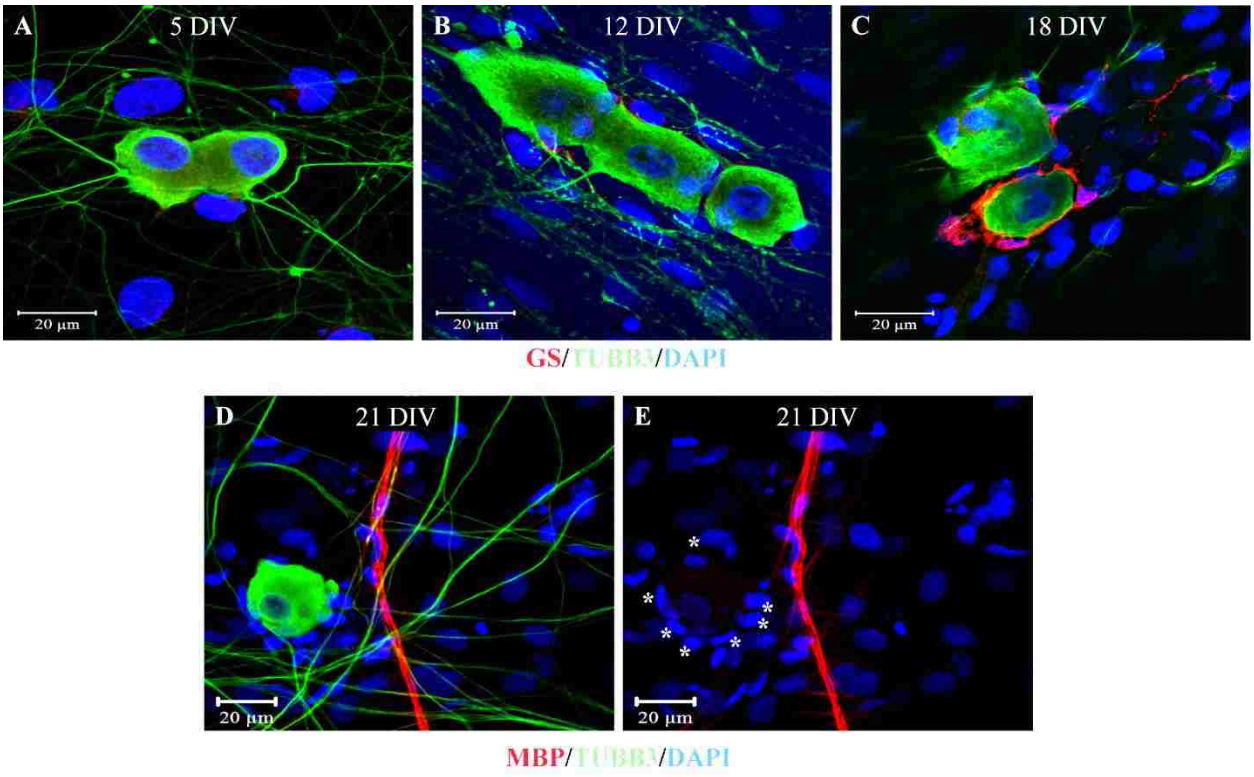

Figure 7. Non-neuronal cells within the embryonic DRG are glial precursors

Dissociated embryonic (E15) at (**A**) 5DIV (**B**) 12DIV and (**C**) 18DIV showed an increase in the number of glial cells around the neuron and expression of GS only at later time point. (**D-E**) Dissociated embryonic culture grown in myelinating conditions (21DIV) show formation of myelinating SC which is identified by MBP and the cells associating with the neuronal cell body which is indicated by the asterisks. Scale bar represents 20µm.

SGCs Exhibit Characteristics of Early SCs

To further examine lineage commonalities between SCs and SGCs, we stained cryosections of cervical DRGs with antibodies to markers associated with the SC lineage (Jessen & Mirsky, 2005; Liu et al., 2015). As shown in Figure 8A-E, we observed that adult SGCs expressed CDH19, previously described as a unique marker for SC precursors (Takahashi & Osumi, 2005). Expression of this marker paralleled the development of SGCs observed in Figure 6. We also utilized dissociated adult DRGs at 1DIV and noted the expression of GAP43 and BFABP (Figure 8F), which have also been associated with the SC precursor stage of development (Britsch et al., 2001; Curtis et al., 1992).

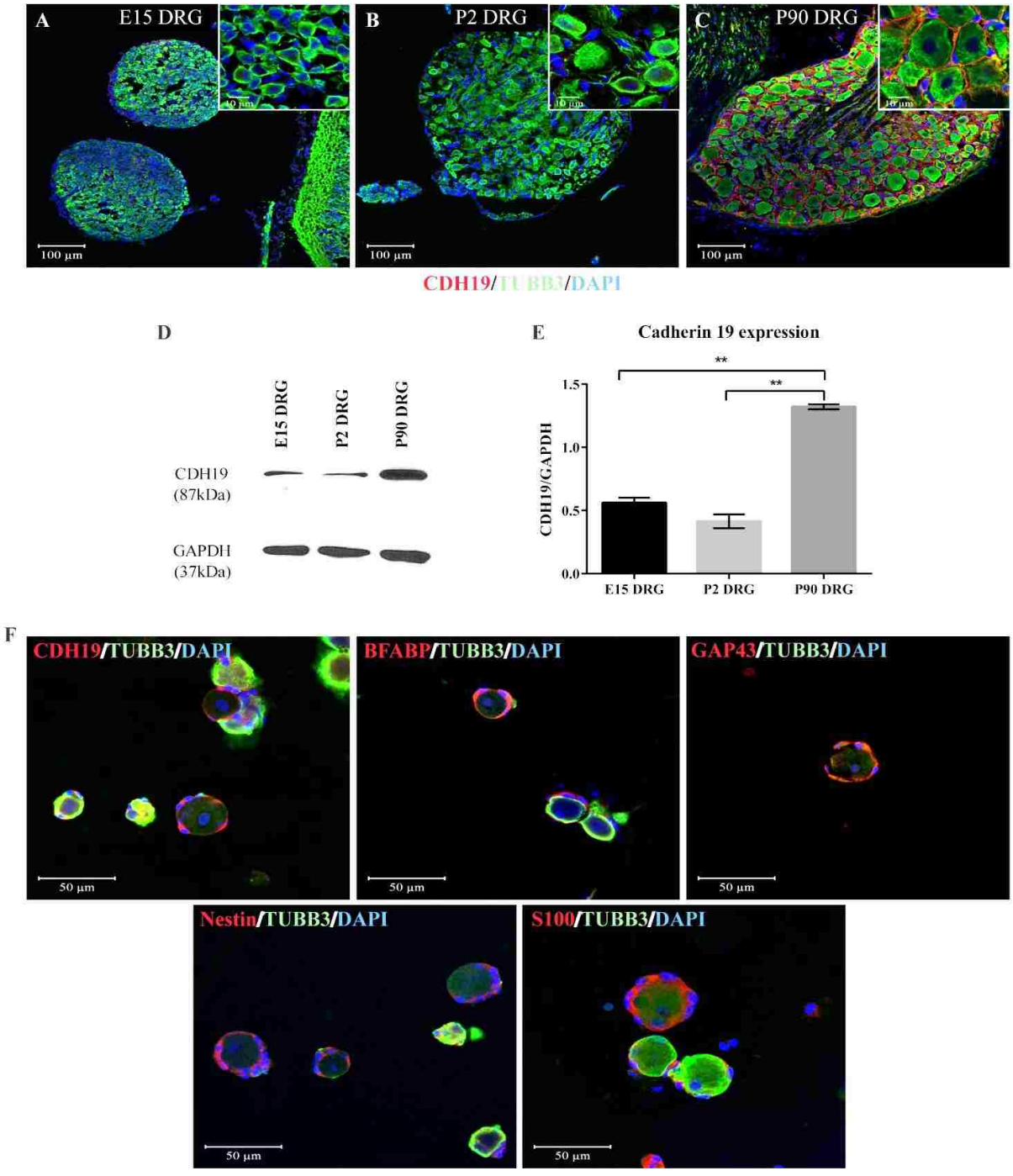

Figure 8. SGCs express CDH19

(**A-C**) 10µm sections of E15, P2 and P90 cervical DRGs stained for CDH19, TUBB3 and DAPI.

(**D**) Western blot showing CDH19 expression at the different developmental stages (**E**) the

quantification of CDH19 expression normalized with GAPDH expression (n=2) showed a significant increase in CDH19 expression in mature SGCs. Data are presented as $\bar{x}$ ± SEM. $^{**}p < 0.01$. (**F**) Dissociated P90 SGCs at 24 hours after plating stained for CDH19, BFABP, GAP43, Nestin and S100.

We set out to purify SGCs from adult rat cervical DRGs and developed a method utilizing BSA cushions. Briefly, we harvested the adult DRGs, trimmed the nerve roots and dissociated the ganglia in collagenase. Figure 9A shows the dissociated DRG culture with the several GS negative cells (indicated by arrows). Once a uniform suspension was obtained, the solution was separated twice on a BSA cushion. The myelin debris and SCs were effectively removed at the end of this separation, leaving neurons with closely adhered SGCs (fraction 1; Figure 9B). This cell suspension was further treated with trypsin solution to further dissociate SGCs from the neurons. BSA cushion separation was performed again to obtain an enriched population of SGCs (fraction 3; Figure 9D) leaving the pellet containing neurons (fraction 2; Figure 9C). SGC population was identified by the expression of GS (we have observed that although the smaller neurons have SGCs ensheathing the cell body, these SGCs do not express GS (Figure 10)) and the neurons were identified by TUBB3 staining. The other non-neuronal cells were identified by DAPI and the absence of both TUBB3 and GS. SGCs were released from the neurons following trypsin treatment (Figure 9F) and as seen in Figures 9D and E, this protocol generated SGCs of greater than 90% purity. When initially cultured, these cells exhibited a flattened fibroblastic morphology (Figure 11A and B). However, after a single passage, the cells appear as bipolar spindles, similar to the shape of a SC (Figure 11C). We see significant differences in cell surface area between passage 0

and passage 1 at 7 days (Figure 11D). Glial marker S100 was used to identify these cells and it is important to note that this morphological change occurred in the absence of axons. Previous studies have also reported that SGCs appear to take on a SC morphology in prolonged culture (V. Belzer et al., 2010; Poulsen et al., 2014). We isolated mRNA and performed an analysis of the transcriptome of passage 1 SGCs (Figure 12A) grown in culture for 7DIV and compared it with the transcriptome of purified passage 5 adult SCs (Figure 12B). As shown in Figure 12C and D, there was a high degree of correlation between the two transcriptomes with less than a 0.2% difference in transcripts analyzed. The expression levels of only 59 transcripts out of the 28,407 analyzed were observed to be significantly different (Figure 12D). The corresponding gene description and the fold change in expression levels between the two cell types are shown in table 1 and table 2.

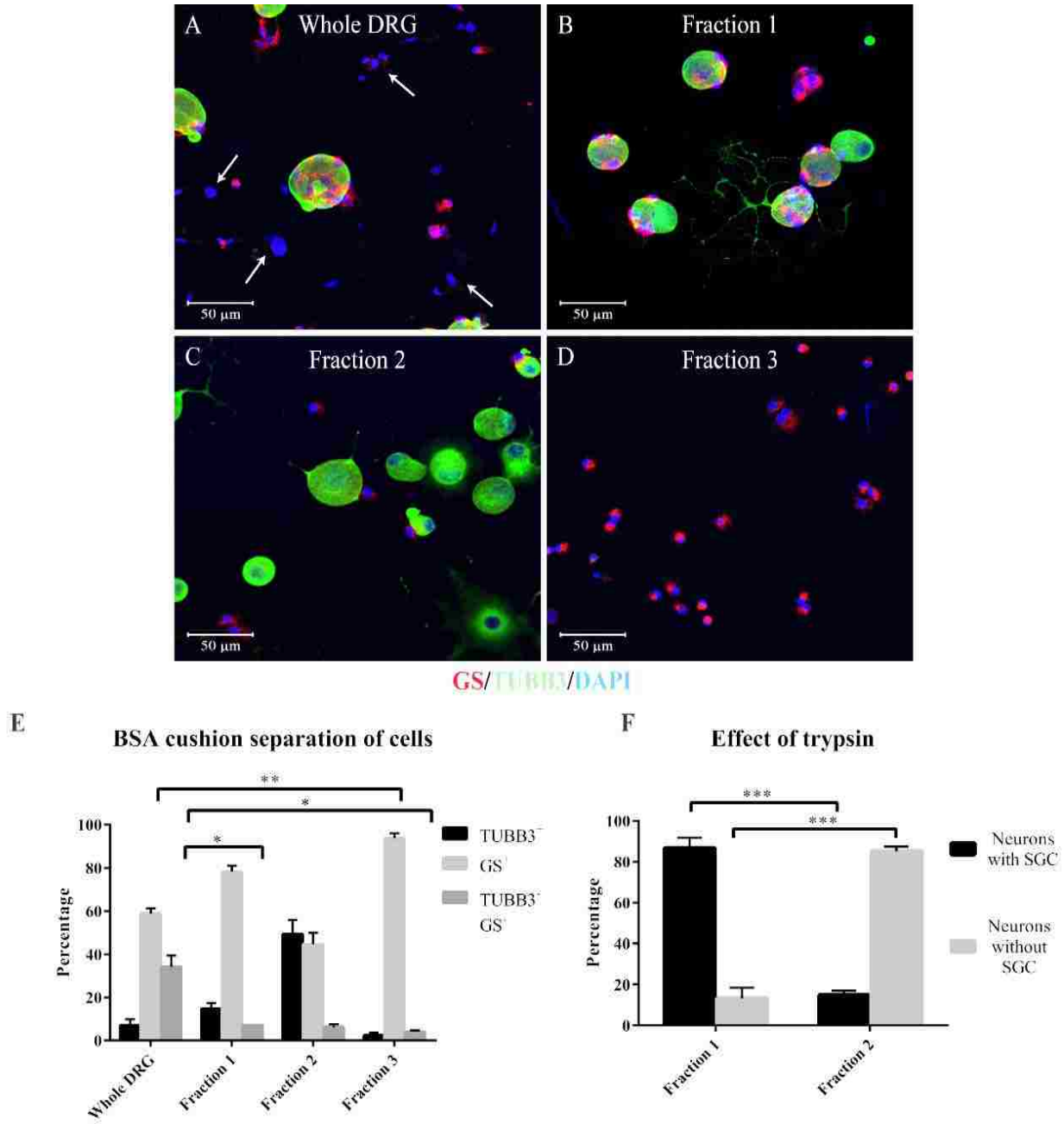

Figure 9. Isolation of SGCs

(**A**) P90 DRGs treated with collagenase and plated prior to BSA separation. Arrows identify glial cells that are GS negative. (**B**) The pellet after separation on BSA cushion. (**C**) Pellet and (**D**) supernatant after further treatment with trypsin followed by separation on BSA cushion. SGCs are

identified by GS, neurons by TUBB3 and other glial cells are identified by the absence of both markers. (**E**) Percentage of different cell types in whole dissociated ganglia and in each of the fractions (n = 3). (**F**) Effect of trypsin on SGC separation from the neurons. Data are presented as $\bar{x}$ ± SEM, ***p* < 0.05.

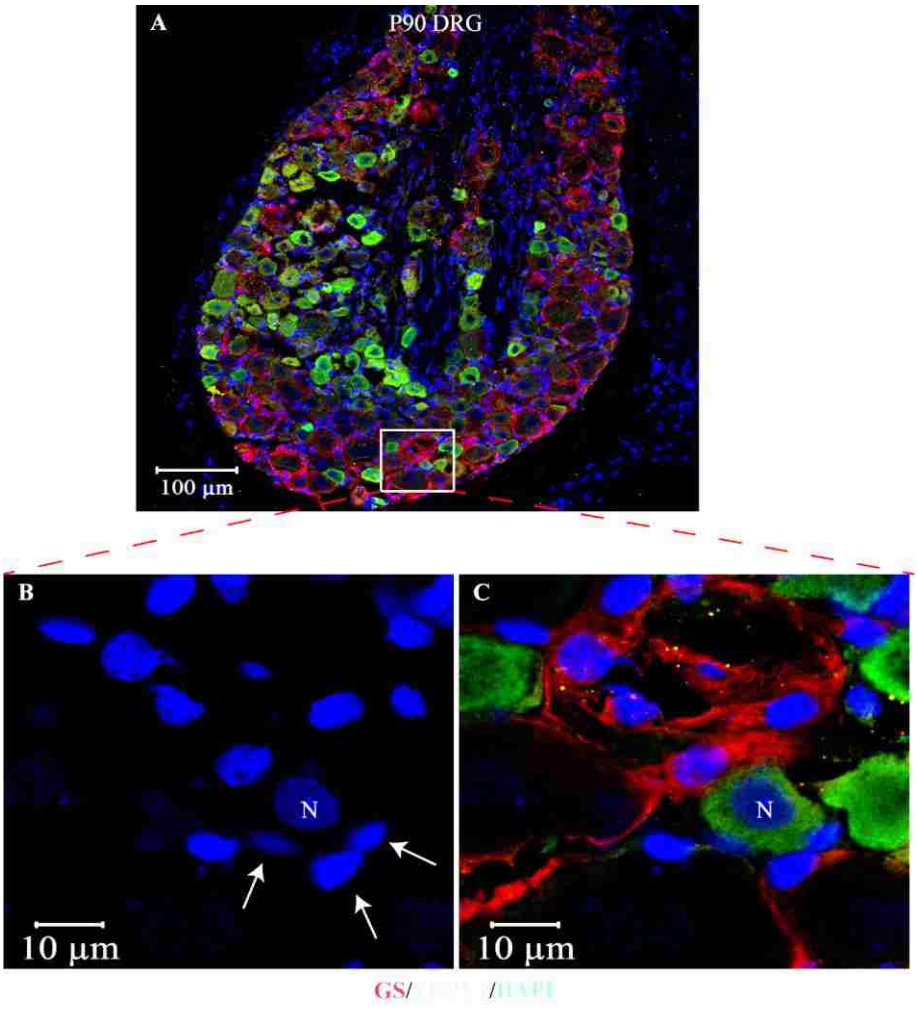

Figure 10. TRPV1 positive neurons do not express GS

(**A**) Immunohistochemistry of P90 DRG shows SGCs around larger neurons expressing GS whereas the smaller TRPV1 positive neurons do not have GS positive SGCs. (**B-C**) Inset is a magnified image of the section. (**B**) Arrows point to DAPI showing the presence of SGCs surrounding the neuron (N) (**C**) Neuron (N) is TRPV1 positive and lacks GS positive glia.

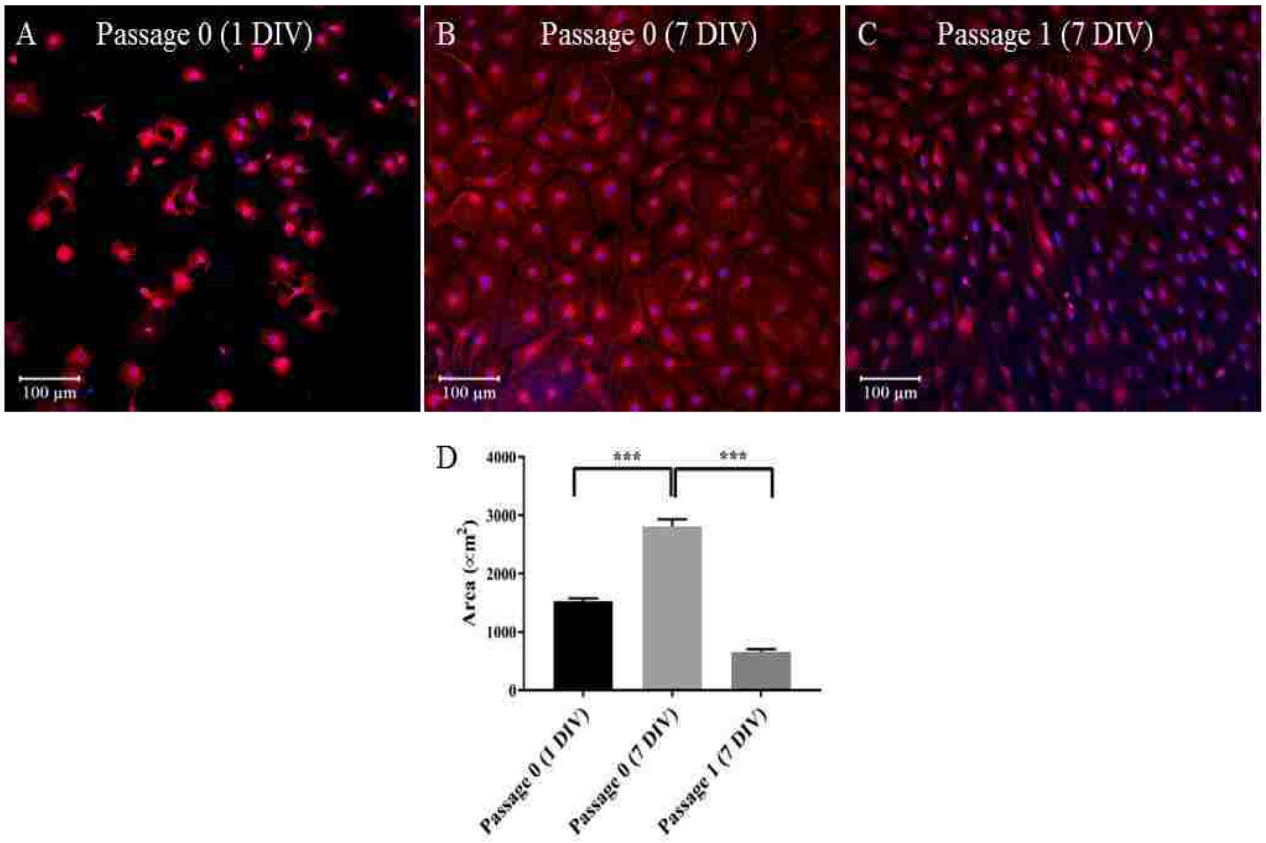

Figure 11. Morphological changes of SGCs

(**A**) 1 day after plating (**B**) 7 days after plating and (**C**) 7DIV after one passage (P1). (**D**) Quantification of the cell surface area between P0 (1DIV, 7DIV) and P1 (7DIV) 100 cells were measured from each condition. Data are presented as $\bar{x}$ ± SEM ***$p < 0.001$. Cells are identified by S100 staining and nuclei by DAPI. Images indicate a morphological change from a flattened fan shape to a bipolar spindle shape after passaging.

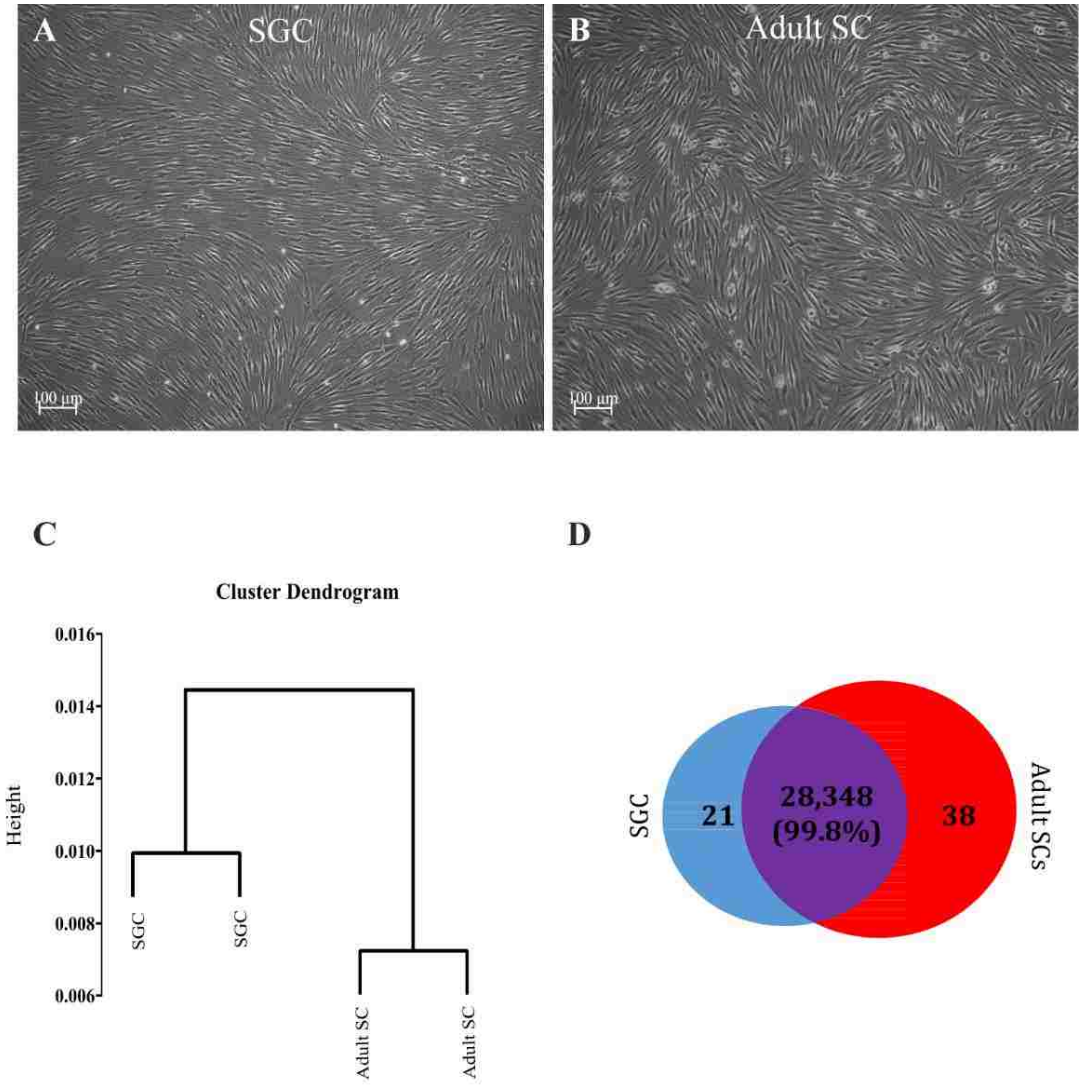

Figure 12. SGCs and SCs are closely related cell types

(**A**) Isolated passage 1 SGCs and (**B**) passage 5 adult SCs grown in similar conditions at 7DIV. (**C**) Dendrogram of Affymetrix Rat Gene 2.0 array comparison between the replicates of each cell type and between the two different cell types show a high degree of correlation. (**D**) Illustration showing the number of transcripts that are differentially expressed between the two cell types.

Table 1. Transcripts with higher expression levels in SGCs

Gene Description	SGC	SGC	SC	SC	Log2FC (SC/SGC)	p value
Fatty acid binding protein, brain	10.24095	7.598433	3.922492	4.171316	-4.873	0.00294
Protein phosphatase1, regulatory (inhibitor) subunit 1C	10.12096	8.543543	5.42678	6.099573	-3.569	0.0018
Carbonic anhydrase 5b, mitochondrial	10.57911	10.75434	7.278402	7.222755	-3.416	0
Zinc finger protein 658B-like	6.480721	4.31133	2.31878	1.822333	-3.325	0.00693
Transmembrane protein 176B	12.17163	9.177574	7.8796	7.715805	-2.877	0.03447
LIM domain binding 2	10.28695	7.278443	5.874477	6.300641	-2.695	0.04434
Interaction protein for cytohesin exchange factors 1	8.175984	8.125478	5.467092	5.477365	-2.679	0
Homeo box A2	6.787416	7.452611	4.483123	4.807213	-2.475	0.00031
Synuclein, gamma	12.2291	10.9459	9.379388	8.903334	-2.446	0.0036
ELOVL fatty acid elongase 2	9.083694	6.536357	5.848471	4.889462	-2.441	0.04304
Leucine rich repeat containing G protein coupled receptor 5	10.52314	8.392814	7.265714	6.939879	-2.355	0.02258
Phospholipase A2, group XVI	8.641899	6.065925	5.216479	4.804748	-2.343	0.04291
Leucine rich repeat neuronal 3	8.346226	6.370303	5.087136	5.005742	-2.325	0.0179
Solute carrier family 16 (monocarboxylate transporter), member 7	8.6614	8.262614	5.91989	6.525473	-2.239	0.00045
Netrin G1	6.76474	7.436815	4.638986	5.265791	-2.148	0.00133
Fibulin 2	8.868303	10.11878	7.04572	7.70642	-2.117	0.00735
Interleukin 33	6.50084	6.466847	4.31787	4.540732	-2.055	0.00003
Plexin domain containing 2	11.24584	11.18015	8.867145	9.461807	-2.049	0.00034
Midkine	9.72899	7.770844	6.77838	6.666795	-2.027	0.02763
Zinc finger protein 521	7.519093	8.091207	5.583355	5.983865	-2.022	0.00062
Myosin Vb	7.513097	6.950174	5.365945	5.057861	-2.02	0.00046

Table 2. Transcripts with higher expression levels in SCs

Gene Description	SGC	SGC	SC	SC	Log2FC (SC/SGC)	p value
Glutamate receptor, ionotropic, AMPA 1	4.339376	5.049667	7.993583	8.371711	3.488	0.00009
Secretogranin II	3.745154	4.010756	7.05478	7.550909	3.425	0.00003
Transforming growth factor, beta induced	6.320231	7.427352	9.814057	10.7823	3.424	0.00114
Meis homeobox 2	5.518019	8.213129	10.15273	10.09727	3.259	0.01543
Leucine rich adaptor protein 1-like	6.018113	5.734979	9.299845	8.806058	3.176	0.00004
Peripheral myelin protein 2	8.47366	6.665875	10.66794	10.05507	2.792	0.00767
MicroRNA 19b-2	3.032256	2.603317	5.751867	5.397797	2.757	0.00007
Somatomedin B and thrombospondin, type 1 domain containing	8.163711	8.86568	11.50944	10.91121	2.696	0.00049
mab-21-like 1 (C. elegans)	4.437928	4.119211	7.160288	6.692215	2.648	0.00009
Homeobox protein Hox-D8-like	4.912837	6.919669	8.527472	8.532732	2.614	0.01196
BTB (POZ) domain containing 16	6.048716	6.048716	8.796915	8.528403	2.614	0.00001
POU class 3 homeobox 1	6.825703	6.805931	9.570774	9.179165	2.559	0.00003
Fibroblast growth factor 1 (acidic)	5.721413	6.718378	8.996104	8.534381	2.545	0.00127
Thrombospondin 2	10.01996	10.40276	12.84675	12.5542	2.489	0.00007
Muscular LMNA-interacting protein	5.580262	5.355801	8.064244	7.799314	2.464	0.00003
SH3-domain GRB2-like 3	7.314805	8.039347	10.17944	9.846105	2.336	0.00053
Protease, serine, 12 neurotrypsin (motopsin)	6.818745	7.013252	9.489999	8.992291	2.325	0.00013
Phosphodiesterase 4D, cAMP-specific	8.490598	8.309664	11.06317	10.36349	2.313	0.00038
Palmdelphin	6.171412	7.945516	9.427964	9.304221	2.308	0.01231
Carboxypeptidase A4	4.572556	4.623984	6.759602	6.798272	2.181	0.00001
Membrane metallo-endopeptidase	7.936572	8.678213	10.57476	10.35108	2.156	0.00068
Chimerin 2	5.222805	6.79949	8.227407	8.04189	2.124	0.01116
Chemokine (C-X-C motif) ligand 14	8.40965	8.343615	10.75215	10.24149	2.12	0.00018
Calcium/calmodulin-dependent protein kinase IV	5.570234	7.129077	8.47983	8.444214	2.112	0.01066
SH3-domain GRB2-like (endophilin) interacting protein 1	5.495108	6.92895	8.601629	8.034436	2.106	0.01035
ATP-binding cassette, subfamily G (WHITE), member 3-like 3	9.191216	9.489748	11.54186	11.28379	2.072	0.00009
Ribosomal protein S16	7.902252	6.025511	9.012001	9.050374	2.067	0.02228
Claudin 19	5.572169	5.672629	7.958853	7.389347	2.052	0.0003
Macrophage activation 2 like	5.504892	6.589047	8.266476	7.923917	2.048	0.00368

SGCs and SCs Share Similar Functional Properties

Given the striking similarities between SGCs and SCs we evaluated whether purified SGCs were functionally similar to SCs, by evaluating whether they were capable of myelinating sensory axons. Initially we utilized adult cervical DRGs, as an intact explant (Figure 13A). Switching this culture to a myelin permissive feed for 21 days (35 DIV) allowed the formation of multiple myelin segments as evidenced by staining for MBP. To our knowledge this is the first time that adult axons have been myelinated in culture. As it is possible that the explant contains a number of SCs that could be responsible for the observed myelin segments, we carried out the same experiments using neurons, with their ensheathing SGCs intact, that have been purified on a BSA cushion (fraction 1, Figure 9B). As is observed in figure 9B and E, this process significantly reduces the numbers of non SGC cells (defined as ($TUBB3^-$, GS^-)) present in the preparation. Again, multiple myelin segments were observed when the preparation was switched to myelin feed (Figure 13B). Finally, we used a classic myelinating coculture, utilizing E15 DRG neurons that have been purified to remove non-neuronal cells. After developing extensive axonal processes, BSA cushion purified SGCs (fraction 3, Figure 9D) and adult rat SCs purified from the sciatic nerve, were added to the neurons and cocultured as mentioned before being switched to a myelin permissive media. As is seen in Figures 13C and 13D, both SGCs and adult SCs were capable of forming myelin segments on these axons. Interestingly, although SGCs produced collagen, they failed to assemble it into arrays along the axon (Figure 14).

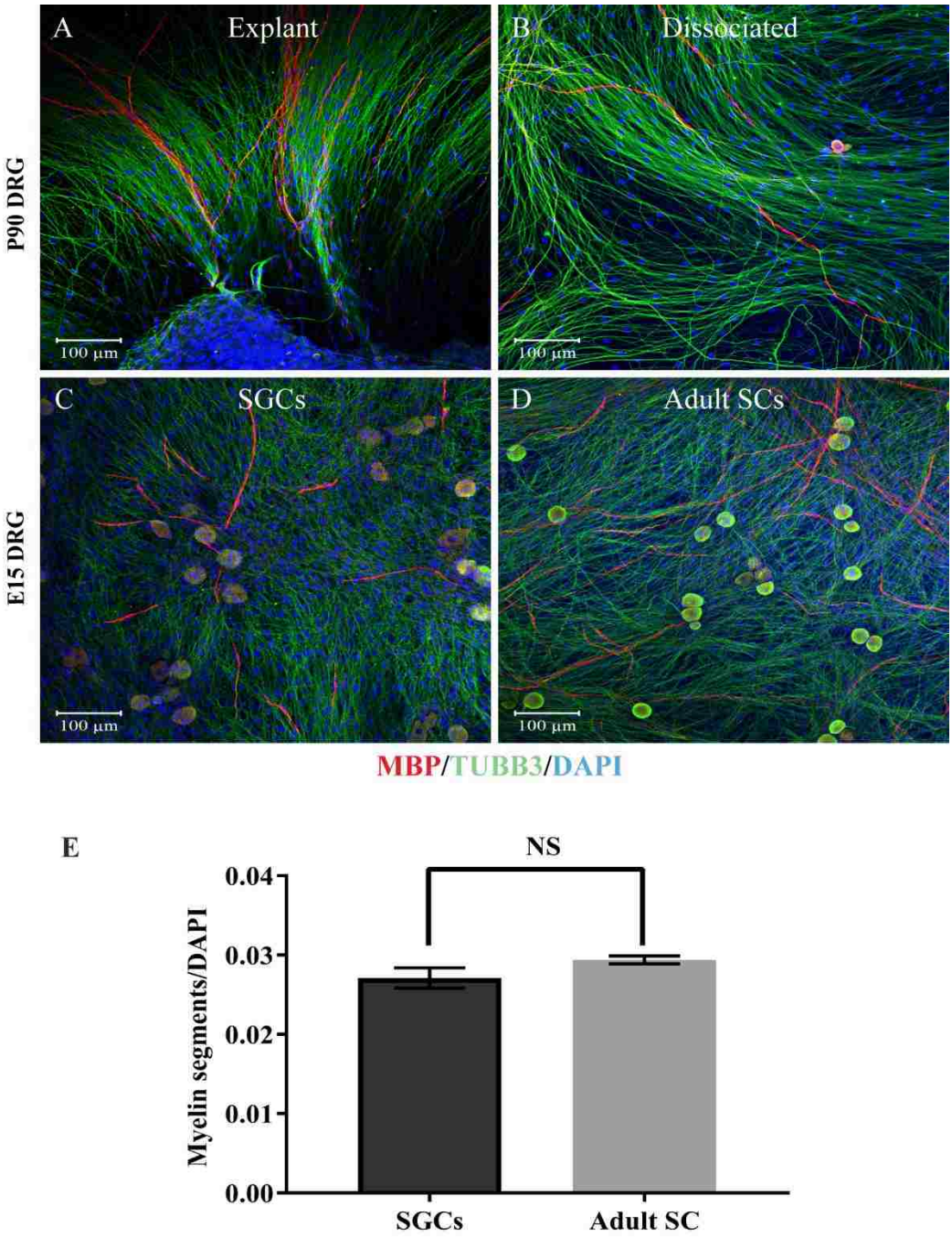

Figure 13. SGCs can myelinate both embryonic and adult axons

(**A**) P90 DRG maintained as an explant and (**B**) dissociated P90 DRG (fraction 2) at 35 DIV in myelin permissive conditions. Purified E15 neurons cocultured with (**C**) SGCs and (**D**) adult SCs

at 40 DIV. Myelin segments are identified by MBP and neurons by TUBB3. Scale bar represents 100µm. (**E**) The number of segments formed by SGCs and SCs normalized with DAPI count. Data were analyzed by unpaired t test (n=3) and presented as mean ± SEM.

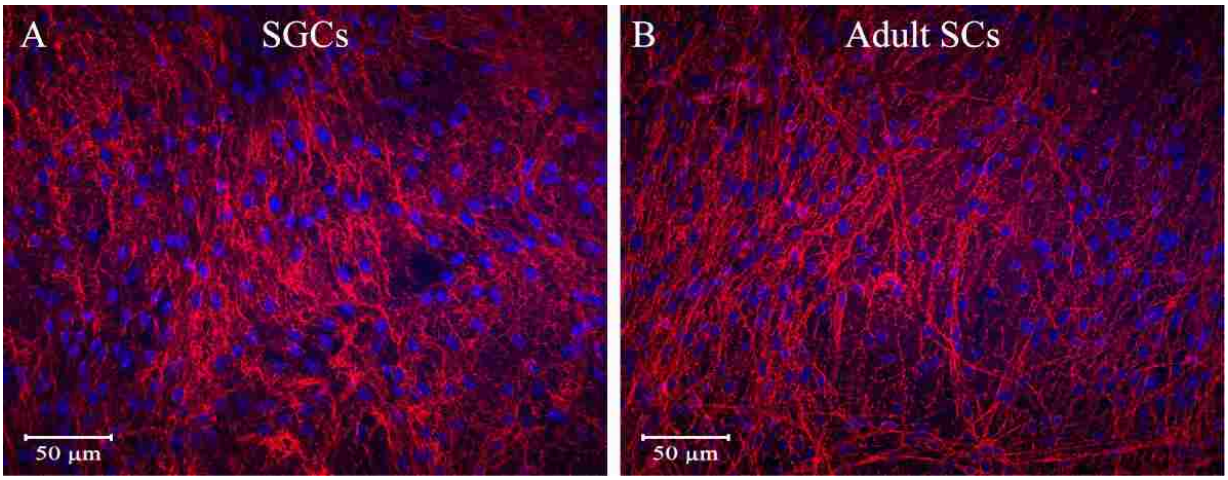

Figure 14. Difference in collagen assembly between SCs and SGCs

(**A**) Collagen assembly appeared to be more diffuse when SGCs were co-cultured on embryonic axons in similar conditions. (**B**) Collagen was assembled into arrays when SCs were co-cultured with purified embryonic axons in myelinating conditions. Cultures were grown for 21 days and immunostained for collagen and DAPI. Scale bar represents 50µm.

Discussion

In this study we have examined the development of SGCs, cells that ensheathe sensory neuronal soma. We have shown that these cells arise postnatally and express early SC markers such as

CDH19, which has previously been described as a unique marker for SC precursors (Takahashi & Osumi, 2005). To examine the relationship between SGCs and SCs, we developed a novel method for the purification of SGCs and showed that these cells are transcriptionally and morphologically similar to SCs even in the absence of axonal contacts. Finally, we were able to assess how functionally similar SGCs are to SCs by demonstrating that purified SGCs were able to myelinate sensory axons in both organotypic and mixed cocultures. Based on these observations we hypothesize that SGCs represent a population of SC precursors whose further development has been arrested as a result of the ganglia microenvironment and/or contact with neuronal soma.

CDH19 has been described as the only unique marker for SC precursors (Takahashi & Osumi, 2005) and this marker is down regulated as these precursors differentiate into immature SCs in response to axonal contact. In this study we show that 'adult' SGCs that surround neuronal cell bodies also express CDH19 and that, when purified, these cells adopt the characteristic bipolar spindle cell shape of the SC, even in the absence of axonal contact, to become functional myelinating cells. Recent studies indicate that in addition to SCs, SC precursors can also give rise to parasympathetic neurons (Dyachuk et al., 2014; Espinosa-Medina et al., 2014b), suggesting that these cells exhibit a degree of plasticity outside of the SC lineage. SGCs have also been described as being potentially plastic and have been proposed to give rise to a number of different cell types including sensory neurons and even oligodendrocytes (Fex Svenningsen et al., 2004). It has been proposed that SGCs may represent a reservoir of multipotent cells that could replenish damaged neurons within the ganglia. Our study supports this idea by demonstrating that SGCs exhibit properties of SC precursors.

The differentiation of SC precursors to immature SCs and finally myelinating SCs has been well characterized in the context of the developing peripheral nerve (Jessen & Mirsky, 2005; Mirsky et al., 2008). In those studies the SC precursor has been shown to require the neuregulin growth factor for its survival, propagation and differentiation into an immature SC. *In vivo*, this is provided by contact of the SC precursor with the axonal bound neuregulin. In our studies we note that markers such as CDH19 are quickly downregulated once SGCs are no longer in contact with neuronal soma and that SGCs quickly adopt a SC morphology when placed in culture. There these cells can be propagated in the absence of neuregulin or axonal contact and can be added to DRG neurons to form myelin segments. It should also be noted that they exhibit a different pattern of ECM deposition, and appear less organized than their counterparts derived from purified adult rat SCs. We believe that this may reflect differences in the differentiation of SGCs to a myelinating cell type compared with SC precursors or simply technical differences resulting from the preparation of SGCs.

It is well-established that the embryonic DRG is a source for the generation of viable population of SCs (Wood, 1976), and several previous studies (Fex Svenningsen et al., 2004; Maro et al., 2004; Wakamatsu, Maynard, & Weston, 2000; Weider et al., 2015) have referred to non-neuronal cells within the embryonic DRG as SGCs. Although these cells lie within the DRG (where neuronal cell bodies are clustered), we have shown that these cells in the embryonic DRG are not yet mature SGCs as they neither envelope the neuronal cell body nor express characteristic SGC markers such as GS. This observation suggests that these non-neuronal embryonic cells might represent an earlier neural crest derivative. In the first two weeks of the postnatal period, Ki67

staining suggests that most cells in the ganglia have ceased proliferation and are starting to differentiate into SGCs in close proximity with the neuronal soma.

The role of CDH19 in SGC function remains to be determined. When adult DRGs, complete with their ensheathment of SGCs are placed into culture, CDH19 is quickly downregulated, concomitant with the migration of SGCs away from the neuronal cell body (unpublished observations), suggesting a potential role for CDH19 in maintaining SGC-somal/SGC-SGC interactions. In support of this idea, it is interesting to note that the distance between the neuronal surface and SGCs is 20nm (E. Pannese, 1981) which is comparable with the distance between cells in the cadherin-based adherens junction.

In this study we purified SGCs from adult rat DRGs and demonstrated their ability to myelinate purified sensory neurons. We were aware of the presence of contaminating cells (including SCs) within the harvested adult ganglion. However, in the method used to isolate SGCs, we typically obtained about 90% SGCs and a small percentage of neurons. The neurons failed to attach and thrive on PLL coated surfaces and passaging resulted in their complete loss. We also observed SCs (GS negative, TUBB3 negative) but noted a fivefold reduction in SC numbers when the separation was performed, with the total percentage of SCs in fraction 3 less than five percent. It is unlikely that this small percentage of SCs in culture contribute to the formation of myelin segments observed in the cocultures experiments.

SGCs have been proposed to regulate the electrical activity of DRGs and have been shown to undergo several changes during nerve injury that are thought to underlie the recruitment of additional neurons to an injury response (M. Hanani et al., 2002b; Ohara, Vit, Bhargava, & Jasmin,

2008; E. Pannese, Ledda, Cherkas, Huang, & Hanani, 2003; Siemionow, Klimczak, Brzezicki, Siemionow, & McLain, 2009; Stephenson & Byers, 1995; Vit, Jasmin, Bhargava, & Ohara, 2006). Recent progress has been made in understanding the signaling exchange between the SGC and the neuronal soma as well as between adjacent SGCs, with the idea that perturbing these pathways can lead to the development of novel therapeutics for dealing with neuropathic pain. Greater understanding of the differentiation of the SGC as proposed in this study could facilitate the development of such therapeutics.

CHAPTER THREE: DEVELOPMENT AND CHARACTERIZATION OF A FUNCTIONAL MODEL OF THE DRG TO STUDY NEUROPATHIC PAIN

Introduction

Gap in Knowledge

One of the easiest and direct methods of investigating the contribution of SGCs towards the activity of neurons is by measuring the electrical activity of the neurons they ensheathe. Neurophysiological measurements are a direct readout of the function of neurons, and this is valuable in understanding the changes that occur in disease conditions. Unfortunately, 1) there are no *in vitro* models that successfully mimic the SGC-neuronal interaction for long-term monitoring and 2) soma of the neurons are usually the sites where electrical readings are routinely recorded, and this site is not ideal for the acquisition of electrical information as the axonal terminals that innervate the sensory targets are the sites where the stimulus is received. Also, correct ensheathment of the soma by the SGCs would inhibit functional recordings. Here we describe the functional characterization of an *in vitro* model that can preserve the SGC-somal contacts as well as acquire spontaneous and evoked electrical activity from the axons. We integrate an *in vitro* three-dimensional nerve model with a microelectrode array (MEA) to obtain electrical recordings from axonal bundles. We report here the overall design and culture of DRGs using a three-dimensional capillary alginate gel (Capgel™) and its comparison with two-dimensional cultures. We highlight the advantage of the system by performing long-term electrophysiological monitoring of the same bundle of axons. Finally, we show sensitization of nociceptive neurons to

capsaicin and utilize this three-dimensional system to further investigate the role of SGCs in neuropathic pain.

Electrophysiological Readings and their Significance

Neurophysiological assessments provide a wealth of information about the activity of neurons in normal and in disease conditions, as well as their response to drug treatments. The current approach relies heavily on neurophysiological endpoints in animal models and is limited by the cost, time and low throughput (Irons et al., 2008). As the electrical data obtained from *in vivo* and *in vitro* are comparable, *in vitro* systems are beneficial with respect to the cost, reproducibility, and ease of use. The Patch-clamp method is used to assess the electrical activity of individual neurons, but this technique is time-consuming and is restricted by the number of neurons that can be studied at once, thus limiting its use for studying neuronal networks. Planar MEAs overcome these limitations by enabling long-term recording of electrical activity from a population of neurons in culture (Obien, Deligkaris, Bullmann, Bakkum, & Frey, 2014).

Microelectrode array and neural recordings

Planar MEAs are devices that contain a grid of electrodes on which cells can be directly grown. The electrodes are usually about 10-40µm in diameter and are typically made with metallic conductors. The impedance of the electrodes is lowered by increasing the surface area using a conductive material. MEAs offer a non-invasive method of measuring electrical information by detecting electrical changes in the extracellular field around the electrodes in comparison to the ground electrode (Obien et al., 2014).

The use of this system facilitates recording of the action potentials (spikes) that can be analyzed based on characteristics such as spike height and spike width. The polarity of the spike has a strong correlation with the location of the cell on the electrode. The shape of a spike is characteristic of the size and shape of the cell, and can vary depending on the structure/part of the cell that interfaces with the electrode (Nam & Wheeler, 2011). Somatic spikes are typically wide when compared with axonal spikes (Deligkaris, Bullmann, & Frey, 2016). Larger cell structures like the DRG soma (14-75µm) have greater capacitance and generate stronger field potentials. Usually, the action potentials are recorded from the large-sized soma as opposed to the small diameter axon (typically less than 1µm) on an MEA in a two-dimensional culture (Nam & Wheeler, 2011). This necessitates the need for culturing neurons at high densities (Newberry et al., 2016) or patterning the MEA surfaces (John C. Chang, Brewer, & Wheeler, 2000; J. C. Chang, Brewer, & Wheeler, 2001; Griscom, Degenaar, LePioufle, Tamiya, & Fujita, 2002; Ravenscroft et al., 1998; Stenger et al., 1998) to ensure the neuronal cell bodies are in contact with the MEA electrode.

The current *in vitro* models that study peripheral nerve disease are two-dimensional in nature and lack the necessary spatial arrangements of the glial cells, ion channel expression, and extracellular matrix organization to faithfully represent the *in vivo* microenvironment (Breslin & O'Driscoll, 2013; Irons et al., 2008). Moreover, glial cells are often referred to as contaminants and the cultures are treated with antimitotics to prevent glial growth and interference (Newberry et al., 2016). The need for an accurate representation of the *in vivo* cellular behavior is more pronounced in the context of electrophysiological activity and more so in the context of understanding pain. A three-dimensional model is a better platform for investigation of neurophysiological measurements than the traditional two-dimensional cultures.

The Use of Three-Dimensional Systems

Extrapolating two-dimensional observations may not be accurate, as it is now evident that cells exhibit different characteristics in a monolayer system. A three-dimensional system allows a close approximation of the cell-cell, and cell-extracellular matrix (ECM) interactions. Castillon *et al*., have shown that Na+/H+ exchangers polarize correctly in three-dimensional culture and others have shown that two-dimensional cultures have a non-physiological calcium dynamic when compared with the three-dimensional counterparts (Castillon et al., 2002; Desai, Kisaalita, Keith, & Wu, 2006; Mao & Kisaalita, 2004).

There are several commonly used approaches to study cells in a three-dimensional aspect: organotypic explant cultures, microcarrier cultures, micromass cultures, microgravity bioreactors and gel-based culturing, etc. (Edelman & Keefer, 2005). Gel-based matrices offer several advantages over the other methodologies mentioned. Here, cells are embedded within different substrates like matrigel which function as scaffolds to support their growth. The scaffolds can then be engineered to mimic the properties of the ECM.

Capillary Alginate Gel (Capgel™) as a biomaterial for neuronal growth

Capillary Alginate Gel (Capgel™) is a hydrogel that is engineered to have a continuous microtubular architecture (Willenberg, Hamazaki, Meng, Terada, & Batich, 2006). This particular organization is ideal for the growth of DRG neurons as it resembles the organization of fascicles within a nerve. Capgel™ are self-assembled alginate gels that are crosslinked with Cu^{2+} (Willenberg et al., 2006). The diameter of the lumen of the capillaries that are formed can easily be manipulated by altering the Cu^{2+} concentrations or by altering the pH of the system (Thumbs

& Kohler, 1996). Laminin derivatization of the capillary lumen has been previously described by our laboratories (Anderson et al., under review) and it was shown that laminin promotes the growth of neuronal axons within the 50µm diameter channels. The laminin coated Capgel™ was used to grow DRG neurons and it was shown that neurons extend axons through the capillaries forming a nerve fascicle like structure. The axon bundles were surrounded by perineurial glia and the mature myelinating SCs formed myelin sheaths around about 20% of the axons which is similar to the percentage of myelinated axons in the sural nerve. Overall, our previous work promotes the use of Capgel™ as an ideal biomaterial for studying the peripheral nerve (Anderson et al., under review).

We integrated DRGs cultures with a microelectrode array using this biomaterial to study the electrical properties of the DRG neurons in a three-dimensional environment. As mentioned in chapter one, the major limitation in measuring the contribution of SGCs to the electrical activity of neurons is the lack of an *in vitro* model that sufficiently mimic the *in vivo* organization. Additionally, in a two-dimensional culture system, SGCs migrate away from the DRG soma they envelop (Figure 15). Here, we have designed a model where we can not only study SGCs in their native environment but also offers advantages such as the long-term monitoring of electrical signals from these neurons. To further substantiate its use as a neuropathic pain model, we use capsaicin to evoke activity of the nociceptors.

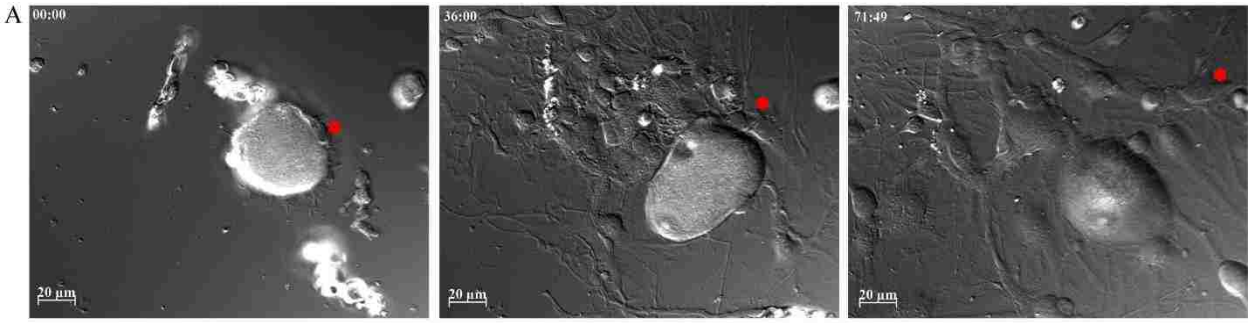

Figure 15. SGCs migrate away from the cell body

Live imaging of adult DRG neuron with SGCs indicates the migration of SGCs away from the cell body with time. The red asterisk follows the migration of a single SGC from the cell body. Three frames were imaged at 36 hours apart.

Capsaicin as an Agent of Neuropathic Pain

Capsaicin (8-methyl *N*-vanillyl 6-noamide) is found commonly in plants of the capsicum family and is used in animals and in cell culture to model neuropathic pain. It causes a wide variety of physiological changes including effects on the cardiovascular and respiratory system. The effect of capsaicin in inducing pain responses and evoking electrical activity is well described (J. N. Wood et al., 1988). Short-term treatment with capsaicin leads to an increase in the firing rate of neurons followed by a period of desensitization to other noxious stimuli. Long-term effects of capsaicin include changes in neuropeptide levels, desensitization, and toxicity leading to neuronal apoptosis. Although the cellular basis of the action of capsaicin is unknown, capsaicin specifically exerts its effects on the nociceptive neurons. The effect of capsaicin is dose-dependent and studies have shown that capsaicin binds to a nonselective cation channel known as the transient receptor

potential cation channel subfamily V member 1 (TRPV1). This receptor is part of the vanilloid family of receptors and TRPV1 is activated by various stimuli like non-physiological temperature and low pH.

While other groups have attempted to model neuropathic pain *in vitro* using capsaicin, we have designed a system that is far more superior than the existing models in terms of recapitulating the *in vivo* organization of neurons and glia, while enabling detection of electrical signals from axons.

Materials and Methods

Animal Use

All animal protocols were reviewed and approved by the University of Central Florida Institutional Animal Care and Use Committee (IACUC). Timed pregnant rats were purchased from Charles River Laboratories (Wilmington, MA) and thoracic DRGs from 15-day old embryos were harvested for culture.

Surface Preparation of MEA

64 electrode single well MEAs (M64-GLx, Axion BioSystems, Atlanta, GA) were treated with 0.01% poly-L-ornithine (Sigma, St. Louis, MO) at room temperature for an hour followed by an overnight treatment of 50µg/ml natural mouse laminin (Invitrogen, Carlsbad, CA) at 37°C.

Capgel™ Block Preparation and Laminin Derivatization

Capgel™ blocks were synthesized as previously described (Willenberg et al., 2011) and derivatized with laminin as previously described (Anderson et al., under review). 5mm by 3mm

by 2.5mm Capgel™ blocks used were large enough to cover the electrode grid area. The blocks were submerged in 0.01% poly-L-ornithine solution for two hours at room temperature on a shaker followed by two hours at 4°C with shaking. Blocks were then submerged in 50µg/ml natural mouse laminin solution for 48 hours with shaking at 4°C, after which the Capgel™ blocks were then transferred to an incubator at 37°C/5% CO_2 for six hours. Immunostaining was performed to confirm the uniform coating of laminin along the length of the capillary channels (Anderson et al., under review).

Media Preparation

Standard neurobasal media was used for maintaining the cultures as previously established (Callizot et al., 2011). Briefly, neurobasal media (Gibco, Waltham, MA) was supplemented with 2% B27 (Invitrogen), 1% GlutaMax (Invitrogen), 1% penicillin-streptomycin (Invitrogen) and 50ng/ml NGF (Harlan Laboratories). Laminin was removed from the MEA surface and about 50µL of media was added. The volume of the media was maintained around 50µL throughout the entire period of culture as this low volume of media facilitates the anchoring of the Capgel™ blocks to the electrode surface. The cultures were fed with 50% change of the media volume every two days after the readings were recorded.

Experimental Design

Four thoracic DRGs explants were placed on top of the derivatized Capgel™ blocks. The Capgel™ blocks were carefully placed and oriented directly on top of the electrode grid such that the blocks covered all 64 electrodes and the capillary channels were perpendicular to the electrode grid. The capillary channels were at a density of around 40channels/mm^2 and no effort was made to align

the capillary channel directly with the electrode. DRG neurons extend their axons through the entire length of the capillaries and make contact with the electrode surface around day 11- day 15. For the two-dimensional cultures, four thoracic DRGs explants were placed either directly on the four quadrants of the electrode grid such that the DRG cell bodies came in direct contact with the electrodes or, they were placed outside the electrode grid so that the DRG cell bodies never made any contact with the electrodes and instead, only the single axons that extend from the DRG made contact with the electrodes. The experimental set-up is outlined in Figure 2. The first day where electrical activity was designated as Day 1 of Firing (DF) for all conditions.

Data Acquisition and Analysis

Readings were recorded using the 2.1.1.16 Axion Integrated Studio (AxIS) software for 10 minutes every two days with the heating element set to 37°C. Adaptive threshold crossing at six standard deviation (STD) and pre-spike 0.84ms and post-spike of 2.16ms was used. Raw data from all 64 electrodes were recorded. Axion spike files were analyzed using the 2.0.4 Neural Metric Tool (Axion Biosystems). Electrodes with a firing rate of ≥ 5spikes/min were included in the analysis. Using 11 different characteristics of the waveform, each spike was analyzed and clustered as the same or distinct population of the waveform using a custom MATLAB script.(Enright et al., 2016; Narula et al., 2017) Mean firing rate was calculated as the average firing rate across 64 electrodes and weighted firing rate was calculated as the average firing rate of the active electrode.

Capsaicin Treatment

1µM capsaicin (Sigma) in dimethyl sulfoxide (DMSO, Sigma-Aldrich, St. Louis, MO) was directly added to the Capgel™ blocks on day 21 and the readings were acquired immediately after

its addition. An equivalent volume of DMSO was added to the culture to obtain comparable basal/control readings.

Capgel™ Processing and Histology

Thoracic DRGs grew through the Capgel™ blocks for 35 days. Blocks were fixed with 4% paraformaldehyde (Electron Microscopy Sciences, Hatfield, PA) for 18 hours. After fixing, blocks were washed in PBS for 24 hours and transferred to a solution of 30% sucrose with 0.02% sodium azide overnight at 4°C. 30% sucrose solution was replaced with 20% OCT (Sakura) in 30% sucrose/PBS solution at 37°C for about 24 hours after which it was then replaced with 50% OCT in 30% sucrose/PBS solution for 24 hours at 37°C. Capgel™ blocks were embedded carefully in OCT compound. 10µm cross sections of the blocks were collected and processed with immunostaining. Briefly, the tissue sections were permeabilized using 0.3% Triton X-100 in 4% PFA for 10 minutes on ice. Tissue samples were then blocked using 10% normal goat serum and incubated overnight at 4°C with primary antibodies (mouse TUBB3 (1:300 Abcam)), followed by addition of secondary antibodies (goat anti-mouse Alexa Flour, 1:1000, Invitrogen) and 4, 6-diamidino-2-phenylindole (DAPI, 1:200, Invitrogen).

Microscopy

A Zeiss LSM 710 confocal microscope was used to acquire images. Acquisition settings were optimized using Zen 2.1 software and the optimal setting was used to obtain identically captured images for comparison.

Cleaning and Re-use of MEAs

Instructions from the manufacturer were followed for cleaning. After the Capgel™ blocks were removed, 0.5% trypsin (Life Technologies, Carlsbad, CA) was added to the MEA well for about 30 minutes at 37°C. Trypsin was removed and the surface was washed with 200 proof ethanol. The surface was then rinsed with sterile water and the MEAs were baked for about 12-16 hours at 55 °C. The MEA wells were viewed under a phase microscope to ensure the surface was clean before they were used again. MEAs were re-used up to two times.

Statistics

Data for the well-wide mean firing rate for soma (n = 6), single axons (n = 8) and bundled axons (n = 6) between DF1 to DF11 were compared using one-way ANOVA with Tukey's multiple comparisons test. DF11 was chosen as the cut-off time period, as the explants in the soma and single axonal conditions detached beyond this time point. The width of the spikes and voltages of soma (n = 42), single axons (n = 8) and bundled axons (n = 91) were also compared by one-way ANOVA with Tukey's multiple comparison test. Weighted mean firing rate and the voltage comparison between control and capsaicin treatment were both analyzed using a paired t test (n = 4). Data are reported as the mean ($\bar{x}$) ± standard error of the mean (SEM).

Results

Culture of DRG Explants on Capgel™ Block Facilitates the Separation of DRG Cell Bodies from the Bundles of Axon

Previous work has shown the generation of a three-dimensional *in vitro* nerve model using Capgel™ (Anderson.et al., under review). We observed that placing DRG explants on top of the

Capgel™ block restricted the migration of DRG neuronal cell bodies (Figure 16C) hence, four thoracic DRG explants were placed on top of the derivatized Capgel™ blocks. The block with explants on top was then carefully placed on the MEA, such that the capillaries were perpendicular to the electrode grid and made direct contact with the electrodes (Figure 16A). The culture was maintained for about 35 DIV after which the Capgel™ block was serially sectioned. An immunostained cross-section close to the DRG explant site (Figure 16B) showed several capillaries were infiltrated with cells and further examination at higher magnification revealed several neuronal cell bodies (identified by β-3 tubulin (TUBB3)) with associated satellite glia (nuclei identified by bright DAPI staining) threading the capillaries (Figure 16C). The maximum distance travelled by the cell bodies within these capillaries was seen to be around 400µm from the explant site (data not are shown). Beyond this distance, we see several axons (TUBB3) with glial cells (nuclei identified by bright DAPI staining) bundled together (Figure 16D and E). The axon bundles grew through the entire length of Capgel™ (2-2.5mm) and the capillary diameter was around 100µm ($\bar{x}$ 102.12 ± 22.10µm, n = 5, Figure 16F). As the bundles exited the capillaries, they were around 8µm ($\bar{x}$ 8.02 ± 0.57µm, n = 5) in diameter (single axons are typically less than 1µm in diameter) and make contact with the electrode (Figure 16F). Different waveform populations on each individual electrode were analyzed using clustering criteria as described in the materials and methods section. The waveforms that result from the action potentials of each neuron will be characteristic and so, the number of waveform populations on each electrode will indicate the number of neurons contributing to the electrical activity on that electrode. Figure 16G shows that only about 8% of the electrodes had a single waveform and 92% of the electrodes

analyzed had two or more waveforms and suggesting that multiple different axons within the same bundle are contributing to the firing observed at a single electrode.

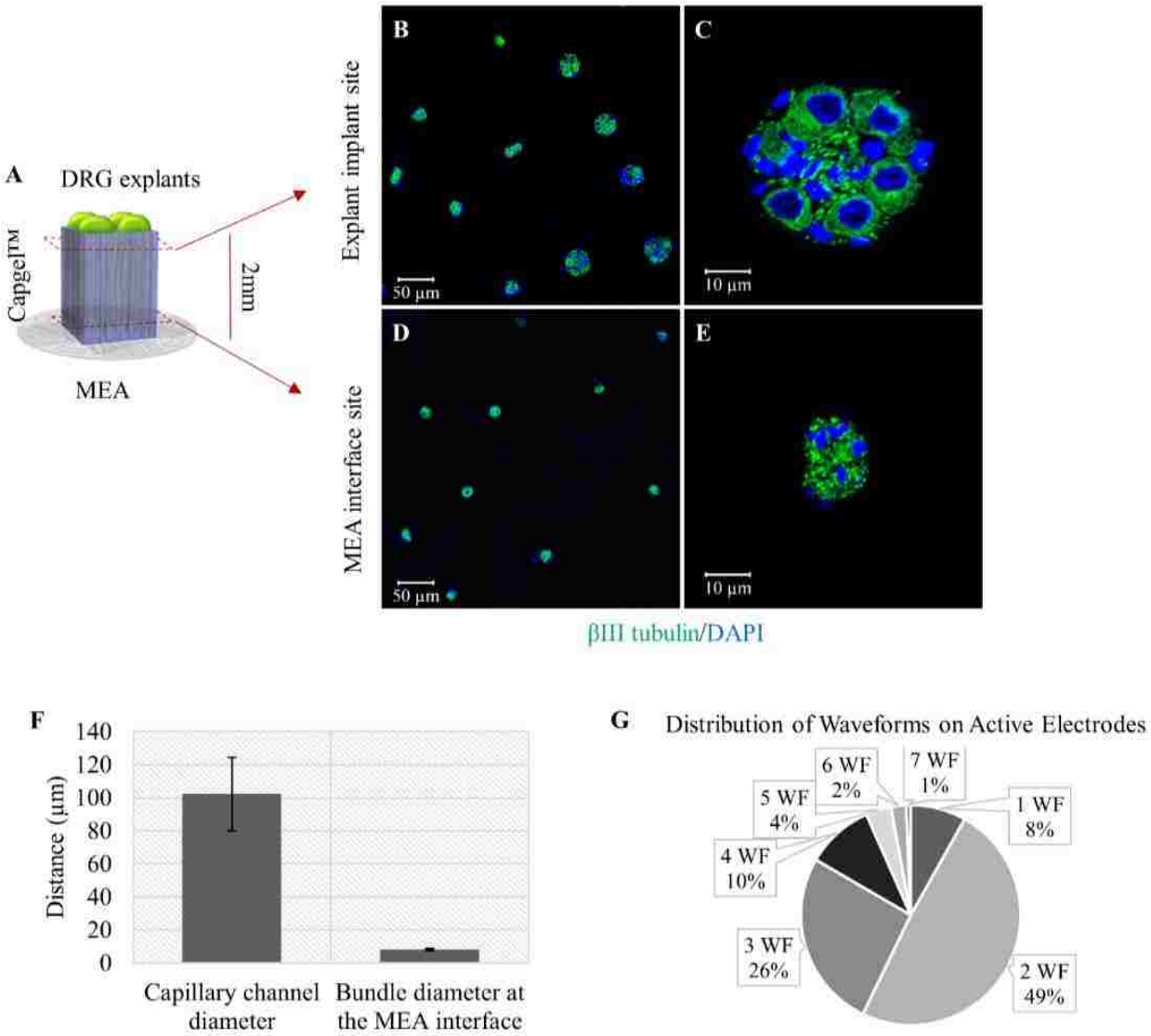

Figure 16. Characterization of bundles within Capgel™

(**A**) Capgel with DRG explants (on top) interfaced with the MEA (**B**) A 10µm section of Capgel™ block near the explant implant site showing several capillaries infiltrated with cells (**C**) Image of a single capillary channel indicates the organization of neuronal soma with closely associated

SGCs (**D**) 10μm section of Capgel™ block at the MEA interface site and (**E**) Image of a single capillary channel shows the compact organization of axons and glia. Axons are identified in green and the neuronal and glial nuclei are identified by DAPI. (**F**) Characterization of the capillary channel diameter and bundle diameter at the MEA interface. (**G**) Distribution of waveform numbers (WF) on each electrode.

We placed four thoracic DRG explants directly on top of the electrodes in the absence of a Capgel™ block with a single explant being large enough to completely cover one quadrant of the electrode grid (Figure 17A). This design allows us to measure electrical activity generated from the soma of the DRG neurons. Similarly, to determine the electrical properties of individual single axons, four thoracic DRGs were carefully placed along the circumference of the ground electrode (which is about 2.2mm away from the electrode grid center). As shown in the schematic and phase image (Figure 17B), DRG explants extended their axons radially and around three days in culture we can see axons with glia along the electrode grid. Although some neuronal cell bodies migrated away from the explant they were not observed to migrate distances large enough to reach the electrode grid. This experimental set-up facilitates the measurement of extracellular electrical currents largely from populations of axons. Similarly, the phase contrast image of Capgel™ block on the electrode grid (Figure 17C) shows that the block covers the electrode grid and several of the capillaries appear darker suggesting that these capillaries are infiltrated with cells and axons. The spontaneous activity of the two-dimensional cultures was then compared with the three-dimensional axonal bundles generated using Capgel™.

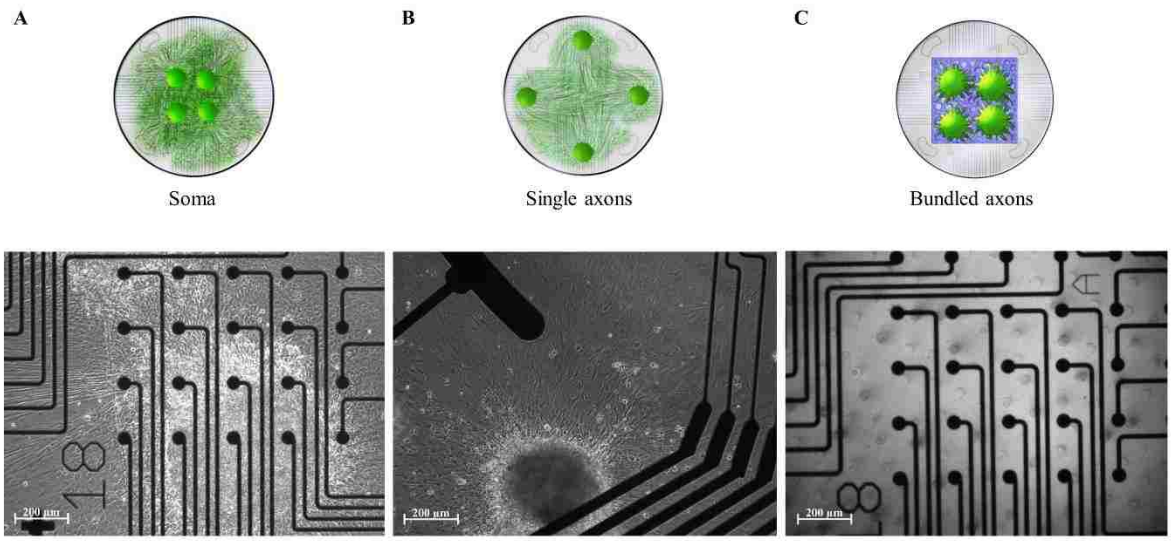

Figure 17. Schematic and phase images of the experimental set-up

Top down view of (**A**) DRG explants placed directly on top of the electrode grid (**B**) DRG explants placed outside of the electrode grid and (**C**) Capgel™ blocks with DRG explants are placed on top of the electrode grid

Bundling of Axons Using Capgel™ Lead to Detectable Action Potentials and Higher Firing Rates

Extracellular recordings from axons are challenging as they do not generate signals large enough to pass the threshold settings (van Pelt, Wolters, Corner, Rutten, & Ramakers, 2004). Single axons extending across the electrode do not achieve sufficient sealing with electrodes and instead form a loose meshwork across the MEA surface. We were curious to know whether bundling the axons in a manner similar to what is seen *in vivo* would generate detectable signals. Comparison of the

well-wide mean firing rate between the somatic ($\bar{x}$ 0.02, n = 6), single axons ($\bar{x}$ 0.01, n = 8), and bundled axons ($\bar{x}$ 0.18, n = 6) (using Capgel™) from the first day of firing (1DF) to 11DF revealed that bundled axons have a firing rate that is significantly higher than the soma (p = 0.03) and single axons (Figure 18A, p = 0.01). There is negligible electrical activity seen where single axons makes contact with the electrodes but bundling of axons generated consistently higher readings when compared with the two-dimensional cultures. The bundle of axons started off with low well-wide firing rate, as fewer bundles made contacts with the electrodes. This is reflected in the small number of active electrodes during early time points (data not shown). With time, there is an increase in the well-wide firing rates that peaks between 9DF and 13DF (Figure 18B).

Figure 18C shows a representative image of waveform populations that were recorded on a single electrode in the three different experimental designs. We see distinct waveforms in the soma and the bundled axons and single axons. Single axons have waveforms that are typical of noise (these populations have the same shape in both positive and negative directions and these spikes were not considered for further analysis) and less than ten data points were available for axonal measurements. Somatic spikes are known to be wider than axonal spikes (Buitenweg, Rutten, & Marani, 2002; van Pelt et al., 2004) and our analysis of the waveform indicated a significant difference in the width of spikes between the soma ($\bar{x}$ 0.24 ± 0.01ms, n = 42) and single axons ($\bar{x}$ 0.21 ± 0.01ms, n = 8, p = 0.02) as well between soma and bundled axons ($\bar{x}$ 0.19 ± 0.00ms, n = 91, p < 0.01). No significant difference were observed between the single and bundled axons (p = 0.33) further establishing the idea that the cell bodies did not contribute to the detected signals and that only axons were present at the interface of Capgel™ block and the MEA (Figure 18D). Interestingly, we did not see an amplification of the voltage in the bundled axons (Figure 18E, $\bar{x}$

31.99 ± 1.22μV, n = 93) as reported by other groups that attempted to acquire axonal readings using microtunnels (Dworak & Wheeler, 2009; Lewandowska, Bakkum, Rompani, & Hierlemann, 2015; Narula et al., 2017).

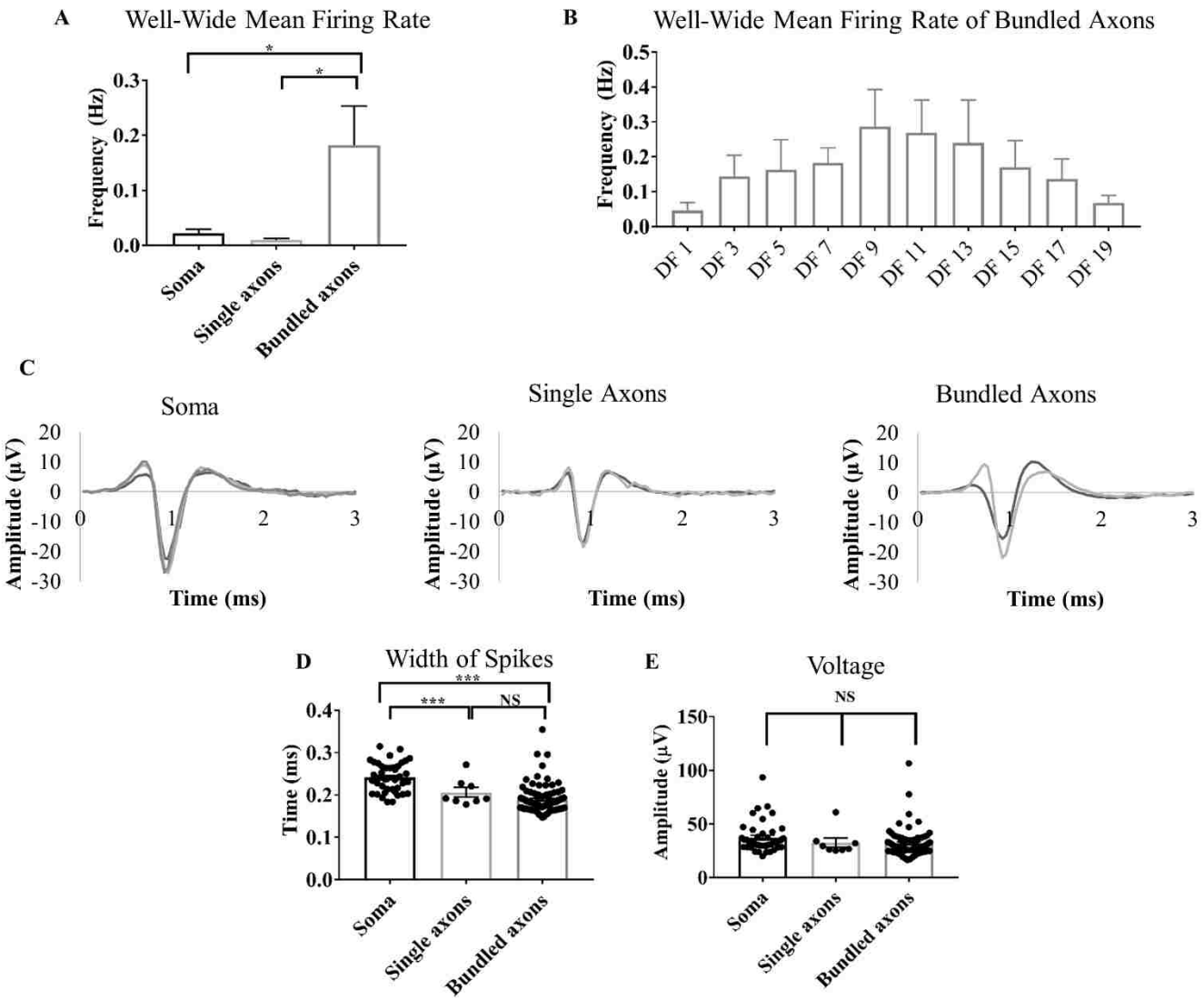

Figure 18. Comparison of firing rates and waveform populations between soma, single axons and bundled axons.

(**A**) Well-wide mean firing rate comparison between the experimental designs. Data represented as an average across all 64 electrode (data analyzed by using one-way ANOVA with Tukey's multiple comparisons test; error bars represent SEM, $*p \leq 0.05$). (**B**) Analysis of well-wide mean firing rate of bundled axons over time. (**C**) Representative waveforms from each condition. Each line represents a population of spikes that have consistently fired and clustered as a distinct waveform. (**D**) Comparison of the width of spikes and (**E**) voltage between soma, single and bundled axons. (**D and E**) Data analyzed by using one-way ANOVA followed by Tukey's multiple comparisons test; error bars represent SEM, $***p \leq 0.01$.

In our three-dimensional system, the bundle of axons that make contact with an electrode continued to maintain the same connections with time because the Capgel™ block was stationary. This was advantageous as we could monitor the electrical activity of the same bundle of axons long-term. We show in Figure 19, the same electrode tracked for over 20 days. Two distinct populations of waveforms that consistently appeared over this period and the firing rate of each of the populations is shown. The spike shapes were remarkably consistent and reproducible each day but changes in the waveform were observed over time. Changes in the spike shape could be a result of developmental or maturation differences as previously reported (Lewandowska et al., 2015). This model can be used as a tool to study and understand these changes.

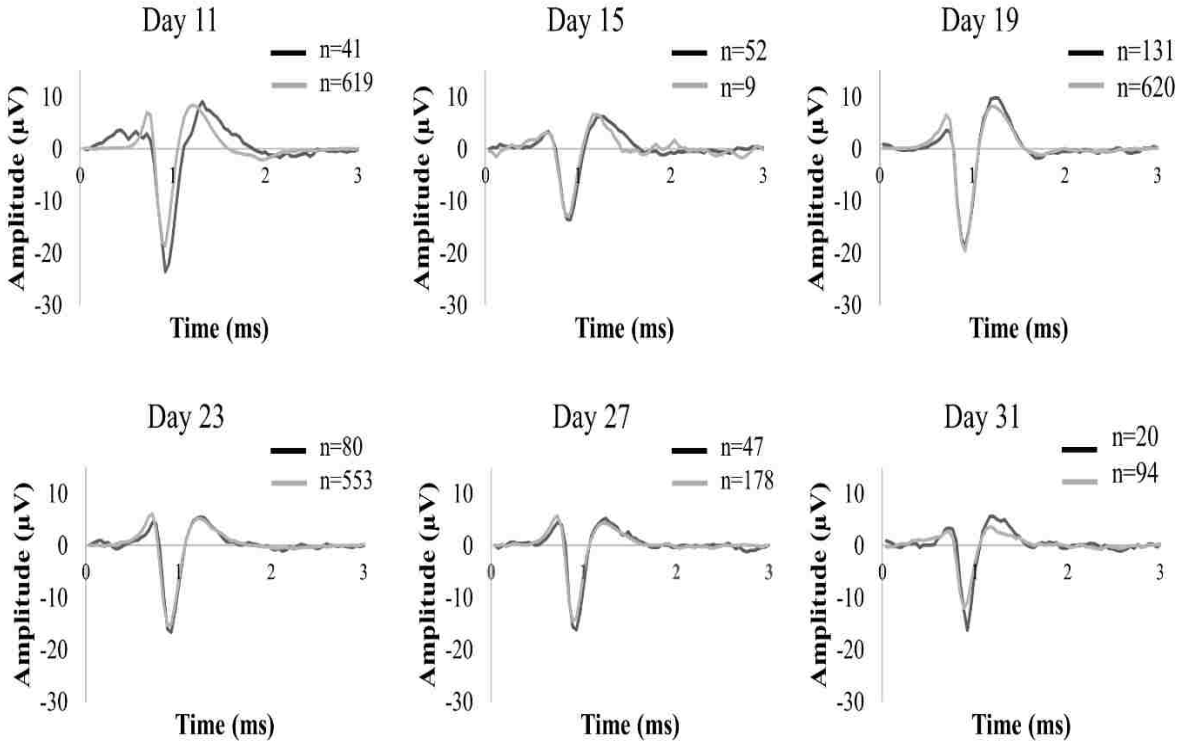

Figure 19. Long term monitoring of population of waveforms

Waveplots of the same electrode and the same population of waveforms from 11DIV to 31DIV. The frequency of firing of each of these population is indicated.

The Bundle of Axons within the Capgel™ Blocks are a Heterogeneous Population of Axons Similar to an In Vivo Nerve

DRG are composed of several different types of neurons – nociceptive, mechanoreceptive and proprioceptive, which are involved in transmitting different types of sensory inputs to the CNS

(Marmigere & Ernfors, 2007; Montano, Perez-Pinera, Garcia-Suarez, Cobo, & Vega, 2010; Scott, 1992). To further study the composition of the axon bundles formed within the Capgel™ capillaries, we added capsaicin, a TRPV1 receptor agonist, to the culture, in order to model pain (Caterina et al., 2000; Caterina et al., 1997; Heinricher, Cheng, & Fields, 1987; Tominaga et al., 1998). Figure 20A shows the weighted firing rate for the DMSO control and after the addition of capsaicin at 21DIV. We see here that the addition of capsaicin led to an overall increase in the mean firing rate (control $\bar{x}$ 3.01 ± 0.33, n = 4; capsaicin $\bar{x}$ 10.49 ± 2.23, n = 4, p = 0.02). This augmentation in firing rate in response to capsaicin treatment is well documented (Caterina et al., 2000; Newberry et al., 2016; B. J. Wainger et al., 2015). Analysis of the waveforms indicated a change in the firing rates with no changes in the voltage (Figure 20B, control $\bar{x}$ 24.32 ± 1.60, n = 4; capsaicin $\bar{x}$ ± SEM 25.49 ± 1.69, n = 4, p = 0.63)

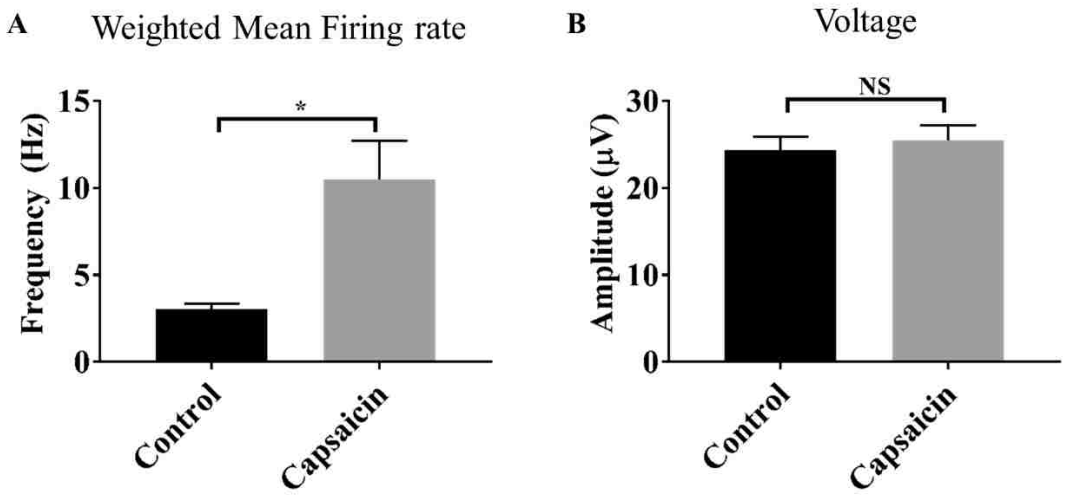

Figure 20. Analysis of activity metrics in response to capsaicin treatment

(**A**) Weighted mean firing rate (**B**) voltage comparison between control and capsaicin treated sample. Data analyzed using unpaired t-test, error bars represent SEM, *$p \leq 0.05$.

Electrode level analysis was then performed to further understand the composition of the bundles. In figure 21A, a representative graph shows changes in firing rate in response to capsaicin treatment (silent electrodes have been omitted) on each electrode and we see that several of the electrodes shown exhibited an increase in firing rate in response to capsaicin. We know that capsaicin elicits a response exclusively from TRPV1 expressing nociceptive neurons (Caterina et al., 2000) and so we wanted to investigate how individual axons within a bundle responded to capsaicin treatment.

For this, we further teased out each population of waveforms on individual electrodes. Analysis of electrode 36 is shown in figure 21B and C. Here, we see two distinct waveforms from two separate axons, a negative monophasic and a negative biphasic waveform which we refer to as population 1 and population 2. The firing rate of each of these populations is shown in figure 21C and it suggests that both these waveforms were consistent and reproducible. Interestingly, we see here that population 1 has no change in the firing rate in response to capsaicin whereas population 2 showed a significant increase in firing rates in response to the capsaicin. This suggested that population 2 is sensitive to capsaicin indicating that it is nociceptive in nature, whereas population 1 could be a different subclass of DRG neurons lacking the TRPV1 receptors. We see that about 64% of the waveforms analyzed showed a doubling of firing rates and about 35% (Figure 21D, n = 42) did not show any change to the addition of capsaicin.

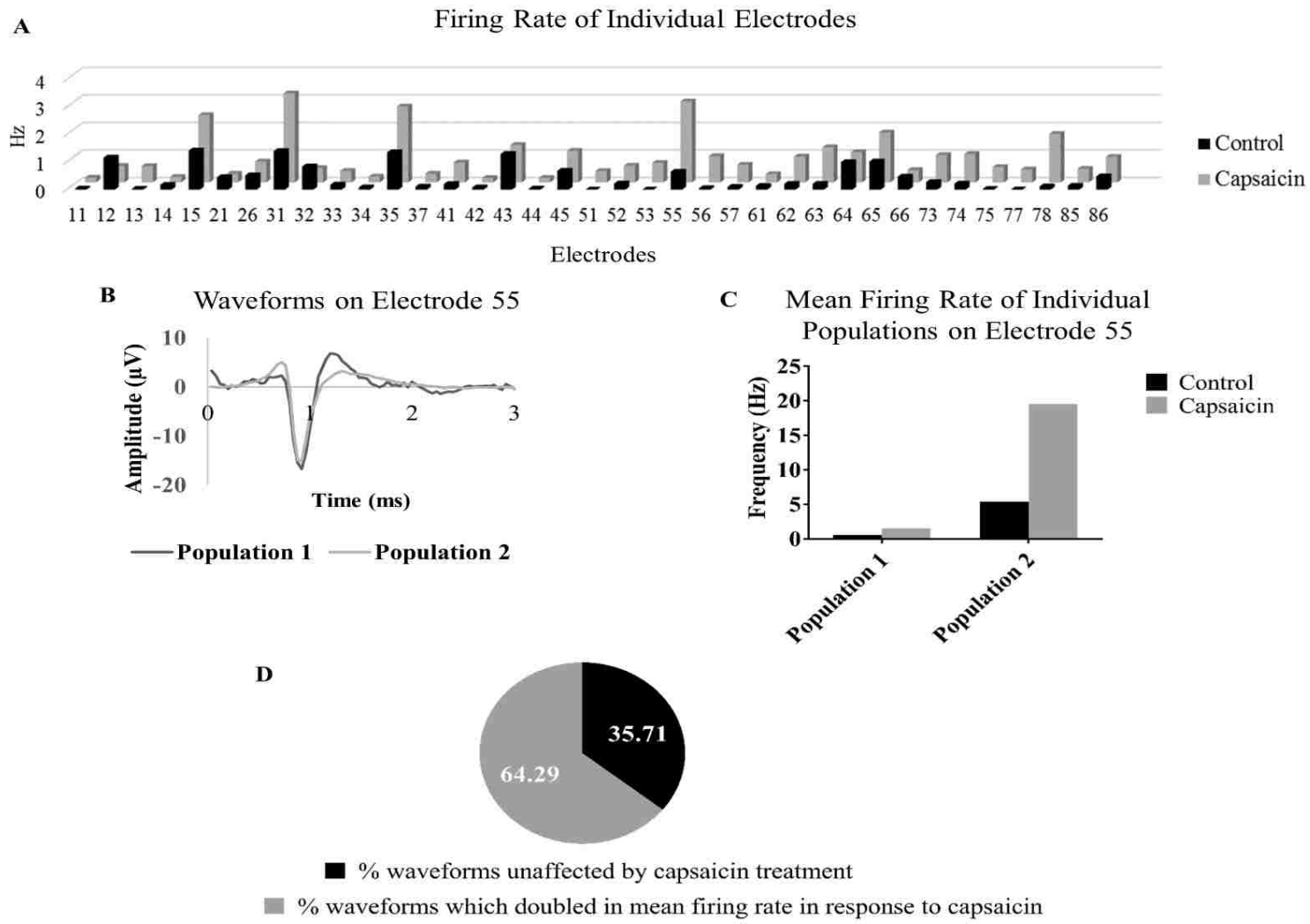

Figure 21. Analysis of firing rates of individual electrodes and populations of waveforms

(**A**) Firing rate of individual electrodes in response to capsaicin treatment (**B**) Analysis of waveforms on individual electrodes (**C**) Analysis of individual population of waveforms (**D**) Overall percentage of waveforms that respond to capsaicin treatment (n = 42)

Discussion

In this study, we have integrated an *in vitro* cultured three-dimensional 'nerve' on a microelectrode array. We have shown that this design and integration is a better model for investigating electrical activity from axons compared to traditional two-dimensional systems in terms of the ability to detect axonal activity. Moreover, by simply bundling the axons through Capgel™, we greatly improved our ability to record the spontaneous activity of DRG. We have also successfully shown that, this system facilitates the long-term monitoring of electrical activity of the same bundle of axons. Finally, we show here that the axon bundle composition within the capillaries is strikingly similar to an *in vivo* nerve.

There has been a renewed interest in acquiring axonal electrophysiological readings (Dworak & Wheeler, 2009; FitzGerald, Lacour, McMahon, & Fawcett, 2009; Lewandowska et al., 2015) but, these approaches required either patterning (Erickson, Tooker, Tai, & Pine, 2008; Nam, Chang, Khatami, Brewer, & Wheeler, 2004) or complex modification of the MEA surface (Dworak & Wheeler, 2009; Lewandowska et al., 2015; Musick, Khatami, & Wheeler, 2009; Wheeler & Brewer, 2010). The model we described here requires no modification to the commercially available MEAs and instead, we use a cheap and easily synthesizable biomaterial to generate the bundles of axons which can then be simply placed on top of the electrodes. Furthermore, most of the established models involving patterning lack the structural three-dimensional complexity that

is observed *in vivo*. Using Capgel™, we were able to generate a three-dimensional structure which offers a more realistic milieu in which the functional properties of neurons can be observed.

Capsaicin was used to chemically stimulate and sensitize DRG neurons in an attempt to show that heterogeneity with respect to the neuronal subtypes also exists within the bundles. Other groups have shown that 1µM concentration of capsaicin was sufficient to depolarize nociceptors (J. N. Wood et al., 1988). The growth media used in our experiments was supplemented with 50ng/ml NGF for axonal growth and survival of the nociceptive neurons. Interestingly, NGF is known to increase sensitization of the capsaicin receptor TRPV1 (Zhang, Huang, & McNaughton, 2005). Our analysis of waveforms whose frequency doubled or more in response to capsaicin treatment was shown to be around 64% which is similar to the reported percentage of nociceptor neurons within the DRG (Bautista et al., 2006). Overall, this supported the idea that we were able to recreate a functional model which closely resembled an *in vivo* nerve.

The microtunnel technology to detect axonal readings is based on the idea of increasing resistance to amplify the voltage of the axonal signals. Here, we showed that there is no increase in the voltage when axons were bundled and yet, we had improved firing rates. We speculate that this high rate of firing could be a result of ephaptic coupling of axons. Typical axonal bundles shown in figure 16D and E reveal the organization of the axonal bundles. We see several axons identified by punctate β-3-tubulin staining along with glial cells identified by DAPI and these are compact structures. Because of the tightness and the close proximity of the axons within the bundle, it is possible that a single depolarization event could induce an action potential in another axon within the same bundle and contribute to the high firing rates observed. Interestingly, this arrangement was similar to the structure of the early developing nerve seen *in vivo* (Jessen & Mirsky, 2005).

Around embryonic day 14-18 in rats, the nerve remains as a compact structure with early Schwann cells within and outside the bundles of axons with no connective tissue space. The process of myelination is initiated shortly after birth and the organization of the nerves drastically change, which includes segregation of axons for radial sorting necessary for myelination and the formation of connective tissue. We have previously shown that we can induce myelination in the DRG axons grown within Capgel™ (Anderson et al., under review) and it would be interesting to determine whether induction of myelination would affect this ephaptic phenomenon. Alternatively, we also consider the possibility that the improved firing rates could be a result of how tightly the bundles interface with the electrode (Buitenweg et al., 2002). It is possible the alginate component of the biomaterial acts as an uptake reservoir for cations such as sodium and potassium which may influence ephaptic coupling by altering local osmotic and electrochemical pressure and thus membrane charge (L. Mongar & Wassermann, 1949; Silva, Manso, Rodrigues, & Lagoa, 2008; Tveito et al., 2017).

The model described here offers the structural complexity that allows us to directly investigate these observations and further evaluate the DRG excitability especially in the context of pain. The development of this functional artificial nerve and integration with an MEA offers high throughput, non-invasive measurement of electrical properties, which can be used as a platform for modeling neuropathic pain.

CHAPTER FOUR: CONCLUSIONS

This project provides insight into the development and differentiation potential of the elusive SGCs and promotes the idea of the regenerative potential within the DRG. We describe here, for the first time, a detailed description of the isolation of SGCs which could be highly valuable for the field in general. Further, we also show the development and characterization of an *in vitro* model where SGC-somal contacts are retained, and this facilitates the use of this model as a tool to study SGCs especially in the context of neuropathic pain. These findings are highly exciting, and this work opens up new avenues that warrant further investigation.

Questions remain about the signals that are involved in the specification of SCGs. It remains to be determined whether a simple removal of these signals results in the differentiation of SGCs to SCs or whether the spatial expression of signals (soma vs. axonal signals) are important in this differentiation pathway. Neuregulins are an obvious candidate that could be playing an important role in SGC differentiation. Neuregulins are a family of proteins that are important in SC differentiation. Neuregulin isoforms are differentially expressed on the axon and the soma, SMDF being the major axonal form. It was shown that knockdown of SMDF affected only SC numbers and not SGCs numbers (Garratt, Britsch, & Birchmeier, 2000) which suggested that the SMDF signal was not crucial for SGC specification. It also invites the question whether it is a lack of this axonal neuregulin signal that leads to the formation of SGCs.

Notch is another important signal that could be involved in SGC development and maintenance. We know that Notch signaling is vital for glial specification of neural crest cells, and moreover, it was shown that ablation of the effectors of Notch signaling impairs SGC development (Woodhoo

et al., 2009). Expression of Notch on the DRG soma could possibly arrest SGCs in their native state. But much remains to be explored, including determining whether the components of notch are present in the adult ganglia.

Cadherin-19 (CDH19) is a type II classic calcium-dependent cell adhesion molecule and Takahashi *et al*. have shown a temporal expression of CDH19 in the SC developmental pathway by exclusive expression in the SC precursor state. But, the significance of this expression and the role it plays in the developmental pathway has not been explored (Takahashi & Osumi, 2005). Similarly, although we identified the expression of CDH19 in SGCs within the adult DRG, we were not any closer to identifying the role of this signaling molecule. We noted a downregulation in the expression of CDH19 as soon as SGCs migrated away from the soma, and based on this observation, it is likely that expression and downregulation might be essential signals specifying the maintenance and differentiation of SGCs respectively.

Adding to the complexity of these observations is that adult SCs, which do not appear to express CDH19, are capable of ensheathing mature DRG soma (unpublished observations, Figure 22) suggesting that, other unidentified adhesion molecules may also play a role in the SGC/neuronal cell body interaction. Although these SCs can ensheathe the neuronal cell body they do not express SGC markers such as GS. Figure 22 identifies SCs ensheathing purified neurons using P0 marker, a marker expressed in SC precursors and immature SCs.

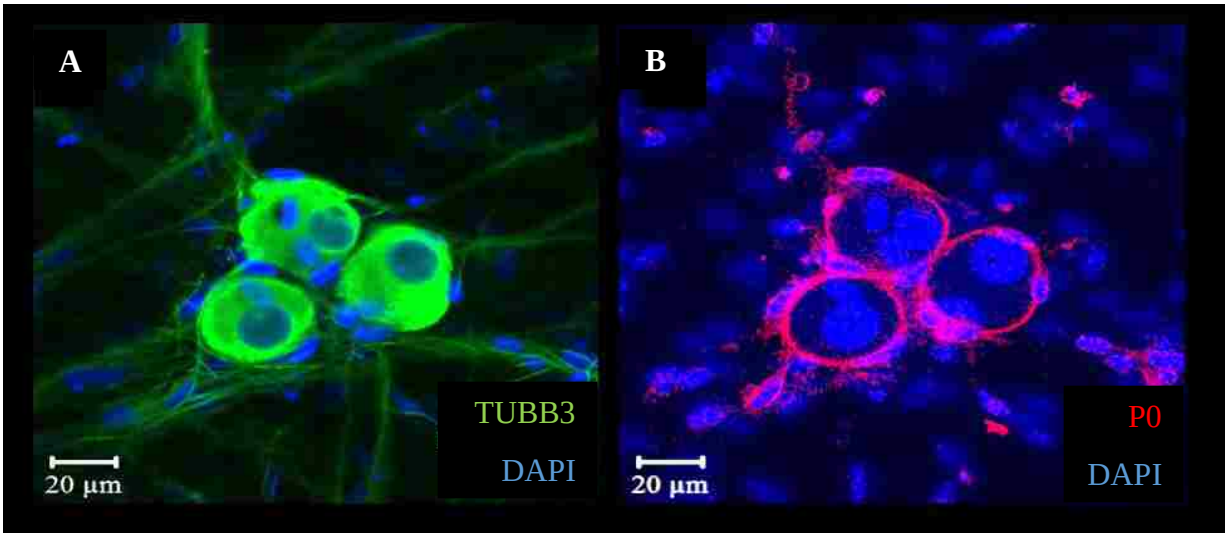

Figure 22. SCs ensheathing neurons

(A, B) FUdR treated E15 DRG neurons where SCs isolated from postnatal day 2 rats were added at 10 DIV.

We observed in our two-dimensional cultures an increase in the number of SGCs that expressed Ki67 after 48 hours of capsaicin treatment (unpublished data, Figure 23) but, our efforts to investigate the mechanism underlying this change was thwarted by the fact that SGCs migrated away from the neurons. We had previously determined that this increase in Ki67 expression was a neuron-specific effect as SGCs (fraction 3) when treated with capsaicin in the absence of neurons showed no changes to Ki67 expression. Interestingly, contact inhibition of proliferation is a downstream signaling effect of cadherins (Klezovitch & Vasioukhin, 2015) and it would be interesting to see if these signals are at play here.

Alternatively, ATP signaling is known to promote proliferation, and combining the fact that SGCs expresses the receptor for ATP (P2X7) and that an increase in gap junction-mediated coupling is observed in response to injury (Menachem Hanani, 2012), we hypothesize that neuronal ATP released via gap junctions modulate the proliferation of SGCs (Figure 24). Again, the significance of proliferation can only be speculated. Studies have implicated SGCs as the source of cells that replenish the neurons that have undergone apoptosis in response to capsaicin treatment (Z. Gallaher, T. Johnston, & Czaja, 2014). Considering the expression of Sox2 in SGCs, a factor important in the regulation of pluripotency (Koike et al., 2015) and our work that establishes the plasticity of SGCs, it would be within reason to predict that given the right cues, SGCs could differentiate to neurons.

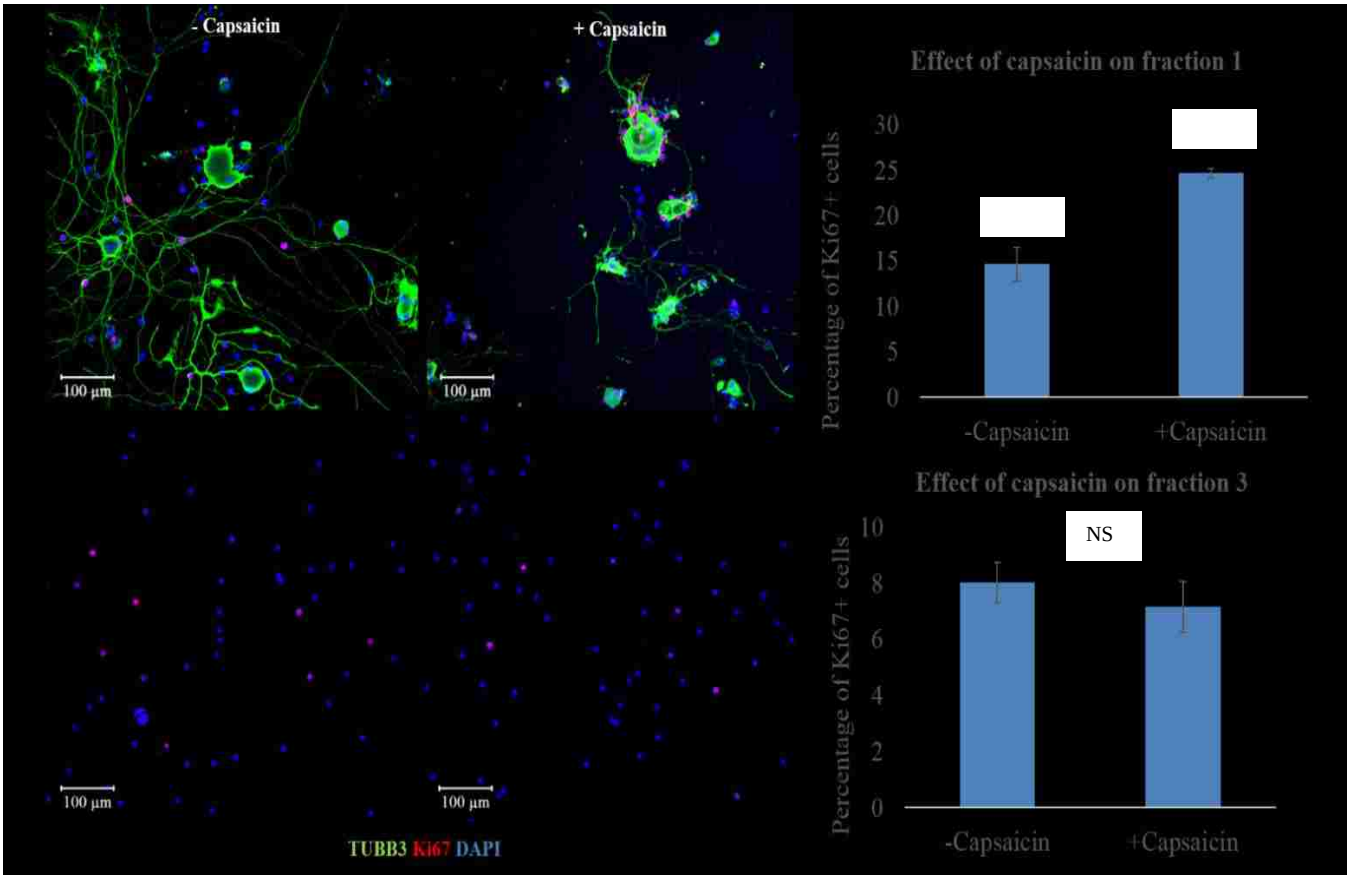

Figure 23. Ki67 staining in response to capsaicin treatment in fraction 1 and fraction 3

Images show fraction 1 and fraction 3 identified using TUBB3, Ki67 and DAPI. Data compared using student's t-test.

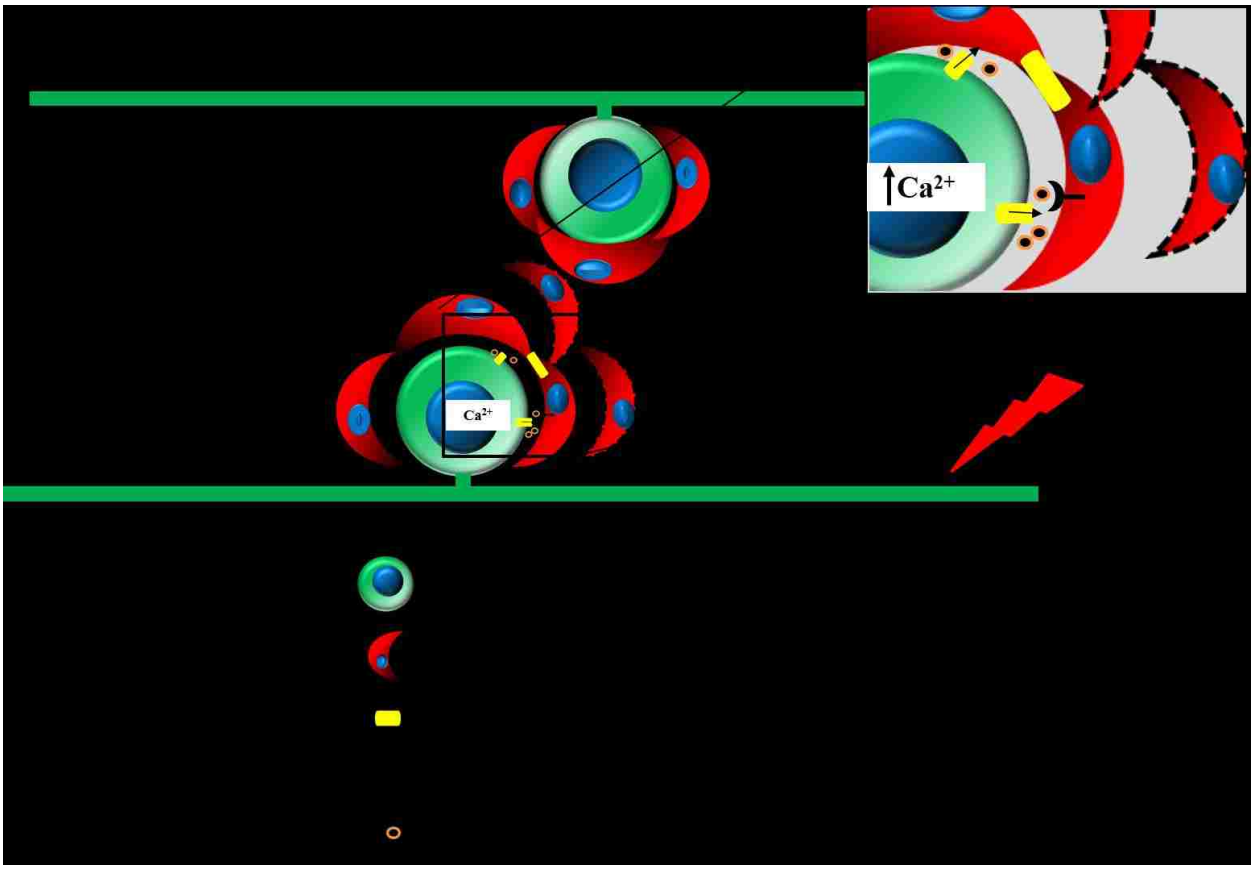

Image by author

Figure 24. Proposed model

Dotted cells indicate the newly formed cells that arise in response to the ATP signaling after neuropathic injury

We can now start to uncover the mechanism by which this expression change occurs using our three-dimensional model. Our overall motivation was to design a system wherein we could study changes that occur in SGCs under neuropathic pain conditions. Although we successfully developed and characterized the novel model described, we were not able to directly assess the

changes in SGCs that contributed to the capsaicin-evoked hyperexcitability of the neurons because we ran out of time. The potential for further studies in this area is promising.

DRGs do not undergo synchronous firing as these neurons lack dendrites. But, studies have shown that increased coupling occurs between SGCs surrounding different neurons in response to injury. When we added capsaicin to our three-dimensional model, we were able to detect network burst/synchrony in firing across many electrodes (Figure 25). It would be important to determine whether this bursting activity is a mediated via SGCs. Participation of SGCs in this manner could explain the underlying basis of neuronal hyperexcitability that is observed in injury.

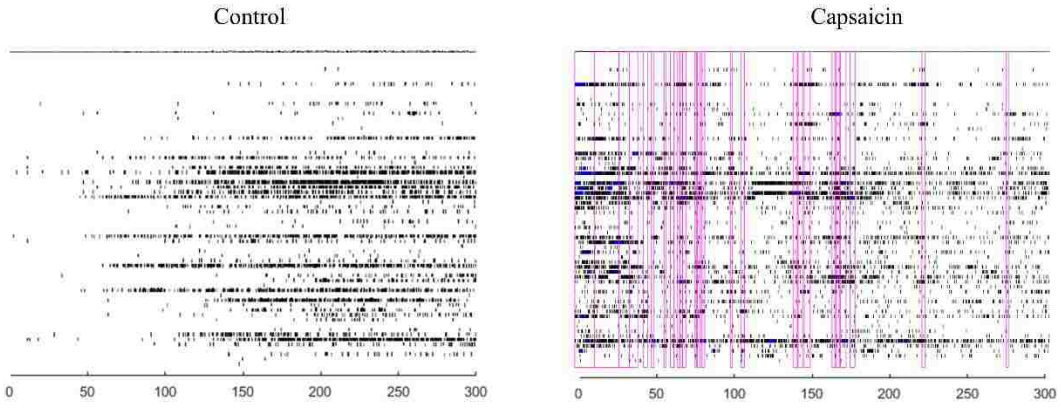

Figure 25. Raster plot showing spike trains
Network burst criteria min # spikes 10, max interspike interval 100ms, min electrodes (%) 30

One way to determine their contribution would be to use drugs like carbenoxolone that block gap junctions and measure changes in network bursts. An alternate approach would be to utilize fractions of neurons with and without SGCs directly placed on top of Capgel™ blocks to assess activity differences. In line with the idea that SGCs may be involved in inducing this sort of

network synchrony, it would be interesting to electrically stimulate axonal bundles to determine the changes in firing rates in the axonal bundles apposed on different electrodes.

As shown in figure 16, the Capgel™ blocks can be sectioned near the explant implant site to study the structure and organization of SGCs around the DRG soma. For example, we can specifically examine SGCs that surround nociceptive neurons by using specific markers like TRPV1 and determine the changes that occur in response to capsaicin treatment including the expression of Ki67. Although the three-dimensional model is discussed here only in the perspective of a neuropathic pain model, the system itself has enormous potential applications and can be used as a tool to study electrical properties during development.

APPENDIX: COPYRIGHT PERMISSION LETTER

JOHN WILEY AND SONS LICENSE TERMS AND CONDITIONS

Mar 16, 2018

This Agreement between Mrs. Dale George ("You") and John Wiley and Sons ("John Wiley and Sons") consists of your license details and the terms and conditions provided by John Wiley and Sons and Copyright Clearance Center.

License Number	4310890035238
License date	Mar 16, 2018
Licensed Content Publisher	John Wiley and Sons
Licensed Content Publication	GLIA
Licensed Content Title	Satellite glial cells represent a population of developmentally arrested Schwann cells
Licensed Content Author	Dale George,Paige Ahrens,Stephen Lambert
Licensed Content Date	Mar 9, 2018
Licensed Content Pages	1
Type of use	Dissertation/Thesis
Requestor type	Author of this Wiley article
Format	Print and electronic
Portion	Full article
Will you be translating?	No
Title of your thesis / dissertation	Dissecting the Components of Neuropathic Pain
Expected completion date	Apr 2018
Expected size (number of pages)	100
Requestor Location	Mrs. Dale George 13221 Silver strand falls drive ORLANDO, FL 32824 United States Attn: Mrs. Dale George
Publisher Tax ID	EU826007151
Total	0.00 USD

REFERENCES

Aldskogius, H., & Arvidsson, J. (1978). Nerve cell degeneration and death in the trigeminal ganglion of the adult rat following peripheral nerve transection. *Journal of Neurocytology, 7*(2), 229-250. doi:10.1007/bf01217921

Aldskogius, H., & Kozlova, E. N. (1998). Central neuron–glial and glial–glial interactions following axon injury. *Progress in Neurobiology, 55*(1), 1-26. doi:https://doi.org/10.1016/S0301-0082(97)00093-2

Allen, D. T., & Kiernan, J. A. (1994). Permeation of proteins from the blood into peripheral nerves and ganglia. *Neuroscience, 59*(3), 755-764. doi:https://doi.org/10.1016/0306-4522(94)90192-9

Amir, R., & Devor, M. (2003). Electrical excitability of the soma of sensory neurons is required for spike invasion of the soma, but not for through-conduction. *Biophys J, 84*(4), 2181-2191. doi:10.1016/S0006-3495(03)75024-3

Arvidson, B. (1979). Distribution of intravenously injected protein tracers in peripheral ganglia of adult mice. *Experimental Neurology, 63*(2), 388-410. doi:https://doi.org/10.1016/0014-4886(79)90134-1

Attal, N., Jazat, F., Kayser, V., & Guilbaud, G. (1990). Further evidence for 'pain-related' behaviours in a model of unilateral peripheral mononeuropathy. *Pain, 41*(2), 235-251.

Backonja, M., & Woolf, C. J. (2010). Future directions in neuropathic pain therapy: closing the translational loop. *Oncologist, 15 Suppl 2*, 24-29. doi:10.1634/theoncologist.2009-S502

Bala, U., Tan, K. L., Ling, K. H., & Cheah, P. S. (2014). Harvesting the maximum length of sciatic nerve from adult mice: a step-by-step approach. *BMC Res Notes, 7*, 714. doi:10.1186/1756-0500-7-714

Barber, L. A., & Vasko, M. R. (1996). Activation of protein kinase C augments peptide release from rat sensory neurons. *J Neurochem, 67*(1), 72-80.

Bautista, D. M., Jordt, S.-E., Nikai, T., Tsuruda, P. R., Read, A. J., Poblete, J., . . . Julius, D. (2006). TRPA1 Mediates the Inflammatory Actions of Environmental Irritants and Proalgesic Agents. *Cell, 124*(6), 1269-1282. doi:https://doi.org/10.1016/j.cell.2006.02.023

Belzer, V., Shraer, N., & Hanani, M. (2010). *Phenotypic changes in satellite glial cells in cultured trigeminal ganglia* (Vol. 6).

Belzer, V., Shraer, N., & Hanani, M. (2010). Phenotypic changes in satellite glial cells in cultured trigeminal ganglia. *Neuron Glia Biol, 6*(4), 237-243. doi:10.1017/S1740925X1100007X

Berger, U. V., & Hediger, M. A. (2000). Distribution of the glutamate transporters GLAST and GLT-1 in rat circumventricular organs, meninges, and dorsal root ganglia. *J Comp Neurol, 421*(3), 385-399. Retrieved from http://www.ncbi.nlm.nih.gov/pubmed/10813794

Bowery, N. G., Brown, D. A., & Marsh, S. (1979). gamma-Aminobutyric acid efflux from sympathetic glial cells: effect of 'depolarizing' agents. *J Physiol, 293*, 75-101. Retrieved from http://www.ncbi.nlm.nih.gov/pubmed/501652

Breslin, S., & O'Driscoll, L. (2013). Three-dimensional cell culture: the missing link in drug discovery. *Drug Discov Today, 18*(5-6), 240-249. doi:10.1016/j.drudis.2012.10.003

Britsch, S., Goerich, D. E., Riethmacher, D., Peirano, R. I., Rossner, M., Nave, K. A., . . . Wegner, M. (2001). The transcription factor Sox10 is a key regulator of peripheral glial development. *Genes Dev, 15*(1), 66-78. Retrieved from http://www.ncbi.nlm.nih.gov/pubmed/11156606

Buitenweg, J. R., Rutten, W. L., & Marani, E. (2002). Modeled channel distributions explain extracellular recordings from cultured neurons sealed to microelectrodes. *IEEE Trans Biomed Eng, 49*(12 Pt 2), 1580-1590. doi:10.1109/TBME.2002.805555

Callizot, N., Combes, M., Steinschneider, R., & Poindron, P. (2011). A new long term in vitro model of myelination. *Exp Cell Res, 317*(16), 2374-2383. doi:10.1016/j.yexcr.2011.07.002

Castillon, N., Hinnrasky, J., Zahm, J. M., Kaplan, H., Bonnet, N., Corlieu, P., . . . Puchelle, E. (2002). Polarized expression of cystic fibrosis transmembrane conductance regulator and associated epithelial proteins during the regeneration of human airway surface epithelium in three-dimensional culture. *Lab Invest, 82*(8), 989-998. Retrieved from http://www.ncbi.nlm.nih.gov/pubmed/12177237

Caterina, M. J., Leffler, A., Malmberg, A. B., Martin, W. J., Trafton, J., Petersen-Zeitz, K. R., . . . Julius, D. (2000). Impaired nociception and pain sensation in mice lacking the capsaicin receptor. *Science, 288*(5464), 306-313. Retrieved from http://www.ncbi.nlm.nih.gov/pubmed/10764638

Caterina, M. J., Schumacher, M. A., Tominaga, M., Rosen, T. A., Levine, J. D., & Julius, D. (1997). The capsaicin receptor: a heat-activated ion channel in the pain pathway. *Nature, 389*(6653), 816-824. doi:10.1038/39807

Chang, J. C., Brewer, G. J., & Wheeler, B. C. (2000). Microelectrode Array Recordings of Patterned Hippocampal Neurons for Four Weeks. *Biomedical Microdevices, 2*(4), 245-253. doi:10.1023/a:1009946920296

Chang, J. C., Brewer, G. J., & Wheeler, B. C. (2001). Modulation of neural network activity by patterning. *Biosens Bioelectron, 16*(7-8), 527-533.

Cherkas, P. S., Huang, T. Y., Pannicke, T., Tal, M., Reichenbach, A., & Hanani, M. (2004). The effects of axotomy on neurons and satellite glial cells in mouse trigeminal ganglion. *Pain, 110*(1-2), 290-298. doi:10.1016/j.pain.2004.04.007

Courteix, C., Eschalier, A., & Lavarenne, J. (1993). Streptozocin-induced diabetic rats: behavioural evidence for a model of chronic pain. *Pain, 53*(1), 81-88.

Curtis, R., Stewart, H. J., Hall, S. M., Wilkin, G. P., Mirsky, R., & Jessen, K. R. (1992). GAP-43 is expressed by nonmyelin-forming Schwann cells of the peripheral nervous system. *J*

Cell Biol, 116(6), 1455-1464. Retrieved from http://www.ncbi.nlm.nih.gov/pubmed/1531832

Deligkaris, K., Bullmann, T., & Frey, U. (2016). Extracellularly Recorded Somatic and Neuritic Signal Shapes and Classification Algorithms for High-Density Microelectrode Array Electrophysiology. *Front Neurosci, 10*, 421. doi:10.3389/fnins.2016.00421

Desai, A., Kisaalita, W. S., Keith, C., & Wu, Z. Z. (2006). Human neuroblastoma (SH-SY5Y) cell culture and differentiation in 3-D collagen hydrogels for cell-based biosensing. *Biosens Bioelectron, 21*(8), 1483-1492. doi:10.1016/j.bios.2005.07.005

Dubin, A. E., & Patapoutian, A. (2010). Nociceptors: the sensors of the pain pathway. *J Clin Invest, 120*(11), 3760-3772. doi:10.1172/JCI42843

Dworak, B. J., & Wheeler, B. C. (2009). Novel MEA platform with PDMS microtunnels enables the detection of action potential propagation from isolated axons in culture. *Lab Chip, 9*(3), 404-410. doi:10.1039/b806689b

Dyachuk, V., Furlan, A., Shahidi, M. K., Giovenco, M., Kaukua, N., Konstantinidou, C., . . . Adameyko, I. (2014). Neurodevelopment. Parasympathetic neurons originate from nerve-associated peripheral glial progenitors. *Science, 345*(6192), 82-87. doi:10.1126/science.1253281

Edelman, D. B., & Keefer, E. W. (2005). A cultural renaissance: in vitro cell biology embraces three-dimensional context. *Exp Neurol, 192*(1), 1-6. doi:10.1016/j.expneurol.2004.10.005

Egan, M. D. Talmage D. (2005). Miller's Anesthesia, 6th Edition. *Anesthesiology, 103*(3), 673-673. Retrieved from http://dx.doi.org/

Elson, K., Ribeiro, R. M., Perelson, A. S., Simmons, A., & Speck, P. (2004). The life span of ganglionic glia in murine sensory ganglia estimated by uptake of bromodeoxyuridine. *Experimental Neurology, 186*(1), 99-103. doi:https://doi.org/10.1016/j.expneurol.2003.10.017

Enright, H. A., Felix, S. H., Fischer, N. O., Mukerjee, E. V., Soscia, D., McNerney, M., . . . Pannu, S. (2016). Long-term non-invasive interrogation of human dorsal root ganglion neuronal cultures on an integrated microfluidic multielectrode array platform. *Analyst, 141*(18), 5346-5357. doi:10.1039/c5an01728a

Erickson, J., Tooker, A., Tai, Y. C., & Pine, J. (2008). Caged neuron MEA: a system for long-term investigation of cultured neural network connectivity. *J Neurosci Methods, 175*(1), 1-16. doi:10.1016/j.jneumeth.2008.07.023

Espinosa-Medina, I., Outin, E., Picard, C. A., Chettouh, Z., Dymecki, S., Consalez, G. G., . . . Brunet, J.-F. (2014a). Parasympathetic ganglia derive from Schwann cell precursors. *Science, 345*(6192), 87-90. doi:10.1126/science.1253286

Espinosa-Medina, I., Outin, E., Picard, C. A., Chettouh, Z., Dymecki, S., Consalez, G. G., . . . Brunet, J. F. (2014b). Neurodevelopment. Parasympathetic ganglia derive from Schwann cell precursors. *Science, 345*(6192), 87-90. doi:10.1126/science.1253286

Fex Svenningsen, A., Colman, D. R., & Pedraza, L. (2004). Satellite cells of dorsal root ganglia are multipotential glial precursors. *Neuron Glia Biol, 1*(1), 85-93. doi:doi:10.1017/S1740925X04000110

Fex Svenningsen, A., Shan, W. S., Colman, D. R., & Pedraza, L. (2003). Rapid method for culturing embryonic neuron-glial cell cocultures. *J Neurosci Res, 72*(5), 565-573. doi:10.1002/jnr.10610

FitzGerald, J. J., Lacour, S. P., McMahon, S. B., & Fawcett, J. W. (2009). Microchannel electrodes for recording and stimulation: in vitro evaluation. *IEEE Trans Biomed Eng, 56*(5), 1524-1534. doi:10.1109/TBME.2009.2013960

Fleetwood-Walker, S. M., Quinn, J. P., Wallace, C., Blackburn-Munro, G., Kelly, B. G., Fiskerstrand, C. E., . . . Dalziel, R. G. (1999). Behavioural changes in the rat following infection with varicella-zoster virus. *J Gen Virol, 80 (Pt 9)*, 2433-2436. doi:10.1099/0022-1317-80-9-2433

Gallaher, Z., T. Johnston, S., & Czaja, K. (2014). *Neural Proliferation in the Dorsal Root Ganglia of the Adult Rat Following Capsaicin-Induced Neuronal Death* (Vol. 522).

Gallaher, Z. R., Ryu, V., Larios, R. M., Sprunger, L. K., & Czaja, K. (2011). Neural Proliferation and Restoration of Neurochemical Phenotypes and Compromised Functions Following Capsaicin-Induced Neuronal Damage in the Nodose Ganglion of the Adult Rat. *Frontiers in Neuroscience, 5*, 12. doi:10.3389/fnins.2011.00012

Garratt, A., Britsch, S., & Birchmeier, C. (2000). *Garratt AN, Britsch S, Birchmeier C.. Neuregulin, a factor with many functions in the life of a Schwann cell. Bioessays 22: 987-996* (Vol. 22).

Goldman, S. (2003). Glia as neural progenitor cells. *Trends in Neurosciences, 26*(11), 590-596. doi:https://doi.org/10.1016/j.tins.2003.09.011

Griscom, L., Degenaar, P., LePioufle, B., Tamiya, E., & Fujita, H. (2002). Techniques for patterning and guidance of primary culture neurons on micro-electrode arrays. *Sensors and Actuators B: Chemical, 83*(1), 15-21. doi:https://doi.org/10.1016/S0925-4005(01)01022-X

Haines, D. E., & Mihailoff, G. A. (2018). *Fundamental neuroscience for basic and clinical applications*.

Hall, A. K. (2006). Rodent sensory neuron culture and analysis. *Curr Protoc Neurosci, Chapter 3*, Unit 3 19. doi:10.1002/0471142301.ns0319s36

Hanani, M. (2005). Satellite glial cells in sensory ganglia: from form to function. *Brain Res Brain Res Rev, 48*(3), 457-476. doi:10.1016/j.brainresrev.2004.09.001

Hanani, M. (2010). Satellite glial cells: more than just 'rings around the neuron'. *Neuron Glia Biol, 6*(1), 1-2. doi:10.1017/S1740925X10000104

Hanani, M. (2012). Intercellular communication in sensory ganglia by purinergic receptors and gap junctions: Implications for chronic pain. *Brain Research, 1487*, 183-191. doi:https://doi.org/10.1016/j.brainres.2012.03.070

Hanani, M., Huang, T. Y., Cherkas, P. S., Ledda, M., & Pannese, E. (2002a). Glial cell plasticity in sensory ganglia induced by nerve damage. *Neuroscience, 114*(2), 279-283. Retrieved from http://www.ncbi.nlm.nih.gov/pubmed/12204197

Hanani, M., Huang, T. Y., Cherkas, P. S., Ledda, M., & Pannese, E. (2002b). Glial cell plasticity in sensory ganglia induced by nerve damage. *Neuroscience, 114*(2), 279-283. doi:https://doi.org/10.1016/S0306-4522(02)00279-8

HANSSON, E., & RÖNNBÄCK, L. (2003). Glial neuronal signaling in the central nervous system. *The FASEB Journal, 17*(3), 341-348. doi:10.1096/fj.02-0429rev

Harper, A. A., & Lawson, S. N. (1985). Conduction velocity is related to morphological cell type in rat dorsal root ganglion neurones. *The Journal of Physiology, 359*, 31-46. Retrieved from http://www.ncbi.nlm.nih.gov/pmc/articles/PMC1193363/

Haydon, P. G. (2001). Glia: listening and talking to the synapse. *Nature Reviews Neuroscience, 2*, 185. doi:10.1038/35058528

Heinricher, M. M., Cheng, Z. F., & Fields, H. L. (1987). Evidence for two classes of nociceptive modulating neurons in the periaqueductal gray. *J Neurosci, 7*(1), 271-278. Retrieved from http://www.ncbi.nlm.nih.gov/pubmed/3806198

Holmes, D. (2016). The pain drain. *Nature, 535*(7611), S2-3. doi:10.1038/535S2a

Hosli, L., Andres, P. F., & Hosli, E. (1978). Neuron-glia interactions: indirect effect of GABA on cultured glial cells. *Exp Brain Res, 33*(3-4), 425-434. Retrieved from http://www.ncbi.nlm.nih.gov/pubmed/215433

Huang, T. Y., Cherkas, P. S., Rosenthal, D. W., & Hanani, M. (2005). Dye coupling among satellite glial cells in mammalian dorsal root ganglia. *Brain Res, 1036*(1-2), 42-49. doi:10.1016/j.brainres.2004.12.021

Humbertson, A., Jr., Zimmermann, E., & Leedy, M. (1969). A chronological study of mitotic activity in satellite cell hyperplasia associated with chromatolytic neurons. *Z Zellforsch Mikrosk Anat, 100*(4), 507-515. Retrieved from http://www.ncbi.nlm.nih.gov/pubmed/5351191

Humbertson, A., Zimmermann, E., & Leedy, M. (1969). A chronological study of mitotic activity in satellite cell hyperplasia associated with chromatolytic neurons. *Zeitschrift für Zellforschung und Mikroskopische Anatomie, 100*(4), 507-515. doi:10.1007/bf00344371

Immke, D. C., & Gavva, N. R. (2006). The TRPV1 receptor and nociception. *Semin Cell Dev Biol, 17*(5), 582-591. doi:10.1016/j.semcdb.2006.09.004

Irons, H. R., Cullen, D. K., Shapiro, N. P., Lambert, N. A., Lee, R. H., & Laplaca, M. C. (2008). Three-dimensional neural constructs: a novel platform for neurophysiological investigation. *J Neural Eng, 5*(3), 333-341. doi:10.1088/1741-2560/5/3/006

Jessen, K. R., Brennan, A., Morgan, L., Mirsky, R., Kent, A., Hashimoto, Y., & Gavrilovic, J. (1994). The Schwann cell precursor and its fate: a study of cell death and differentiation during gliogenesis in rat embryonic nerves. *Neuron, 12*(3), 509-527.

Jessen, K. R., & Mirsky, R. (1997). Embryonic Schwann cell development: the biology of Schwann cell precursors and early Schwann cells. *J Anat, 191 (Pt 4)*, 501-505. Retrieved from http://www.ncbi.nlm.nih.gov/pubmed/9449069

https://www.ncbi.nlm.nih.gov/pmc/articles/PMC1467717/pdf/joa_1914_0501.pdf

Jessen, K. R., & Mirsky, R. (1998). Origin and early development of Schwann cells. *Microsc Res Tech, 41*(5), 393-402. doi:10.1002/(sici)1097-0029(19980601)41:5<393::aid-jemt6>3.0.co;2-r

Jessen, K. R., & Mirsky, R. (2005). The origin and development of glial cells in peripheral nerves. *Nat Rev Neurosci, 6*(9), 671-682. doi:10.1038/nrn1746

Joseph, N. M., Mukouyama, Y. S., Mosher, J. T., Jaegle, M., Crone, S. A., Dormand, E. L., . . . Morrison, S. J. (2004). Neural crest stem cells undergo multilineage differentiation in developing peripheral nerves to generate endoneurial fibroblasts in addition to Schwann cells. *Development, 131*(22), 5599-5612. doi:10.1242/dev.01429

Klezovitch, O., & Vasioukhin, V. (2015). Cadherin signaling: keeping cells in touch. *F1000Research, 4*(F1000 Faculty Rev), 550. doi:10.12688/f1000research.6445.1

Koike, T., Wakabayashi, T., Mori, T., Hirahara, Y., & Yamada, H. (2015). Sox2 promotes survival of satellite glial cells in vitro. *Biochem Biophys Res Commun, 464*(1), 269-274. doi:10.1016/j.bbrc.2015.06.141

Kumamoto, T., Fukuhara, N., Miyatake, T., Araki, K., Takahashi, Y., & Araki, S. (1986). Experimental Neuropathy Induced by Methyl Mercury Compounds: Autoradiographic Study of GABA Uptake by Dorsal Root Ganglia. *European Neurology, 25*(4), 269-277. Retrieved from https://www.karger.com/DOI/10.1159/000116020

L. Mongar, J., & Wassermann, A. (1949). *Fully swollen alginate gels as permutites: kinetics of calcium?sodium ion exchange* (Vol. 7).

Lawson, S. N., Caddy, K. W., & Biscoe, T. J. (1974). Development of rat dorsal root ganglion neurones. Studies of cell birthdays and changes in mean cell diameter. *Cell Tissue Res, 153*(3), 399-413. Retrieved from http://www.ncbi.nlm.nih.gov/pubmed/4458950

Ledda, M., De Palo, S., & Pannese, E. (2004). Ratios between number of neuroglial cells and number and volume of nerve cells in the spinal ganglia of two species of reptiles and three species of mammals. *Tissue Cell, 36*(1), 55-62.

Lee, K. H., Chung, K., Chung, J. M., & Coggeshall, R. E. (1986). Correlation of cell body size, axon size, and signal conduction velocity for individually labelled dorsal root ganglion cells in the cat. *J Comp Neurol, 243*(3), 335-346. doi:10.1002/cne.902430305

Lewandowska, M. K., Bakkum, D. J., Rompani, S. B., & Hierlemann, A. (2015). Recording large extracellular spikes in microchannels along many axonal sites from individual neurons. *PLoS One, 10*(3), e0118514. doi:10.1371/journal.pone.0118514

Li, L., & Zhou, X.-F. (2001). Pericellular Griffonia simplicifolia I isolectin B4-binding ring structures in the dorsal root ganglia following peripheral nerve injury in rats. *The Journal of Comparative Neurology, 439*(3), 259-274. doi:10.1002/cne.1349

Liu, Z., Jin, Y. Q., Chen, L., Wang, Y., Yang, X., Cheng, J., . . . Shen, Z. (2015). Specific marker expression and cell state of Schwann cells during culture in vitro. *PLoS One, 10*(4), e0123278. doi:10.1371/journal.pone.0123278

Malin, S. A., Davis, B. M., & Molliver, D. C. (2007). Production of dissociated sensory neuron cultures and considerations for their use in studying neuronal function and plasticity. *Nat Protoc, 2*(1), 152-160. doi:10.1038/nprot.2006.461

Mao, C., & Kisaalita, W. S. (2004). Characterization of 3-D collagen hydrogels for functional cell-based biosensing. *Biosens Bioelectron, 19*(9), 1075-1088. doi:10.1016/j.bios.2003.10.008

Marchand, S. (2008). The physiology of pain mechanisms: from the periphery to the brain. *Rheum Dis Clin North Am, 34*(2), 285-309. doi:10.1016/j.rdc.2008.04.003

Marmigere, F., & Ernfors, P. (2007). Specification and connectivity of neuronal subtypes in the sensory lineage. *Nat Rev Neurosci, 8*(2), 114-127. doi:10.1038/nrn2057

Maro, G. S., Vermeren, M., Voiculescu, O., Melton, L., Cohen, J., Charnay, P., & Topilko, P. (2004). Neural crest boundary cap cells constitute a source of neuronal and glial cells of the PNS. *Nat Neurosci, 7*(9), 930-938. doi:10.1038/nn1299

Martini, R., Mohajeri, M. H., Kasper, S., Giese, K. P., & Schachner, M. (1995). Mice doubly deficient in the genes for P0 and myelin basic protein show that both proteins contribute to the formation of the major dense line in peripheral nerve myelin. *J Neurosci, 15*(6), 4488-4495.

Millan, M. J. (1999). The induction of pain: an integrative review. *Prog Neurobiol, 57*(1), 1-164. Retrieved from http://www.ncbi.nlm.nih.gov/pubmed/9987804

Miller, K. E., Richards, B. A., & Kriebel, R. M. (2002). Glutamine-, glutamine synthetase-, glutamate dehydrogenase- and pyruvate carboxylase-immunoreactivities in the rat dorsal root ganglion and peripheral nerve. *Brain Research, 945*(2), 202-211. doi:https://doi.org/10.1016/S0006-8993(02)02802-0

Mirsky, R., Woodhoo, A., Parkinson, D. B., Arthur-Farraj, P., Bhaskaran, A., & Jessen, K. R. (2008). Novel signals controlling embryonic Schwann cell development, myelination and dedifferentiation. *J Peripher Nerv Syst, 13*(2), 122-135. doi:10.1111/j.1529-8027.2008.00168.x

Montano, J. A., Perez-Pinera, P., Garcia-Suarez, O., Cobo, J., & Vega, J. A. (2010). Development and neuronal dependence of cutaneous sensory nerve formations: Lessons from neurotrophins. *Microsc Res Tech, 73*(5), 513-529. doi:10.1002/jemt.20790

Morrissey, T. K., Kleitman, N., & Bunge, R. P. (1991). Isolation and functional characterization of Schwann cells derived from adult peripheral nerve. *J Neurosci, 11*(8), 2433-2442. Retrieved from http://www.ncbi.nlm.nih.gov/pubmed/1869923

Musick, K., Khatami, D., & Wheeler, B. C. (2009). Three-dimensional micro-electrode array for recording dissociated neuronal cultures. *Lab Chip, 9*(14), 2036-2042. doi:10.1039/b820596e

Nadeau, J. R., Wilson-Gerwing, T. D., & Verge, V. M. (2014). Induction of a reactive state in perineuronal satellite glial cells akin to that produced by nerve injury is linked to the level of p75NTR expression in adult sensory neurons. *Glia, 62*(5), 763-777. doi:10.1002/glia.22640

Nam, Y., Chang, J., Khatami, D., Brewer, G. J., & Wheeler, B. C. (2004). Patterning to enhance activity of cultured neuronal networks. *IEE Proc Nanobiotechnol, 151*(3), 109-115. doi:10.1049/ip-nbt:20040706

Nam, Y., & Wheeler, B. C. (2011). In vitro microelectrode array technology and neural recordings. *Crit Rev Biomed Eng, 39*(1), 45-61. Retrieved from http://www.ncbi.nlm.nih.gov/pubmed/21488814

Narula, U., Ruiz, A., McQuaide, M., DeMarse, T. B., Wheeler, B. C., & Brewer, G. J. (2017). Narrow microtunnel technology for the isolation and precise identification of axonal communication among distinct hippocampal subregion networks. *PLoS One, 12*(5), e0176868. doi:10.1371/journal.pone.0176868

Newberry, K., Wang, S., Hoque, N., Kiss, L., Ahlijanian, M. K., Herrington, J., & Graef, J. D. (2016). Development of a spontaneously active dorsal root ganglia assay using multiwell multielectrode arrays. *J Neurophysiol, 115*(6), 3217-3228. doi:10.1152/jn.01122.2015

Obien, M. E. J., Deligkaris, K., Bullmann, T., Bakkum, D. J., & Frey, U. (2014). Revealing neuronal function through microelectrode array recordings. *Frontiers in Neuroscience, 8*, 423. doi:10.3389/fnins.2014.00423

Ohara, P. T., Vit, J.-P., Bhargava, A., Romero, M., Sundberg, C., Charles, A. C., & Jasmin, L. (2009). Gliopathic Pain: When Satellite Glial Cells Go Bad. *The Neuroscientist : a review journal bringing neurobiology, neurology and psychiatry, 15*(5), 450-463. doi:10.1177/1073858409336094

Ohara, P. T., Vit, J. P., Bhargava, A., & Jasmin, L. (2008). Evidence for a role of connexin 43 in trigeminal pain using RNA interference in vivo. *J Neurophysiol, 100*(6), 3064-3073. doi:10.1152/jn.90722.2008

Ohara, P. T., Vit, J. P., Bhargava, A., Romero, M., Sundberg, C., Charles, A. C., & Jasmin, L. (2009). Gliopathic pain: when satellite glial cells go bad. *Neuroscientist, 15*(5), 450-463. doi:10.1177/1073858409336094

Pacifici, M., & Peruzzi, F. (2012). Isolation and culture of rat embryonic neural cells: a quick protocol. *J Vis Exp*(63), e3965. doi:10.3791/3965

Pannese, E. (1956). [Research on the morphology of the perineuronal satellite cells in the spinal and sympathetic ganglia of mammals. I. Phase-contrast findings]. *Boll Soc Ital Biol Sper, 32*(1-2), 72-74. Retrieved from http://www.ncbi.nlm.nih.gov/pubmed/13374026

Pannese, E. (1981). The satellite cells of the sensory ganglia. *Adv Anat Embryol Cell Biol, 65*, 1-111. Retrieved from http://www.ncbi.nlm.nih.gov/pubmed/7013430

Pannese, E. (2002). Perikaryal surface specializations of neurons in sensory ganglia *International Review of Cytology* (Vol. 220, pp. 1-34): Academic Press.

Pannese, E. (2010). The structure of the perineuronal sheath of satellite glial cells (SGCs) in sensory ganglia. *Neuron Glia Biol, 6*(1), 3-10. doi:10.1017/S1740925X10000037

Pannese, E., Ledda, M., Cherkas, P. S., Huang, T. Y., & Hanani, M. (2003). Satellite cell reactions to axon injury of sensory ganglion neurons: increase in number of gap junctions and formation of bridges connecting previously separate perineuronal sheaths. *Anat Embryol (Berl), 206*(5), 337-347. doi:10.1007/s00429-002-0301-6

Pannunzio, M. E., Jou, I. M., Long, A., Wind, T. C., Beck, G., & Balian, G. (2005). A new method of selecting Schwann cells from adult mouse sciatic nerve. *J Neurosci Methods, 149*(1), 74-81. doi:10.1016/j.jneumeth.2005.05.004

Pini, A., Baranowski, R., & Lynn, B. (1990). Long-Term Reduction in the Number of C-Fibre Nociceptors Following Capsaicin Treatment of a Cutaneous Nerve in Adult Rats. *European Journal of Neuroscience, 2*(1), 89-97. doi:10.1111/j.1460-9568.1990.tb00384.x

Poulsen, J. N., Larsen, F., Duroux, M., & Gazerani, P. (2014). Primary culture of trigeminal satellite glial cells: a cell-based platform to study morphology and function of peripheral glia. *Int J Physiol Pathophysiol Pharmacol, 6*(1), 1-12. Retrieved from http://www.ncbi.nlm.nih.gov/pubmed/24665354

Ravenscroft, M. S., Bateman, K. E., Shaffer, K. M., Schessler, H. M., Jung, D. R., Schneider, T. W., . . . Hickman, J. J. (1998). Developmental Neurobiology Implications from Fabrication and Analysis of Hippocampal Neuronal Networks on Patterned Silane-

Modified Surfaces. *Journal of the American Chemical Society, 120*(47), 12169-12177. doi:10.1021/ja973669n

Relieving Pain in America: A Blueprint for Transforming Prevention, Care, Education, and Research. (2016). *Mil Med, 181*(5), 397-399. doi:10.7205/MILMED-D-16-00012

Romao, L. F., Sousa Vde, O., Neto, V. M., & Gomes, F. C. (2008). Glutamate activates GFAP gene promoter from cultured astrocytes through TGF-beta1 pathways. *J Neurochem, 106*(2), 746-756. doi:10.1111/j.1471-4159.2008.05428.x

Savastano, L. E., Laurito, S. R., Fitt, M. R., Rasmussen, J. A., Gonzalez Polo, V., & Patterson, S. I. (2014). Sciatic nerve injury: a simple and subtle model for investigating many aspects of nervous system damage and recovery. *J Neurosci Methods, 227*, 166-180. doi:10.1016/j.jneumeth.2014.01.020

Scholz, J., & Woolf, C. J. (2007). The neuropathic pain triad: neurons, immune cells and glia. *Nat Neurosci, 10*(11), 1361-1368. doi:10.1038/nn1992

Scott, S. A. (1992). *Sensory neurons : diversity, development, and plasticity*. New York: Oxford University Press.

Shinder, V., & Devor, M. (1994). Structural basis of neuron-to-neuron cross-excitation in dorsal root ganglia. *Journal of Neurocytology, 23*(9), 515-531. doi:10.1007/bf01262054

Shinder, V., Govrin-Lippmann, R., Cohen, S., Belenky, M., Ilin, P., Fried, K., . . . Devor, M. (1999). Structural basis of sympathetic-sensory coupling in rat and human dorsal root ganglia following peripheral nerve injury. *Journal of Neurocytology, 28*(9), 743-761. doi:10.1023/A:1007090105840

Siemionow, K., Klimczak, A., Brzezicki, G., Siemionow, M., & McLain, R. F. (2009). The effects of inflammation on glial fibrillary acidic protein expression in satellite cells of the dorsal root ganglion. *Spine (Phila Pa 1976), 34*(16), 1631-1637. doi:10.1097/BRS.0b013e3181ab1f68

Silva, R. M., Manso, J. P., Rodrigues, J. R., & Lagoa, R. J. (2008). A comparative study of alginate beads and an ion-exchange resin for the removal of heavy metals from a metal plating effluent. *J Environ Sci Health A Tox Hazard Subst Environ Eng, 43*(11), 1311-1317. doi:10.1080/10934520802177953

Sleigh, J. N., Weir, G. A., & Schiavo, G. (2016). A simple, step-by-step dissection protocol for the rapid isolation of mouse dorsal root ganglia. *BMC Res Notes, 9*, 82. doi:10.1186/s13104-016-1915-8

Sparrow, N., Manetti, M. E., Bott, M., Fabianac, T., Petrilli, A., Bates, M. L., . . . Fernandez-Valle, C. (2012). The actin-severing protein cofilin is downstream of neuregulin signaling and is essential for Schwann cell myelination. *J Neurosci, 32*(15), 5284-5297. doi:10.1523/JNEUROSCI.6207-11.2012

Stenger, D. A., Hickman, J. J., Bateman, K. E., Ravenscroft, M. S., Ma, W., Pancrazio, J. J., . . . Cotman, C. W. (1998). Microlithographic determination of axonal/dendritic polarity in cultured hippocampal neurons. *Journal of Neuroscience Methods, 82*(2), 167-173. doi:https://doi.org/10.1016/S0165-0270(98)00047-8

Stephenson, J. L., & Byers, M. R. (1995). GFAP immunoreactivity in trigeminal ganglion satellite cells after tooth injury in rats. *Exp Neurol, 131*(1), 11-22. Retrieved from http://www.ncbi.nlm.nih.gov/pubmed/7895805

Suadicani, S. O., Cherkas, P. S., Zuckerman, J., Smith, D. N., Spray, D. C., & Hanani, M. (2010). Bidirectional calcium signaling between satellite glial cells and neurons in cultured mouse trigeminal ganglia. *Neuron Glia Biol, 6*(1), 43-51. doi:10.1017/S1740925X09990408

Takahashi, M., & Osumi, N. (2005). Identification of a novel type II classical cadherin: rat cadherin19 is expressed in the cranial ganglia and Schwann cell precursors during development. *Dev Dyn, 232*(1), 200-208. doi:10.1002/dvdy.20209

Thumbs, J., & Kohler, H. H. (1996). Capillaries in alginate gel as an example of dissipative structure formation. *Chemical Physics, 208*(1), 9-24. doi:https://doi.org/10.1016/0301-0104(96)00031-6

Tominaga, M., Caterina, M. J., Malmberg, A. B., Rosen, T. A., Gilbert, H., Skinner, K., . . . Julius, D. (1998). The cloned capsaicin receptor integrates multiple pain-producing stimuli. *Neuron, 21*(3), 531-543. Retrieved from http://www.ncbi.nlm.nih.gov/pubmed/9768840

Tveito, A., Jaeger, K. H., Lines, G. T., Paszkowski, L., Sundnes, J., Edwards, A. G., . . . Einevoll, G. T. (2017). An Evaluation of the Accuracy of Classical Models for Computing the Membrane Potential and Extracellular Potential for Neurons. *Front Comput Neurosci, 11*, 27. doi:10.3389/fncom.2017.00027

van Pelt, J., Wolters, P. S., Corner, M. A., Rutten, W. L., & Ramakers, G. J. (2004). Long-term characterization of firing dynamics of spontaneous bursts in cultured neural networks. *IEEE Trans Biomed Eng, 51*(11), 2051-2062. doi:10.1109/TBME.2004.827936

Vit, J. P., Jasmin, L., Bhargava, A., & Ohara, P. T. (2006). Satellite glial cells in the trigeminal ganglion as a determinant of orofacial neuropathic pain. *Neuron Glia Biol, 2*(4), 247-257. Retrieved from http://www.ncbi.nlm.nih.gov/pubmed/18568096

von Hehn, C. A., Baron, R., & Woolf, C. J. (2012). Deconstructing the neuropathic pain phenotype to reveal neural mechanisms. *Neuron, 73*(4), 638-652. doi:10.1016/j.neuron.2012.02.008

Wainger, B. J., Buttermore, E. D., Oliveira, J. T., Mellin, C., Lee, S., Saber, W. A., . . . Woolf, C. J. (2015). Modeling pain in vitro using nociceptor neurons reprogrammed from fibroblasts. *Nature neuroscience, 18*(1), 17-24. doi:10.1038/nn.3886

Wainger, B. J., Buttermore, E. D., Oliveira, J. T., Mellin, C., Lee, S., Saber, W. A., . . . Woolf, C. J. (2015). Modeling pain in vitro using nociceptor neurons reprogrammed from fibroblasts. *Nat Neurosci, 18*(1), 17-24. doi:10.1038/nn.3886

Wakamatsu, Y., Maynard, T. M., & Weston, J. A. (2000). Fate determination of neural crest cells by NOTCH-mediated lateral inhibition and asymmetrical cell division during gangliogenesis. *Development, 127*(13), 2811-2821. Retrieved from http://www.ncbi.nlm.nih.gov/pubmed/10851127

Weider, M., Wegener, A., Schmitt, C., Kuspert, M., Hillgartner, S., Bosl, M. R., . . . Wegner, M. (2015). Elevated in vivo levels of a single transcription factor directly convert satellite glia into oligodendrocyte-like cells. *PLoS Genet, 11*(2), e1005008. doi:10.1371/journal.pgen.1005008

Wheeler, B. C., & Brewer, G. J. (2010). Designing Neural Networks in Culture: Experiments are described for controlled growth, of nerve cells taken from rats, in predesigned geometrical patterns on laboratory culture dishes. *Proc IEEE Inst Electr Electron Eng, 98*(3), 398-406. doi:10.1109/JPROC.2009.2039029

Willenberg, B. J., Hamazaki, T., Meng, F. W., Terada, N., & Batich, C. (2006). Self-assembled copper-capillary alginate gel scaffolds with oligochitosan support embryonic stem cell growth. *J Biomed Mater Res A, 79*(2), 440-450. doi:10.1002/jbm.a.30942

Willenberg, B. J., Zheng, T., Meng, F. W., Meneses, J. C., Rossignol, C., Batich, C. D., . . . Weiss, M. D. (2011). Gelatinized copper-capillary alginate gel functions as an injectable tissue scaffolding system for stem cell transplants. *J Biomater Sci Polym Ed, 22*(12), 1621-1637. doi:10.1163/092050610X519453

Wood, J., Winter, J., James, I., Rang, H., Yeats, J., & Bevan, S. (1988). Capsaicin-induced ion fluxes in dorsal root ganglion cells in culture. *The Journal of Neuroscience, 8*(9), 3208-3220. Retrieved from http://www.jneurosci.org/content/jneuro/8/9/3208.full.pdf

Wood, J. N., Winter, J., James, I. F., Rang, H. P., Yeats, J., & Bevan, S. (1988). Capsaicin-induced ion fluxes in dorsal root ganglion cells in culture. *J Neurosci, 8*(9), 3208-3220.

Wood, P. M. (1976). Separation of functional Schwann cells and neurons from normal peripheral nerve tissue. *Brain Res, 115*(3), 361-375. Retrieved from http://www.ncbi.nlm.nih.gov/pubmed/135599

Woodhoo, A., Alonso, M. B., Droggiti, A., Turmaine, M., D'Antonio, M., Parkinson, D. B., . . . Jessen, K. R. (2009). Notch controls embryonic Schwann cell differentiation, postnatal myelination and adult plasticity. *Nat Neurosci, 12*(7), 839-847. doi:10.1038/nn.2323

Woolf, C. J. (2011). Central sensitization: implications for the diagnosis and treatment of pain. *Pain, 152*(3 Suppl), S2-15. doi:10.1016/j.pain.2010.09.030

Woolf, C. J., & Mannion, R. J. (1999). Neuropathic pain: aetiology, symptoms, mechanisms, and management. *Lancet, 353*(9168), 1959-1964. doi:10.1016/S0140-6736(99)01307-0

Xie, W., Strong, J. A., & Zhang, J.-M. (2010). Increased excitability and spontaneous activity of rat sensory neurons following in vitro stimulation of sympathetic fiber sprouts in the isolated dorsal root ganglion. *Pain, 151*(2), 447-459. doi:10.1016/j.pain.2010.08.006

Yin, K., Baillie, G. J., & Vetter, I. (2016). Neuronal cell lines as model dorsal root ganglion neurons: A transcriptomic comparison. *Mol Pain, 12*. doi:10.1177/1744806916646111

Zhang, X., Huang, J., & McNaughton, P. A. (2005). NGF rapidly increases membrane expression of TRPV1 heat-gated ion channels. *The EMBO Journal, 24*(24), 4211-4223. doi:10.1038/sj.emboj.7600893

Zhu, W., & Oxford, G. S. (2011). Differential gene expression of neonatal and adult DRG neurons correlates with the differential sensitization of TRPV1 responses to nerve growth factor. *Neurosci Lett, 500*(3), 192-196. doi:10.1016/j.neulet.2011.06.034